Regeneration of the Optic Nerve in *Danio rerio* (Hamilton, 1822)

Identification of Novel Genes and Analysis of the *robo2* Mutant

Dissertation zur Erlangung des Doktorgrades der Naturwissenschaften des Fachbereichs Biologie der Universität Hamburg

vorgelegt von Dipl.-Biol. Anselm M. H. Ebert

Hamburg/Edinburgh, Mai 2010

Genehmigt vom Department Biologie
der Fakultät für Mathematik, Informatik und Naturwissenschaften
an der Universität Hamburg
auf Antrag von Frau Professor Dr. C. BECKER
Weiterer Gutachter der Dissertation:
Professor Dr. L. RENWRANTZ
Tag der Disputation: 02. Juli 2010

Hamburg, den 17. Juni 2010

Professor Dr. Axel Temming
Leiter des Departments Biologie

Gutachter: **Frau PD Dr. C.G. Becker**
Herr Prof. Dr. L. Renwrantz

CONTENT

1 Introduction

One of the most puzzling questions that occupies researchers in the field of regeneration of the central nervous system is "Why do fish regenerate their central nervous system while mammals do not?"

Axonal regeneration in the central nervous system (CNS) of mammals is practically non-existent (Chaudhry and Filbin 2007), whereas adult zebrafish (*Danio rerio*) have the ability to successfully repair injuries in their central nervous system (Tanaka and Ferretti 2009). For example, following spinal cord lesions, descending motor axons are able to re-grow from the injury site to their proper targets which results in recovery of swimming behavior (Becker, Wullimann et al. 1997; Becker, Lieberoth et al. 2004). Moreover, severed optic axons, which also belong to the CNS, are capable of correctly growing along their original pathways and of functional target re-innervation (Becker and Becker 2007). Axons from injured retinal ganglion cells (RGCs) traverse optic nerve injury sites and re-grow to the optic tectum with resulting return of vision (Bernhardt, Tongiorgi et al. 1996; McDowell, Dixon et al. 2004). These abilities are largely absent in mammals. Several theories try to explain this situation. The diminished intrinsic regenerative capacities of mature CNS neurons after axotomy might be inadequate to overcome the obstacles involved in the task of regeneration. Furthermore, neurotrophic factors and cell adhesion molecules in the CNS may not be upregulated strongly enough to support lesioned axons. Thirdly, the regeneration of axons in the CNS could be prevented by molecules, which inhibit neurite outgrowth. Recently, researchers have managed to induce regeneration of the optic nerve of adult mice by a virus-assisted in vivo knock-out of PTEN (phosphatase and tensin homologe), deleting a negative regulator of the mammalian target of rapamycin (mTOR) pathway (Park, Liu et al. 2008). On the other hand, neutralizing the extrinsic growth inhibitors resulted only in a limited axonal regeneration (Harel and Strittmatter 2006; Yiu and He 2006). Additionally, whereas a lesion site in a peripheral nerve is rapidly repopulated by Schwann cells, more than 90% of the retina ganglion cells (RGCs) die in mammals (Becker 2007). Some examples of possible reasons for the differences in regenerative capacity between fish and mammals could be e.g. the expression of netrins and semaphorins in the CNS. Netrin receptor messenger-RNA (mRNA) is down-regulated in axotomized RGCs in rats and does not reappear even 28 days later compared to fish which show expression, additionally regenerating RGC axons express netrin receptors, as indicated by binding of a Netrin-1-Fc to regenerating optic axons (Petrausch, Jung et al. 2000). Another

difference is the presence of Sema3 in the spinal cord transection scar in mammals (Pasterkamp, Giger et al. 1999), whereas in lampreys it is semaphorin-negative (Becker 2007). In general, there is no evidence of a major astrocytic scar formation in fish compared to mammals (Becker 2007). Nevertheless, regenerating axons in fish are also confronted with myelin debris (Becker 2007). It appears that in zebrafish the prominent myelin-associated inhibitor of axon growth, nogo-A, lacks one of the domains crucial to inhibition of axon growth (Diekmann, Klinger et al. 2005). Nonetheless most of the regenerating axons coming from the brainstem do not re-grow through the myelin debris, but take a detour through the central gray matter caudal to the lesion site, where they are normally not located, suggesting that fish myelin is less inhibitory than that of mammals but is not a growth promoting substrate (Becker 2007). An additional question is, whether the mammalian ability to regenerate the CNS has been lost during evolution. A hypothesis to explain extensive adult neurogenesis and regeneration in fish is the mechanism of tissue growth in these animals. In contrast to mammals, in which muscle tissue growth post-birth occurs by increasing the size of cells but not their number, in fish the number of fibers continues to increase throughout their entire life cycle. This type of growth may require a matching increase in neuronal input and therefore exerts selective pressure to maintain neurogenesis (Tanaka and Ferretti 2009).

This thesis has been undertaken in the hope of gaining insight into the lack of a regeneration response in mammals by obtaining a more detailed view of the regulation of genes necessary for optic nerve regeneration in zebrafish, and by looking at pathfinding features of optic axons. The resulting data might be useful for suggesting new strategies concerning mammalian CNS regeneration.

In fish regenerating axons have to grow much greater distances during regeneration than during development. Additionally, the adult brain environment is markedly altered compared to development. Thus, the question arises how precise navigation and target re-innervation is accomplished. Of further interest is, whether correct growth trajectories of regenerating optic axons in fish may be achieved by mechanical or molecular interactions with the denervated brain tracts. For example, in the regenerating peripheral nervous system of mice, denervated Schwann cell tubes provide mechanical guidance for regenerating axons (Nguyen, Sanes et al. 2002). At the same time, Schwann cells up-regulate a number of axon growth promoting molecules (Oudega and Xu 2006), which is also true for oligodendrocytes in the CNS of fish (Stuermer, Bastmeyer et al. 1992). Alternatively, regenerating optic axons may actively read specific molecular cues, similar to those that guide developing axons to their targets (Becker

and Becker 2007). It is difficult to distinguish between these mechanisms in vivo, since degenerating tracts always overlap with the appropriate trajectories of regenerating axons, thus providing potential guidance cues. Therefore, a new approach is needed to address this problem.

One method is to identify genes that are regulated during CNS regeneration in zebrafish – in our case, after an optic nerve lesion. We chose the optic nerve lesion paradigm for the following reasons: a) The optic nerve belongs to the CNS, b) the optic fibers regenerate fully in 4 weeks and the topography is restored, c) the optic system is anatomically discrete and highly accessible for experimentation, d) 100% survival rate of the fish with one lesioned optic nerve. Following a crush or cut lesion of the optic nerve, retinal ganglion cells (RGCs) re-enter a growth state indicated by the re-expression of a number of genes that have been developmentally down-regulated, e.g. GAP-43, tubulin and L1.1 (Becker and Becker 2007). But many of the regulated genes are still unknown. Which genes are involved and how does regeneration differ from a simple recapitulation of development?
A new approach to the question whether pathfinding needs denervated brain tracts in the zebrafish could be to use a mutant with known developmental pathfinding errors and combine it with a lesion paradigm. Is the pathfinding of adult regenerating axons in this mutant executed correctly in vivo? And if errors occur, are they the same as those committed during developmental pathfinding?

1.1 Aim of the Study

The aim of this study was twofold: First, to find previously unknown genes related to the regeneration of axons occurring after a lesion of the optic nerve. Secondly, to examine the regeneration of CNS axons in a mutant strain, developmentally impaired in CNS axon guidance functions, in vivo. The idea of combining a mutant fish, rather than a transgenic fish, with a regeneration paradigm has not been employed in this field of research to date.
To pursue the first aim, a microarray study approach, using retinae samples after optic nerve lesion, was chosen to identify genes involved in CNS regeneration of zebrafish. The collapsin response mediator protein (CRMP) family (Schweitzer, Becker et al. 2005) and some other genes discovered in the screen, sparked our interest and were investigated further. Regulation of the mRNA of these genes in the retina ganglion cell layer was investigated by *in situ* hybridizations. Furthermore, gene expression of *robo2* was down-regulated in the RGCs in

vivo, using a modified antisense oligonucleotide, a so-called morpholino (Nasevicius and Ekker 2000), which inhibits correct splicing or translation of pre-mRNA, trying to influence optic axon regeneration.

To approach the second aim of the study, the zebrafish *astray* mutant (Karlstrom, Trowe et al. 1996) was used. In this mutant, ectopic optic tracts are formed in a stochastic manner during development. If these tracts acted as non-specific guidance cues for regenerating axons they would divert some of the regenerating optic axons from their correct trajectory towards the tectum and other target areas. To address this problem, optic axons from *astray* fish, which were lesioned beforehand, were traced throughout the whole brain. The brain was sectioned and analyzed for pathfinding, projection and termination errors.

1.2 Zebrafish as a Model System for CNS Regeneration

The zebrafish (*Danio rerio*) belongs to the family of Cyprinidae in the order of Cypriniformes and the category of Osteichthyes. Zebrafish are tropical sweet water fish that are found in India, Pakistan, Nepal and South-Asia.

The zebrafish is a powerful model system to study nervous system development and regeneration, due to its external development, transparency of embryos, capability to regenerate its CNS and the availability of mutants, transgenic lines and gene knock down technology (Beattie, Granato et al. 2002; Hjorth and Key 2002; Lewis and Eisen 2003; Lee and Chien 2004).

The stereotypic patterning of the zebrafish nervous system and other organs occurs during the first 24 hours post fertilization (hpf) and juvenile fish hatch between two and three days post fertilization (dpf). On the fifth day of development the vast majority of cell types have differentiated and the organs have taken up their functions.

Protein expression can be easily manipulated by injection of plasmid DNA, mRNA overexpression constructs, or morpholinos, which inhibit mRNA translation. Since the embryos develop externally, perturbation reagents can be injected directly into the yolk of fertilized eggs or into single cells at various developmental stages.

The zebrafish is easy to breed and produces large numbers of eggs (up to 300 eggs in a week) over the whole year. The size of the zebrafish genome is approximately 1.7×10^9 bp on 25 chromosomes. It is assumed that large parts of the zebrafish genome were subject to an ancient genome duplication event during the evolution of the ray-finned fishes. Retained

duplicates often appear to have subdivided the roles of their single-gene ancestors (Taylor, Van de Peer et al. 2001). The genome duplication was followed by a functional specialization of some of the duplicated genes and the loss of other genes. Consequently an estimated 20% of mammalian genes have two zebrafish orthologs with distinct functions and expression domains (Van de Peer, Taylor et al. 2002). In February 2001, the Sanger Institute started sequencing the genome of the zebrafish and sequences are currently being annotated by the Ensembl project of the Sanger Institute and the European Molecular Biology Laboratory. Genomic information is accessible through a genome browser on the Ensembl website: http://www.ensembl.org/index.html

1.3 Growth of Optic Axons

1.3.1 Morphological Overview of the Zebrafish Brain

In order to understand the structure of the zebrafish brain a short overview is given in Figure 1. For a schematic representation of the zebrafish retina, please refer to Figure 2. The pathways taken by regenerating RGC axons towards the tectum are illustrated in Figure 3.

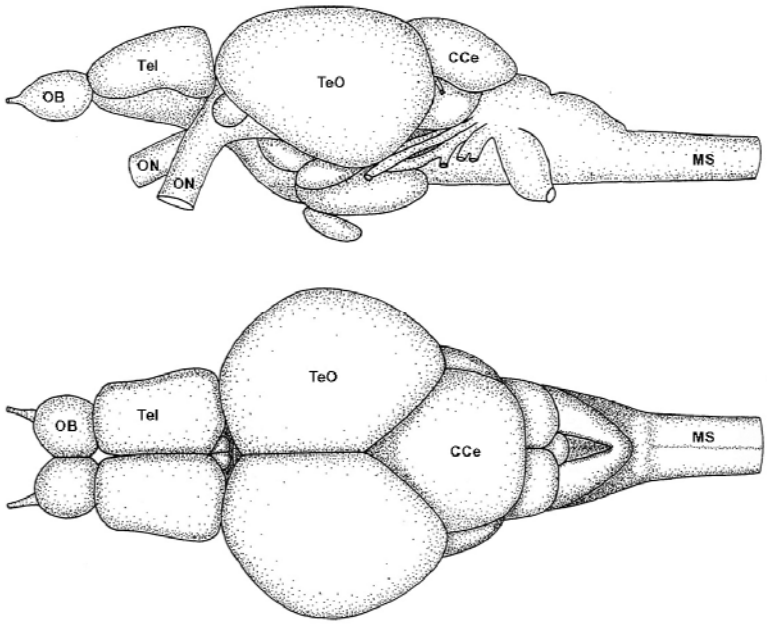

Figure 1: Lateral and dorsal view of the adult zebrafish brain modified after the atlas "Neuroanatomy of the zebrafish brain" (Mario F. Wullimann 1996). Tel: Telencephalon; TeO: Tectum opticum; ON: Optic nerve; MS: Medulla spinalis; OB: Olfactory bulb; Cce: Corpus cerebelli

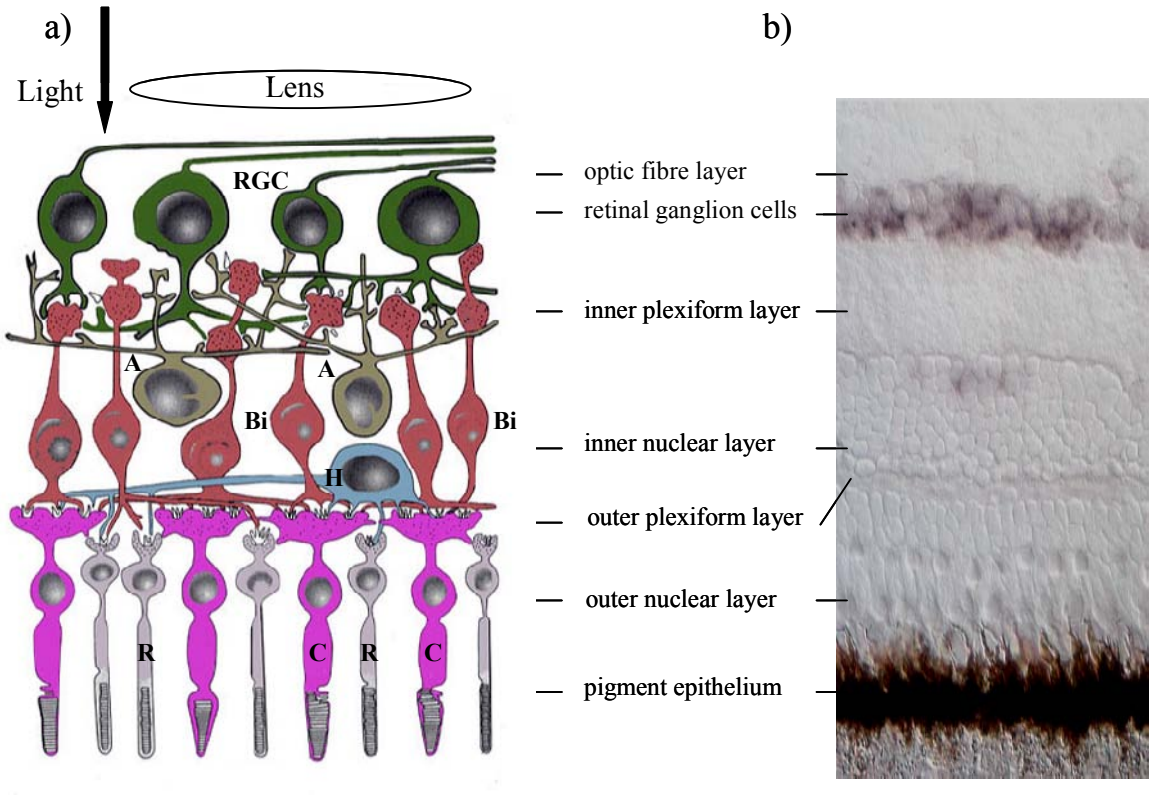

Figure 2: Layers of a retinal cross section. a) Schematic drawing modified after a picture from Scidmore College, New York of a retina including some important cell types. Starting from the top: optic fiber layer: made up of the axons of the retinal ganglion cells, terminating in the brain; retinal ganglion cell layer: place of cell bodies of the retinal ganglion cells (RGCs); inner plexiform layer: place of contact of retinal ganglion cell dendrites and amakrine cell dendrites with bipolar cell axons; inner nuclear layer: mostly cell bodies of amakrine, bipolar, horizontal cells and Müller glia; outer plexiform layer: place of contact of bipolar- and horizontal cell dendrites with the synapses of the photoreceptors; outer nuclear layer: cell bodies of the photoreceptor cells (rods and cones); pigment epithelium: pigmented cell layer which nourishes the photoreceptor cells b) Photo of a retinal cross section with dioxigenin -labeled retinal ganglion cells (cryostat, 14µm) . A: Amacrine cell, Bi: Bipolar cell, C: Cone, H: Horizontal cell, R: Rod, RGC: Retinal ganglion cell.

1.3.2 Time Course of Optic Axon Regeneration

Since all data collected in this work are connected to the regeneration of the optic nerve of zebrafish, supporting information on the path of optic axon regeneration is given in this section. Regenerating optic axons in wild type fish do not commit pathfinding or termination errors, except for a few ipsilateral fibers at the chiasm (Becker, Meyer et al. 2000). To understand the route and pathways these regenerating axons take, a schematic overview is given in the following Figure 3. In goldfish these axons extend from their somata situated in the RGC layer in the eye, cross at the chiasm onto the contralateral side and enter the tectal lobe at its rostroperipheral edges. There, they diverge fan-like, from the brachial entry point, and curve caudally and centrally over the dorsal and ventral hemitecta (Stuermer and Easter 1984). Next to terminating in the tectum, most of the optic axons display collaterals in the pretectum and the tectum (not shown in the schematic overview Figure 3).

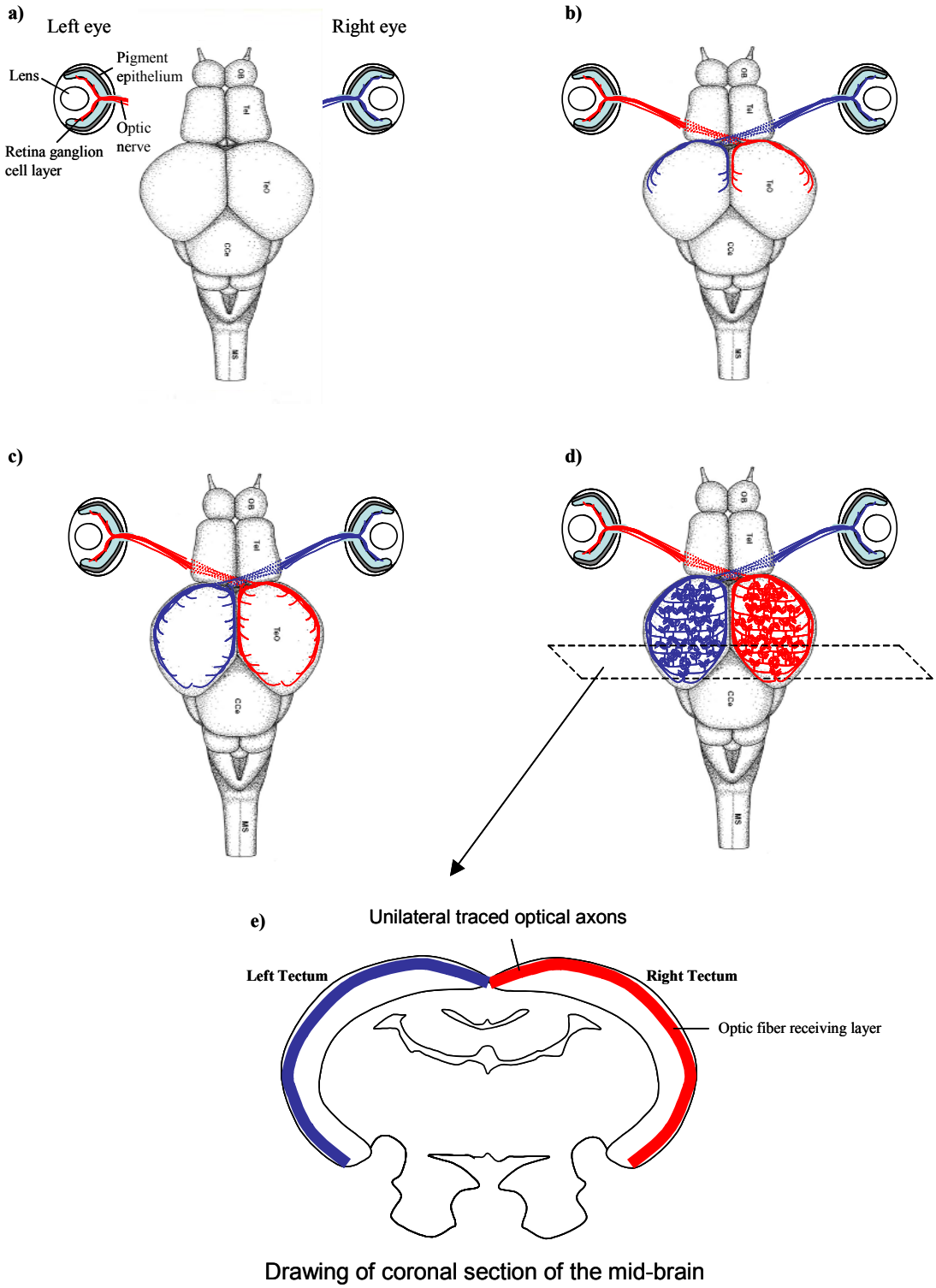

Figure 3: Time course as schematic drawings of optic axons regenerating in a wild type fish after a lesion. a)-d) Ventral view of a zebrafish brain a) 0 days post lesion (dpl): The optic nerve is severed directly behind the eye. b) Approx. 4-6 dpl: Optic axons start to regrow, cross correctly at the chiasm and start to enter the tectum. Thereafter some optic axons terminate at specific pretectal nuclei just rostral to the chiasm (not shown). c) Approx. 8-12 dpl: The other optic axons enter the tectal lobe at its rostroperipheral edges and diverge fanlike, from the brachial entry point, and curve caudally and centrally over the dorsal and ventral hemitecta. d) Approx. 13-28 dpl: Optic axons start growing from the dorsal and ventral hemitecta towards each other, filling the optic fiber receiving layers. e) A coronal section from the mid-brain of a fully regenerated optic tectum depicting the optic fiber receiving layers in blue (left tectum) and red (right tectum).

Figure 4 depicts, in addition to the schematic drawing in Figure 3c, photomicrographs from a regenerating optic projection 8 days after lesioning the optic nerve. At this time point the optic fibers have partially repopulated their final destinations. Optic fibers in the dorsal and ventral tectal region (Figure 4b) start growing towards each other. In the magnification (Figure 4c) pioneering fibers are visible. At the very caudal end of the tectum optic fibers are clearly visible at the ventral edge, starting to grow dorsally (Figure 4d).

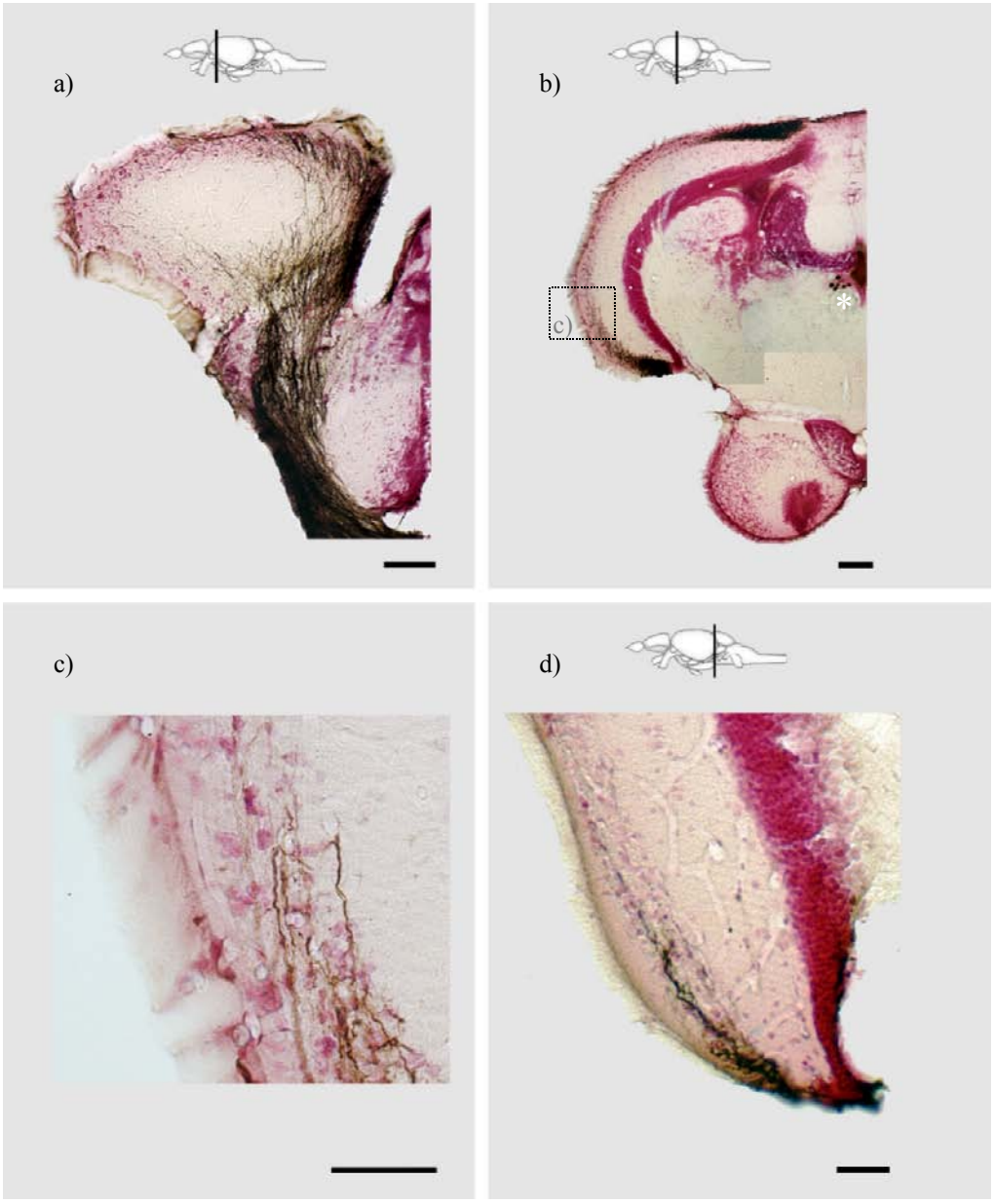

Figure 4: The right eye was lesioned with a crush and the axons traced at 8 days post lesion. Sections of the tectum 8 days after an optic nerve lesion are depicted. They are also shown in the schematical drawing Figure 3c. All pictures show only the left part of the tectum. a) Section posterior of the chiasm at the anterior part of the tectum. Optic nerve fibers are visible, extending onto the tectum starting at the peripheral edges b) Section from the midtectum. Somata of the oculomotorius are clearly visible (indicated by white asterisk). The dorsal and ventral tectal regions already show optic axons growing towards each other. c) Magnification of tectal region. Single axons can be observed growing towards the dorsal part. d) At 8 days optic fibers have already reached the very posterior part of the tectum and start growing dorsally. Scale bars in a) and b) 100µm and in c) and d) 50µm.

1.4 Molecules Involved in Axon Growth and Pathfinding

Axon growth and pathfinding are two main subjects regenerating axons have to cope with. In this thesis we focused on the CRMP (collapsin response mediator protein) family for axon growth and *robo2* for pathfinding. A short overview of the CRMPs is given in section 1.4.1 and for *robo* in section 1.4.2.

1.4.1 Collapsin Response Mediator Proteins – The CRMP Family

CRMPs (collapsin response mediator proteins) belong to the family of cytosolic phosphoproteins. These proteins are prominently expressed in the developing brain and nervous system. In the adult mouse brain, expression is strongly downregulated but remains in structures that retain their capacity for differentiation and plasticity (hippocampus, olfactory bulb and cerebellum). So far, there are five known members of the CRMPs (CRMP1-5) in mammals and 6 in zebrafish CRMP 1-4 and two homologues of CRMP-5 (Schweitzer, Becker et al. 2005). The first to be discovered was CRMP-2, a signal transducer of semaphorin-mediated growth cone collapse, hence the family name. CRMP-2 regulates microtubule dynamics (Gu and Ihara 2000), and it directly binds to tubulin heterodimers (Fukata, Itoh et al. 2002; Stenmark, Ogg et al. 2007). It is crucial for axon outgrowth and determination of the fate of the axon and dendrites, thereby establishing and maintaining neuronal polarity (Yoshimura, Kawano et al. 2005).

Even though the CRMP family shows high sequence identity with the human enzyme dihydropyrimidinase (DHP), which catalyses the second step in pyrimidine degradation, no catalytic activity has been observed and key active site residues of DHP are not conserved in the CRMPs (Wang and Strittmatter 1997).

Apart from axon growth and guidance, CRMPs have been found to also play a role in regeneration (Suzuki, Nakagomi et al. 2003; Zhang, Ottens et al. 2007; Hou, Jiang et al. 2008) apoptosis, neuronal polarity and cell migration in the nervous system (for review see (Quinn, Gray et al. 1999; Liu and Strittmatter 2001; Charrier, Reibel et al. 2003; Arimura, Menager et al. 2004; Schmidt and Strittmatter 2007).

CRMP-1 is involved in Reelin signaling to regulate neuronal migration as well as the semaphorin3A-induced spine development in the cerebral cortex of mice (Yamashita, Uchida et al. 2006; Yamashita, Morita et al. 2007). Looking at axonal injury, major inhibitory factors for growth cone extension in mammals are the proteins of the myelin sheath.

CRMP-2 is involved in the regulation of growth cone collapse by myelin-related inhibitors, and its activation can be induced by the binding of the myelin-associated glycoprotein (MAG) on the axonal surface (Mimura, Yamagishi et al. 2006). It is also expressed in oligodendrocytes, the myelinating cells of the CNS, in a developmentally regulated manner (Ricard, Stankoff et al. 2000), but its exact functions during myelination remain to be characterised. CRMP-2 is regulated by Rho kinase (Hall, Brown et al. 2001) and by that providing a mechanism for dynamic modulation of growth cone guidance. Interaction studies have implicated Rho, Numb, phospholipase D2 (PLD2) (Lee, Kim et al. 2002), the cytosolic tyrosine kinase Fes (Mitsui, Inatome et al. 2002), and intersectin in CRMP function (Quinn, Chen et al. 2003). It also binds directly to cytoplasmic dynein and interferes with its activity, influencing axon formation and neuronal development (Arimura, Hattori et al. 2009) Phosphorylation of CRMP-2 by Rho, Cdk5 and GSK-3β is an event downstream of MAG, NOGO-66, Sema3A and Ephrin-A5 leading either to axonal outgrowth and branching or growth cone collapse and axonal outgrowth arrest (Arimura, Menager et al. 2005; Mimura, Yamagishi et al. 2006). CRMP-2 also interacts with Numb, an endocytosis related protein, possibly indicating a role in the endocytotic recycling of the adhesion molecule L1 at the neuronal growth cone (Nishimura, Fukata et al. 2003). Furthermore, Numb promotes Notch1 ubiquitination and degradation of the Notch1 intracellular domain (McGill and McGlade 2003) possibly influencing the development of oligodendrocytes in zebrafish which require Notch signaling (Schebesta and Serluca 2009). CRMP-2 has also been found to be involved in neurotransmitter release via an interaction with presynaptic calcium channels (Brittain, Piekarz et al. 2009).

A number of studies also suggest a role for CRMP-2 in the etiology of neurological disorders, including Alzheimer's disease (Cole, Knebel et al. 2004; Czech, Yang et al. 2004; Kanninen, Goldsteins et al. 2004; Cole, Noble et al. 2007).

CRMP-3 has been implicated in dendrite and spine morphogenesis in the hippocampus of mice (Quach, Massicotte et al. 2008). It is also a direct target of calpain, which cleaves it at the N-terminus. The subsequent nuclear translocation of the truncated CRMP-3 evokes neuronal death in response to excitotoxicity (Hou, Jiang et al. 2006) and has also been found in connection to the pathogenesis of a paraneoplastic neurologic syndrome (Honnorat, Byk et al. 1999).

CRMP-4 promotes bundling of F-actin and it functionally regulates the actin cytoskeleton in motile cells (Rosslenbroich, Dai et al. 2005). Next to its involvement in neurite outgrowth it also co-localizes with GAP-43 in primary cortical neurons (Kowara, Menard et al. 2007).

GAP-43 is expressed during developmental and regenerative axon growth in zebrafish (Udvadia 2008). Regenerating spinal motoneurons in mammals also upregulate GAP-43 (Linda, Piehl et al. 1992; Yuan, Hu et al. 2009).

CRMP-5 seems to play a role in neuronal process extension and forebrain development in mice (McLaughlin, Vidaki et al. 2008). It is on the other hand a marker for highly aggressive neuroendocrine carcinomas (Meyronet, Massoma et al. 2008). CRMP-5 is expressed in immature olfactory neurons but down-regulated in mature neurons in mice (Veyrac, Giannetti et al. 2005). In contrast to mammalian cell culture (COS-7) where CRMP-5 is thought to interact with CRMP-3 (Inatome, Tsujimura et al. 2000), in zebrafish these two genes have very different expression patterns. The expression pattern of zebrafish CRMP-3 does neither overlap with CRMP-5a nor -5b, even though the human CRMP-5 gene has an amino acid homology of 80% to CRMP-5a and 76% to CRMP-5b gene. In contrast, the human CRMP-3 shows only 67% homology to the zebrafish CRMP-3 (Schweitzer, Becker et al. 2005).

1.4.2 Roundabout and the Mutant *astray*

Originally roundabout (*robo*) was identified through a large-scale screen in *Drosophila* as a mutant affecting the development of CNS axon pathways (Seeger, Tear et al. 1993). *Slit*, which is the ligand for *robo*, belongs to the 4 most studied classes of guidance molecules including ephrins, netrins, semaphorins and *slits*. In *Drosophila*, the *slit/robo* guidance function is critical at a particular choice point, the midline. In the *robo* mutant, many growth cones that normally extend only on their own side now project across the midline, and axons that normally cross the midline only once, appear to cross and recross several times, hence the name “roundabout” (Kidd, Russell et al. 1998).

In vertebrates, there are 3 *slit* ligands for *robo* receptors known. *Slit*s repel several types of extending axons as well as migrating neurons in vertebrates (Itoh, Miyabayashi et al. 1998; Brose, Bland et al. 1999; Nguyen Ba-Charvet, Brose et al. 1999; Yuan, Zhou et al. 1999). In zebrafish *slit1* and *2* are expressed in the midline of the nervous system and in the retina, as well as in other regions (Erskine, Williams et al. 2000).

Robos encode transmembrane receptor proteins which are highly expressed in growth cones (Kidd, Brose et al. 1998). Two of the vertebrate *robo*s – *robo1* and *2* are similar to the *Drosophila robo1*, while a third, *robo3* is more distantly related.

There are 4 *robo* homologues in zebrafish, of which three, *robo1* to *3* are expressed in the CNS (Lee, Ray et al. 2001) and one, *robo*4, is vascular specific and plays a role in angiogenesis and vascular patterning (Park, Morrison et al. 2003).

Robo1 and *3* in zebrafish seem not to be expressed in the developing visual system, whereas *robo2* is (Lee, Ray et al. 2001).

All three *robos* belong to a subgroup of the immunoglobulin cell adhesion molecules (Ig-CAMs). Molecules are categorized as members of the Ig-CAMs based on shared structural features with immunoglobulins, especially the Ig domains, which are about 70-110 amino acids long. *Robo2* is 1513 amino acids (4871 base pairs) long and contains five Ig domains, three fibronectin type III (FnIII) domains, a single transmembrane domain (TM) and a long cytoplasmic domain (CM). The CM domain contains 4 conserved cytoplasmic motifs CM0, 1, 2 and 3. CM0 and CM1 are potential tyrosine phosphorylation sites, whereas CM2 and CM3 are proline rich motifs involved in protein-protein interaction (Kidd, Brose et al. 1998; Lee, Ray et al. 2001).

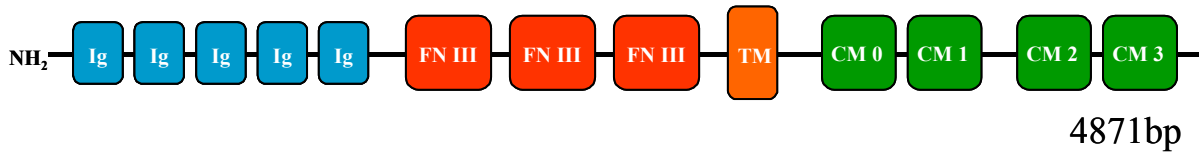

Figure 5: Graphical presentation of the *robo* gene with its domains. Ig = Immunoglobulin domain; FN III = fibronectin type III; TM = transmembrane domain; CM 0,1,2,3 = cytoplasmic motifs.

Robo2 expression starts around 16 hours post fertilization (hpf) with weak expression in the hindbrain. At around that time the principal longitudinal axon tract in the zebrafish forebrain, the postoptic commissure (TPOC) emerges from a ventrorostral cluster (vrc) of neurons. This cluster expresses all three *robos* (Devine and Key 2008). At 24hpf *robo2* is distinctly expressed in the olfactory placode, telencephalon, ventral hypothalamus, hindbrain, trigeminal ganglion, lateral line ganglia and the spinal cord. At 36hpf it is expressed in the whole RGC layer. From 48 to 72hpf there is no expression in the spinal cord anymore, at this stage it can only be detected in the tectum, hindbrain, the peripheral retina and the inner nuclear layer (INL) of the retina. In the nervous system of zebrafish the expression of *robos* indicates possible roles for different neuronal types. *Robo2* may act to determine whether the axons of the interneurons cross the midline. The expression of zebrafish *robos* in interneurons is consistent with the expression of *robo1* in commissural neurons in the developing mammalian spinal cord. The zebrafish and mammalian *robo2* are both expressed in the RGC layer hinting at a role in the guidance of RGC axons (Lee, Ray et al. 2001).

The growth of the retinal ganglion cells in development of zebrafish is characterized, in brief, as follows. At 32hpf the first retinal ganglion cell axons exit the retina and project across the chiasm at around 36hpf. They reach their target, the optic tectum, at around 48hpf (Stuermer 1988); (Burrill and Easter 1995). The expression of *robo2* at 48hpf only in the peripheral retina suggests that it is transiently expressed only in young RGCs and is later turned off, similar to Neurolin-a, which strongly influences the correct development of the RGCs in zebrafish (Diekmann and Stuermer 2009).

The *astray* mutation in zebrafish is a functional null-mutation for *robo2* (Fricke, Lee et al. 2001) and was originally isolated in 1996 (Karlstrom, Trowe et al. 1996) in a large scale screen for retinotectal mutants. Due to the lack of r*obo2*, a receptor for repulsive extracellular matrix (ECM) cues of the *slit* class (Dickson and Gilestro 2006), the *astray* mutants show rostro-caudal pathfinding errors, ectopic midline crossing, and increased terminal arbor sizes of optic axons during development (Fricke, Lee et al. 2001; Campbell, Stringham et al. 2007). Similar pathfinding effects are observed in *slit* or *robo* deficient mice (Plump, Erskine et al. 2002; Plachez, Andrews et al. 2008). Time-lapse analysis indicates that optic axons in *astray* mutants do not correct errors during growth, as opposed to wild type axons which do (Hutson and Chien 2002). The mutant fish line *astray*/*robo2* carries a point mutation changing Arg635 to a Stop codon and thus encoding a truncated *robo2* protein, which could potentially be secreted but not function as a receptor (Fricke, Lee et al. 2001).

For our investigation of optical axon guidance, the *astray*/*robo2* mutant line seemed a perfect tool. Firstly, to study axon guidance defects in detail which occur due to the lack of *robo2* and secondly to elucidate whether guidance during regeneration is also influenced by the lack of *robo2*. Thirdly, we wanted to see whether regenerating axons in the CNS use denervated axon tracts as guidance channels as observed in the peripheral regeneration (Nguyen, Sanes et al. 2002).

The following summarizes shortly our results gained in this thesis.

A group of novel, not yet described, optic axon regeneration associated genes in zebrafish were identified by employing the technique of microarray chip analysis. The CRMP (collapsin response mediator protein) family, identified by microarray analysis, was investigated further for its mRNA expression patterns: a) during development, b) in the unlesioned eye and c) 11 days after an optic nerve lesion. Some family members exhibit regeneration specific expression, whereas others recapitulate their developmental expression patterns, proving that regeneration is different to development. Next to the molecular

approach of identifying new genes by microarray techniques, we compared optic axon pathways of wild type and *astray* mutants (which have a developmental pathfinding defect in the optic projection) both with an unlesioned and regenerated optic projection. Our results indicate that some pathfinding phenotypes in *astray* mutants with a regenerated optic projection are drastically reduced whereas other phenotypes reoccur. Hence, *robo2*, the mutated gene in the *astray* mutant, influences partially the pathfinding of the regenerating optic projection in adult zebrafish. Additionally, gathered data suggests, that the guidance of regenerating axons is not strongly influenced by degenerating tracts, contrary to existing hypotheses gained through research in mice. The approach to perturb in vivo regenerating optic tracts by using CRMP or ROBO morpholinos (chemically stabilized antisense oligonucleotides) in adult fish did not lead to results.

2 Materials and Methods

2.1 Antibodies

Anti-Digoxigenin-AP, Fab fragments	Roche	Welwyn Garden City, UK

2.2 Bacterial Strains

XL1-Blue	Stratagene	Cambridge, UK
Dam^{-}/dcm^{-} Competent E.coli	NEB	Hitchin, UK

2.3 Bacterial Media

All media were autoclaved prior to use.

Luria broth (LB per liter)	10 g NaCl
	10 g tryptone or peptone
	5 g yeast extract
	→ pH 7.0 with 5 N NaOH (optional)
LB agar (per liter)	10 g NaCl
	10 g tryptone or peptone
	5 g yeast extract
	20 g agar
	→ pH 7.0 with 5 N NaOH (optional)

The following antibiotics were added when needed (1000 fold stock solutions): 100 mg/l ampicillin (LB-amp), 25 mg/l kanamycin (LB-kan).

2.4 Buffers and Stock Solutions

Buffers and stock solutions are listed below. All more method-specific solutions are specified in the accompanying sections.

Blocking buffer (whole mount immunohistochemistry)	1 % (v/v) DMSO 1 % (v/v) normal goat serum 1 % (w/v) BSA 0.7 % (v/v) Triton-X 100
DAB-stock solution	6 % (w/v) Diaminobenzidine
Danieau solution	58 mM NaCl 0.7 mM KCl 0.4 mM $MgSO_4$ 0.6 mM $Ca(NO_3)_2$ 5 mM HEPES pH 7.6
dNTP-stock solutions *(PCR)*	25 mM each dATP, dCTP, dGTP, dTTP
Ethidiumbromide-stock solution *(DNA-gels)*	10 mg/ml Ethidiumbromide
4 % Paraformaldehyde	4 % (w/v) Paraformaldehyde dissolved at 60°C under stirring in 1 x PBS and 3 drops of 3M NaOH
2 % PFA / 2% Glutaraldehyde	50% Paraformaldehyde (4%) 8% Glutaraldehyde (25%) 42% PBS (1x)
EDTA stock solution	0.5 M EDTA

	→ pH 8.0		
Phosphate buffered saline (PBS 10 x, Morphology)	1.36 M NaCl 0.1 M Na_2HPO_4 27 mM KCl 18 mM KH_2PO_4 → pH 7.4		
PBST	0.1	% (v/v)	Tween 20 in 1 x PBS
PBSTriton	0.1	% (v/v)	Triton X-100 in 1 x PBS
Saline sodium citrate buffer (SSC, 20 x)	3 0.3	M M → pH 7.4	NaCl *tri*-sodium citrate
TAE (50x) *(DNA-gels)*	2 100	M mM	Tris-Acetat, pH 8.0 EDTA
TE (10x)	0.1 10	M mM	Tris-HCl, pH 7.5 EDTA
Glycine solution (10x)	1	mM (w/v)	Glycine in PBSTriton
$NiCl_2$ (1%)	10	mM	$NiCl_2$ in PBS
$CoSO_4$ (1%)	10	mM	$CoSO_4$ in PBS

2.5 Enzymes and Reaction Kits

Enzymes:

PfuUltra™ High-Fidelity DNA polymerase	Stratagene	Amsterdam, NL

Phosphatase, alkaline (AP)	Roche	Welwyn Garden City, UK
T4 DNA ligase	NEB	Hitchin, UK
Taq DNA polymerase	NEB	Hitchin, UK
Various restriction enzymes	NEB	Hitchin, UK

Kits:

GFX micro plasmid prep kit	Amersham	Buckinghamshire, UK
HiSpeed plasmid midi kit	Qiagen	Crawley,UK
Maxi script SP6/T7 kit	Ambion	Warrington, UK
MinElute PCR purification kit	Qiagen	Crawley,UK
MinElute reaction cleanup kit	Qiagen	Crawley,UK
mirVana™ miRNA isolation kit	Ambion	Warrington, UK
pGEM T-Easy vector kit	Promega	Southampton, UK
QIAquick gel extraction kit	Qiagen	Crawley,UK
Rapid DNA ligation kit	Roche	Welwyn Garden City, UK
SuperScript III RT-kit	Invitrogen	Paisley, UK
Vectastain Elite ABC-kit	VectorLabs	Peterborough, UK

2.6 Instruments

Bioanalyzer 2100	Agilent Technologies	Foster City, US
Centrifuge 3K30C	Sigma Laboratory	Osterode, GER

Centrifuge tabletop	Sigma Laboratory	Osterode, GER
Fridge/freezer Soft Line Plus	Stinol	Lipeck, RO
Gel Doc System	Herolab	Wiesloch, GER
Hotplate stirrer Fisherbrand® metal top	Fisher	Leicestershire, UK
Hybridizer UVP HB-1000	Jencons	Bedfordshire, UK
Incubated shaker MaxQ Mini 4450	Fisher	Leicestershire, UK
Lamp Schott KL200	Schott	Mainz, GER
Magnetic stirrer hotplate	Stuart Scientific	Surrey, UK
Microinjector Narishige Intracel + manipulator IM300	Intracel Ltd.	Herts, UK
Microscope SZ40	Olympus	Hamburg, GER
Microwave oven M8021TP-BI	Empire direct	Leeds, UK
MJ mini gradient thermal cycler	Biorad	Hertfordshire, UK
NanoDrop ND-1000	Thermo Fisher Scientific	Wilmington, US
pH meter MP220	Mettler Toledo	Greifensee, CH
Philips lamps	MGC Lamps Ltd.	Suffolk, UK
Qualicool incubator 260	LTE Scientific Ltd.	Oldham, UK
Stereo microscope - KL 1500	Carl Zeiss Ltd.	Jena, GER
Stereo microscope - STEMI 2000	Carl Zeiss Ltd.	Jena, GER
Stirling mixer	Sandrest Ltd.	Eastbourne, UK
Stirrer plate MR2000	Heidolph	Kehlheim, GER
Sub-Cell GT / Power Pac Basic System	Biorad	Hertfordshire, UK

96/192

2.7 Morpholinos

Morpholine-based antisense oligonucleotides were synthesized by Gene Tools LLC (Philomath, OR, USA). Morpholino sequences are listed in the appendix. For detailed information on morpholinos please refer to Section 2.20.3.1.

2.8 Oligonucleotides

Oligonucleotides/primers were synthesized by VH Bio Limited, Gateshead, UK.

2.9 Reagents and Disposables

If not itemized in this paragraph, origin of enzymes and reaction kits is referenced in the corresponding sections. All chemicals were obtained from the following companies in *pro analysis* quality: Amersham (Buckinghamshire, UK), Fisher (Leicestershire, UK), Invitrogen (Paisley, UK), Sigma-Aldrich (Poole, UK),VWR (Leicestershire, UK). Molecular cloning reagents were obtained from Ambion (Warrington, UK), Promega (Southampton, UK), Qiagen (Crawley, UK) and Stratagene (Amsterdam, NL). DNA and RNA purification kits were purchased from Quiagen (Crawley, UK) and Ambion (Warrington, UK). Nucleic acid molecular weight markers were purchased from Invitrogen (Paisley, UK).

Reagents, disposables, etc.

Fish care:

Artemia	Aquarienbau Schwarz	Göttingen, GER
Coral Pro Salt	Aquarienbau Schwarz	Göttingen, GER
Readsea Salt	Aquarienbau Schwarz	Göttingen, GER

Water test equipment	Palintest	Gateshead, UK
ZM (100 – 400) fish food	Aquarienbau Schwarz	Göttingen, GER
2-Propanol	Sigma-Aldrich	Poole, UK
3,3′-Diaminobenzidine tetrahydrochloride	Sigma-Aldrich	Poole, UK
Acetic anhydride min.98%	Sigma-Aldrich	Poole, UK
Agarose molbiol grade	Fisher	Leicestershire, UK
Albumin from bovine serum fraction V	Sigma-Aldrich	Poole, UK
Aminobenzoic acid ethylmethylester (MS 222)	Sigma-Aldrich	Poole, UK
Ampicillin, Sodium Salt	Fisher	Leicestershire, UK
Anti-Digoxigenin-AP, Fab fragments	Roche	Welwyn Garden City, UK
Bacterial growth encapsulated media	Fisher	Leicestershire, UK
Biocytin	Sigma-Aldrich	Poole, UK
Calcium chloride	Sigma-Aldrich	Poole, UK
Cover slips	VWR	Leicestershire, UK
Cresyl Violet acetate	Sigma-Aldrich	Poole, UK
Denhardt's solution lyophilized powder	Sigma-Aldrich	Poole, UK
Deoxynucleotide Solution Mix	NEB	Hitchin, UK
Dextran sulfate sodium salt	Sigma-Aldrich	Poole, UK

Dextran sulfate sodium salt from Leuconostoc spp.	Sigma-Aldrich	Poole, UK
Digoxigenin-11-UTP, 250nmol (10 mM, 25 µl)	Roche	Welwyn Garden City, UK
Dimethylsulfoxide	Sigma-Aldrich	Poole, UK
DL-Dithiothreitol > = 99.5 %	Sigma-Aldrich	Poole, UK
DNA gel loading buffer 10X	Fisher	Leicestershire, UK
Elite Pap Pen	VWR	Leicestershire, UK
Ethanol 200 proof (absolute)	Sigma-Aldrich	Poole, UK
Ethidium bromide solution	Fisher	Leicestershire, UK
Ethylenediaminetetraacetic acid EDTA	Sigma-Aldrich	Poole, UK
Fluoromount-G	Electron Microscopy Sciences	Hatfield, USA
Formamide reagent grade 98%	Sigma-Aldrich	Poole, UK
Gel loading buffer	Sigma-Aldrich	Poole, UK
Gelatin from porcine skin, Type A	Sigma-Aldrich	Poole, UK
Glass bottles, Duran	Schott	
Glass slides	VWR	Leicestershire, UK
Glutaraldehyde solution 25%	VWR	Leicestershire, UK
Glycerol mol.biol. >= 99%	Sigma-Aldrich	Poole, UK
Heparin sodium salt from porcine	Sigma-Aldrich	Poole, UK

Kanamycin Monosulfate	Fisher	Leicestershire, UK
LB Agar, Miller	Fisher	Leicestershire, UK
Magnesium chloride	Sigma-Aldrich	Poole, UK
Microscope slides, Superfrost Plus	VWR	Leicestershire, UK
Parafilm M	Fisher	Leicestershire, UK
Paraformaldehyde reagent grade, crystalline	Sigma-Aldrich	Poole, UK
Perdrogen-H2O2	Sigma-Aldrich	Poole, UK
Poly A-RNA	Sigma-Aldrich	Poole, UK
Potassium chloride	Sigma-Aldrich	Poole, UK
Potassium phosphate monobasic	Sigma-Aldrich	Poole, UK
Proteinase K solution	Roche	Welwyn Garden City, UK
Random Primers	Promega	Southampton, UK
Ready-Load 1 Kb Plus DNA Ladder	Invitrogen	Paisley, UK
RNase ZAP	Sigma-Aldrich	Poole, UK
RNaseOUT™ Recombinant Ribonuclease Inhibitor	Invitrogen	Paisley, UK
SIGMAFAST™ BCIP/NBT Alkaline Phosphatase Substrate Tablets	Sigma-Aldrich	Poole, UK
Sodium acetate	Sigma-Aldrich	Poole, UK
Sodium Chloride	Sigma-Aldrich	Poole, UK
Sodium citrate	Sigma-	Poole, UK

	Aldrich	
Sodium hydroxide pellets	Sigma-Aldrich	Poole, UK
Sodium phosphate dibasic	Sigma-Aldrich	Poole, UK
T7 Express Competent E.coli	NEB	Hitchin, UK
Tips – all sizes	Starlab	Ahrensburg, GER
Tissue Tek OCT Compound	Electron Microscopy Sciences	Hatfield, USA
Triethanolamine 98%	Sigma-Aldrich	Poole, UK
Trizma base f. molbiol	Sigma-Aldrich	Poole, UK
tRNA from brewer's yeast	Roche	Welwyn Garden City, UK
Tween 20	Sigma-Aldrich	Poole, UK
Water, DNase, RNase and protease free	Fisher	Leicestershire, UK

2.10 Vectors

pGEM® - T Vector	Promega	Cloning vector
pGEM® - T Easy Vector	Promega	Cloning vector

2.11 General Biological Methods

2.11.1 Photometric Quantification of Nucleic Acids

DNA, RNA and oligonucleotides are measured directly in aqueous solutions. The concentration is determined by measuring adsorption at λ = 260 nm against blank and then evaluated via the absorption factor. The absorption of 1 OD (A) is equivalent to approximately 50g/ml sDNA, 40 g/ml RNA and 30 g/ml for oligonucleotides. Interference by contaminants is recognized by the calculation of ratio. The ratio A260 / 280 is used to estimate the purity of nucleic acid, since proteins absorb at 280 nm. Pure DNA should have a ratio of 1.8, whereas pure RNA should give a value of approximately 2.0. Absorption at λ = 230 nm reflects contamination of the sample by substances such as carbohydrates, peptides, phenols or aromatic compounds. In the case of pure samples, the ratio A260 / 230 should be approximately 2.2.

2.11.2 DNA Agarose Gel Electrophoresis

To analyze restriction digests and quality of nucleic acid preparations horizontal agarose gel electrophoresis was performed. Gels are prepared by heating 0.8-1.5 % (w/v) agarose (Fisher, *electrophoresis grade*) in *Tris-acetate* buffer (TAE) and 5µl ethidium bromide from stock solution (10mg/ml) is added. Depending on the size of fragments to be separated DNA samples are adjusted to 1 x DNA sample buffer and are subjected to electrophoresis at 10 V/cm in BioRad gel chambers in 1 x TAE running buffer. Thermo-photographs of transilluminated gels are taken, or bands are made visible on an UV-screen (λ = 360 nm) and desired fragments are cut out with a fresh razor blade. Extraction of DNA fragments from agarose pieces is described in section 2.13.3.

2.11.3 Restriction digest of DNA

Restriction enzyme digestions is performed by incubating dsDNA molecules with an appropriate amount of restriction enzyme(s), the respective buffer as recommended by the supplier(s), and at the optimal temperature for the specific enzyme(s), usually at 37°C. In general, 20 µl digests are planned. For preparative restriction digests the reaction volume is scaled up to 100 µl. Digests are composed of DNA, 1 x restriction buffer, the appropriate number of units of the respective enzyme(s) (due to glycerol content the volume of the

enzyme(s) added should not exceed 1/10 of the digest volume), and the sufficient nuclease-free H_2O to bring the mix to the calculated volume. After incubation at the optimal temperature for a reasonable time period (mostly 2-3 hrs or overnight), digests are purified with the Qiagen MinElute reaction cleanup Kit. If reaction conditions of enzymes are incompatible to each other, DNA is digested successively with the individual enzymes. Between individual reactions, DNA is purified, as described above.

2.11.4 Sequencing of DNA

Sequence determination of dsDNA was performed by the sequencing facility of the University of Dundee, Sequencing Service, School of Life Sciences, MSI/WTB Complex in Scotland.

2.11.5 Maintenance of Plasmids

To maintain important plasmids, 10µl of each plasmid-Midi preparation is put 4 times on a Watmann Paper, circled with a pencil, and put into a folder together with a detailed vector map.

2.11.6 Precipitation of DNA

The salt concentration of an aqueous DNA solution is adjusted by adding 1/10 volume of sodium acetate, pH 5.2. After adding 2.5 volumes of cold ethanol (-20°C) the samples are mixed well. Following incubation on ice for 30 min, samples are centrifuged for 15 min (16000 x g, RT). For optimal purity, the pellet is loosened from the tube during inverting and broken up in ethanol. After removal of the supernatant, a quick 1-2s centrifugation step is performed and residual ethanol is aspirated. The supernatant removed and the DNA pellet air dried (approximately 5 min at RT). DNA is resuspended in an appropriate volume of water at room temperature.

2.11.7 Precipitation of RNA

To precipitate *in situ* RNA probes we use lithium chloride (LiCl) precipitation. It is a convenient and effective way to remove unincorporated nucleotides and most proteins. But lithium chloride precipitation does not precipitate transfer RNA and may not efficiently

precipitate RNAs smaller than 300 nucleotides. The concentration of RNA should be at least 0.1 µg/µl to assure efficient precipitation.

Protocol from the Ambion Megascript Kit:

1. Stop the reaction and precipitate the RNA by adding 30 µl Nuclease-free Water and 30µl LiCl Precipitation Solution.
2. Mix thoroughly. Chill for ≥30 min at –20°C.
3. Centrifuge at 4°C for 15 min at maximum speed to pellet the RNA.
4. Carefully remove the supernatant. Wash the pellet once with ~1 ml 70% ethanol, and re-centrifuge to maximize removal of unincorporated nucleotides.
5. Carefully remove the 70% ethanol, and resuspend the RNA in RNAse free water.
6. Determine the RNA concentration and store frozen at –20°C or –70°C.

2.12 Cloning in Plasmid Vectors

2.12.1 Preparation and Enzymatic Manipulation of Insert DNA

Three different kinds of insert DNA fragments were cloned (see item list below).

Plasmid DNA fragments. For cloning of distinct regions of plasmid DNA, donor molecules are digested with appropriate restriction enzyme(s). Even though direct ligation using DNA from inactivated restriction digest is possible, mostly complete digests are cleaned using the MinElute reaction cleanup kit by Qiagen. Sometimes the complete digests are put on an agarose gel electrophoresis, appropriate bands are cut out and DNA is eluted from agarose pieces, thus avoiding unwanted by-products during subsequent ligation reactions. Non complementary overhanging ends are converted to blunt ends prior to ligation using the Klenow enzyme.

Pfu DNA polymerase-derived products. Due to the 3´- 5´exonuclease activity, a major fraction of DNA species amplified with *PfuTurbo*-DNA polymerase does not contain an additional adenosine at the 3´-end. These products are directly cloned with vector DNA that is cut with enzymes generating blunt ends or subjected to Topo cloning. The Topo cloning technique utilizes the inherent biological activity of DNA topoisomerase I. The linear vector

DNA has the topoisomerase enzyme covalently attached to both of its free 3' ends. The enzyme will link the 5' end of the PCR fragment with the 3' end of the vector. Before ligating DNA from PCR reactions, DNA is cleaned up or DNA fragments are purified.

Taq DNA polymerase-derived products. PCR products amplified with Taq DNA Polymerase, HotStarTaqTM, or enzymes of the AdvantageTM product family DNA polymerases were directly subjected to TA cloning. The latter two products are actually mixtures that contain minor amounts of a proofreading polymerase, but TA cloning is still possible.

Converting a 5´-overhang to a blunt end terminus. Non compatible 5´-overhanging ends are blunted for ligation using Klenow enzyme (DNA polymerase I Large Fragment, Roche). 2U are directly added to a 20 µl heat-inactivated restriction digest complemented to a final concentration of 40 µM of each dNTP and incubated for 30 min at 37°C. The reaction is terminated by incubation at 70°C for 10 min and fragments are directly used for ligation reactions.

2.12.2 Enzymatic Manipulation of Vector DNA Prior to Cloning

When used as vectors, plasmids are digested at one locus either by a single restriction enzyme or by two at a multi-cloning site to achieve insertion of target DNA in a defined orientation. Digestion reactions are carried out as described under section 2.11.3 using 5-10 µg of plasmid DNA as starting material. When digestions are verified as complete and correct by agarose gel electrophoresis, complete restriction digests are subjected to preparative agarose gel electrophoresis and appropriate bands representing digested vectors are cut out and vector DNA is extracted from agarose pieces. To prevent self-circularization by DNA ligase, SAP buffer (Boehringer Ingelheim) and 1 U SAP (shrimp alkaline phosphatase) per 100 ng plasmid DNA are added to remove 5´-phosphates. The reaction is incubated at 37°C for 2 h and terminated by incubation at 70°C for 10 min. The plasmid DNA is used for ligation without further purification.

2.12.3 Ligation of Plasmid Vector and Insert DNA

Ligation of DNA fragments is performed by mixing 50 ng vector DNA with the fivefold molar excess of insert DNA. 1 µl of T4-Ligase and 2 µl of ligation buffer (Roche) are added

and the reaction mix is brought to a final volume of 20 µl. The reaction is incubated either for 2 h at room temperature (sticky ends) or overnight at 16°C (blunt ends). The reaction mixture is used directly for transformation without any further purification.

2.12.4 TA Cloning

TA cloning of PCR products is performed with the pGEM®-T vector. The pGEM®-T and pGEM®-T Easy Vectors by Promega have 3'-thymidine overhangs in the linearized form preventing recircularization of the vector and providing a compatible overhang for PCR products generated by specific thermostable polymerases. The vectors contain T7 and SP6 RNA polymerase promoters flanking a multiple cloning region.

Most of our PCR products for *in situ* probes are ligated into these vectors. In this context primers for the inserts are chosen, if possible, to result in a 1kb fragment. The length of 1kb fragments has two advantages. Firstly, 1kb fragments are convenient to amplify. Secondly, they meet the requirements for *in-situ* probe making which works better the longer the fragment is, but has to be at least 0.5 kb in size.

For the protocol we follow the manufacturer's instructions – but reduce the amount of vector from 1µl (as suggested) to 0.25µl, with very good results.

2.12.5 (Re-) Transformation of DNA into Bacteria

10 ng of plasmid DNA or 20 µl of a ligation mixture are added to 50/100 µl of competent XL1-Blue and incubated for 30 min on ice. After a heat shock (2 min, 42°C) and successive incubation on ice (3 min), 800 µl of LB-medium are added to the bacteria and incubated at 37°C for 30 min. Cells are then centrifuged (5000 x g, 1 min, RT) and the supernatant removed. Cells are resuspended in 100 µl LB medium and plated on LB plates containing the appropriate antibiotics. Colonies formed after incubation at 37°C for 12-16 h.

2.13 Purification of Nucleic Acids

2.13.1 Plasmid DNA Purification from Bacterial Cultures

5 ml LB/Amp-Medium (100 µg/ml ampicillin) are inoculated with a single colony and incubated over night at 37°C with constant agitation. Cultures are transferred into 2 ml Eppendorf tubes and cells are pelleted by centrifugation (12,000 rpm, 1min, RT). Plasmids are

isolated from the bacteria using the GFX *micro* plasmid prep system (Amersham), according to the manufacturer´s protocol. The DNA is eluted from the columns by addition of 50 µl ddH_2O with subsequent centrifugation (12,000 rpm, 2 min, RT). Plasmid DNA is stored at 20°C.

50ml bacterial cultures are used to rapidly obtain higher amounts of DNA, employing the HiSpeed Plasmid Midi Kit by Qiagen. 50 ml LB/Amp-Medium (100 µg/ml ampicillin) are inoculated with a single colony and incubated at 37°C with constant agitation over night. Cultures are transferred into 50 ml Falcon tubes and cells are pelleted by centrifugation (12,000 rpm, 1min, RT) in a 3k30-Sigma centrifuge. Plasmids are isolated from the bacteria according to the manufacturer´s protocol. DNA is eluted from the columns by adding 50 µl of H_2O with subsequent centrifugation (12,000 rpm, 2 min, RT) twice. Finally, the DNA concentration is determined as described in section 2.11.1.

2.13.2 PCR / DNA Fragment Purification

For purification of DNA fragments the silica-gel membrane based MinElute PCR Purification Kit by Qiagen is used according to the manufacturer´s protocol. The DNA is eluted from the column by addition of 10 to 20 µl of ddH_20. The DNA concentration is determined using the undiluted eluate.

2.13.3 DNA Fragment Extraction from Agarose Gels

For isolation and purification of DNA fragments from agarose gels, ethidiumbromide-stained gels are illuminated with UV-light and the appropriate DNA band is excised from the gel with a clean razor balde and transferred into an Eppendorf tube. The fragment is isolated utilizing the silica matrix-based QIAquick Gel Extraction kit (Qiagen) following the manufacturer´s protocol. The fragment is eluted from the column by addition of 50µl Tris-HCl (10 mM, pH 8.0). The DNA-concentration is determined using the undiluted eluate.

2.13.4 Total RNA Extraction from Zebrafish Tissue

Total RNA is purified from whole adult brains or retinas using the mirVana miRNA isolation kit by Ambion. The kit employs an organic extraction followed by immobilization of RNA on glass-fiber filters to purify either total RNA or RNA enriched for small species.

All buffers used are provided by the manufacturer. 5 adult zebrafish brains or retinas are quickly isolated and immediately put into 500µl of the provided lysis buffer. The tissue is homogenized by repeated pipetting of the mixture.
The total RNA is isolated following the manufacturer´s protocol. Finally, total RNA is eluted in 100µl RNAse free water (provided by the kit). The yield was approximately 200ng/µl for 5 brains and 350ng/µl for 5 retinas. Integrity of the purified total RNA is assessed by spectrophotometry using the NanoDrop® and gel electrophoresis using the Bioanalyzer®. Total RNA samples are stored at –80°C.

2.14 Nucleic Acid Amplification

The *in-vitro* amplification of DNA fragments using the polymerase chain reaction (PCR) is usually performed in a MJ mini gradient thermal cycler by Biorad. Routinely, PCR reactions are set up by adding the following ingredients to a 0.2 ml PCR tube: the template DNA (typically plasmid or first strand cDNA), the primers flanking the region to be amplified, dNTPs, buffer and DNA polymerase. Primer sequences are selected manually or electronically determined with the Primer Express 2.0 software programmed by AbiPrism™ (Applied Biosystems, CA, USA). Selected primer sequences are cross checked with the PrimerSelect software from the Lasergene software suite (DNASTAR inc. WI, USA). Routinely, 20-50 µl reactions are performed. The enzymes, which are used during these experiments, are as follows (in brackets typical PCR reactions are cited): (a) *Taq* DNA polymerase (“*general”* PCR reactions), (b) *PfuTurbo*® DNA polymerase (PCR to amplify DNA for further cloning steps).
Table 1 shows cycling parameters for the DNA polymerases (a). Number of cycles (25 up to 40) required for optimum amplification varies depending on the amount of starting material and the efficiency of each amplification step. In some experiments, a touchdown strategy (Don et al., 1991) was adopted. A final incubation step at the extension temperature ensures fully double stranded molecules from all nascent products. Following cycling, typically 5-10 µl aliquots up to complete reactions are analyzed by agarose gel electrophoresis to detect amplified products.

Step	a) *Taq* DNA Polymerase	
1	5 min	95°C
2	0.5 min	95°C
3	1 min	Primer melting temperature
4	1.5 min	72°C
5	Goto 2	25 – 40 times
6	4 min	72°C
7	For ever	4°C

Table 1: Protocol for a "standard" PCR reaction

2.15 Generating RNA by *in-vitro* Transcription

To generate *in-vitro* transcribed RNAs, 5-10 µg of plasmid DNA containing the desired insert and a T3, T7 or SP6 polymerase promotor are digested with restriction endonucleases overnight, at positions that are located 3´ of the designated RNA polymerase promoter and 3´of the strand of DNA to be transcribed. By doing this, the DNA polymerase transcribes only the strand of interest and no vector-specific sequences. Linearized DNA is purified using the MiniElute PCR purification kit according to manufacturers instructions (Qiagen). In order to obtain Digoxigenin (DIG) labeled RNA probes for *in-situ* hybridization, transcription of the desired templates is performed with Ambion´s Megascript system. For the generation of DIG-labeled RNAs, the DIG-UTP mix shown below is used instead of NTPs provided by the manufacturer.

DIG-UTP mix (10x)

10 mM	ATP
10 mM	CTP
10 mM	GTP
6.5 mM	UTP
3.5 mM	DIG-11-dUTP (Roche)

20 µl *in-vitro* transcriptions are essentially performed as recommended by the manufacturer. Generated mRNAs are purified by LiCl precipitation, analyzed on a denaturating agarose gel and stored at –80 °C.

2.16 First Strand Synthesis, Reverse Transcription, PCR

We use the SuperScript™ III Kit by Invitrogen to generate cDNA from extracted RNA.
The first strand synthesis is performed as given in the manufacturer's instructions.

1. Add the following components to a nuclease-free 0.5 or 0.2µl PCR tube:

1 µl random primers, 50ng/µl (reference: Oligonucleotides)
11µl RNA coming from previous RNA Extraction with Ambion mirVana Kit
1 µl 10 mM dNTP Mix (10 mM each dATP, dGTP, dCTP and dTTP at neutral pH)
Sterile, distilled water to get a reaction volume of 13 µl – if volume of added RNA is less than 11µl

2. Heat mixture to 65°C for 5 minutes and incubate on ice for at least 1 minute

3. Collect the contents of the tube by brief centrifugation and add the following (it is recommended to make a mastermix out of the following components):

4 µl 5X First-Strand Buffer
1 µl 0.1 M DTT
1 µl RNaseOUT™ Recombinant RNase Inhibitor
1 µl of SuperScript™ III RT (200 units/µl)

From step 4 on, reaction is carried out in a PCR machine, out of convenience reasons.

4. Mix by pipetting gently up and down. If using random primers, incubate tube at 25°C for 5 minutes

5. Incubate at 50°C for 60 minutes

6. Inactivate the reaction by heating at 70°C for 15 minutes

7. Add a "4°C forever" step at the end, if a PCR machine is used

First strand cDNA is stored at –20°C or directly subjected to PCR reactions (RT-PCR) as described in section 2.14.

2.17 Real Time PCR

The Real time PCR experiments are performed on an AbiPrism™ 7900 HT machine (Applied Biosystems, CA, USA). We use 96-well plates, SYBR Green and the program given by the manufacturer for the runs.

Pipetting protocol for one 20µl reaction:

10x buffer	2.20 µl
$MgCl_2$	1.54 µl
dNTP	0.88 µl
Water	14.56 µl
SYBR green	0.66 µl
Primer	1.50 µl
Template	0.55 µl
Enzyme	0.11 µl
	———
Σ	22 µl

The protocol is for a 20µl reaction volume – the higher end volume is used to account for pipetting errors.
96 well plates are sealed with the special cover foil and stored at 4°C, wrapped in aluminum foil until the run is performed.

2.18 Analysis of Nucleic Acids by Hybridization

2.18.1 RNA *in situ* Hybridization (ISH) on Cryosections

To obtain Digoxigenin (DIG)-labeled RNA sense and anti-sense probes specific for the 15 mRNAs (see appendix) identified in the microarray screen, parts of their ORF are amplified

and cloned into the pGEM-T Easy vector (Promega). The PCR amplicons are mostly 1kb long. Digoxigenin (DIG)-labeled RNA sense and antisense probes are then generated using the Megascript™ system (Ambion) according to the manufacturer´s instructions (see section 2.15).
To perform non-radioactive detection of mRNAs, 14 µm sections are cut from fresh-frozen tissue on a cryostat, mounted on glass slides, probed with a DIG-labeled RNA and visualized with a color substrate reacting on an enzyme bound to the tagged probe.

Day 1:

1. Cut sections in Cryostat and thawmount onto glass slides (Superfrost)

2. Place slide rack into 4 % paraformaldehyde (in PBS) overnight at 4°C

Day 2:

3. Wash slides 3 x 10 min. in PBS (1 x PBS)

4. Place racks into 70 % Ethanol (tech grade) for 10 min.
   - for immediate use keep at room temperature
   - alternatively, slides can be stored that way for several days at 4°C

5. Rinse slides in ddH_2O water, 2 x 10 min.

6. Place into 0.1 M HCl for 10 min.
   - 5 ml 37 % HCl in 500 ml ddH_2O water

7. Wash in 1 x PBS, 2 x for 10 min.

8. Place racks in well-mixed 200 ml 0.1 M triethanolamine (15 ml/1l, adjusted to pH 8.0 with HCl) and add 0.5 ml acetic acid anhydride (quickly added to triethanolamine just before placing the racks into the solution and dispersed with a small magnetic stir bar - always prepare solution fresh).

Incubate for 20 min.

9. Wash in 1 x PBS, 2 x 5 min.

10. Dehydrate in ascending gradient
    a.) 70 % Ethanol in ddH_2O water
    b.) 80 % Ethanol in ddH_2O water for 5 min each
    c.) 95 % Ethanol in ddH_2O water

11. Leave slides in rack and air dry

12. Label all slices with a pencil

13. Encircle sections on slide with a PAP-Pen to minimize volume of hybridization solutions

Prehybridization:

14. Prepare humid incubation chamber with filter paper
    (soaked with formamide/1 x PBS 1:1)

15. Place dried slides into chamber

16. Pipette onto each slide approx. 150 µl formamide/hybridization mix (1:1)

17. Hybridize at 37 °C for 3 hours

Hybridization:

18. Prepare hybridization mix with desired DIG-probe (1:250 to 1:1000)

19. Pour off hybridization mix for prehybridization just by tilting slide and drying the edge with a clean tissue

20. Quickly pipette onto each slide the hybridization mix (up to 50µl) and coverslip slides

21. Seal incubation chamber with parafilm and hybridize at 55 °C overnight

Day 3:

Washing:

TIP: Get three 0.5 l Schott bottles and fill one of them with 200ml and the second with 100ml formamide (pouring is the cleanest!). Now add the same amount of 0.2xSSC. The third one is filled only with 200ml 0.1xSSC. Place these 3 bottles in the 55°C hybridization oven first thing that day. Use these solutions to wash your slides, you will have the exact amount of liquid you need.

22. Remove incubation chamber from 55 °C

23. Place slides into rack after pouring off the hybridization mix

24. Wash in prewarmed 0.1 x SSC/50 % formamide (1:1) at 55 °C. 3 x 90 min
    (take 0.2 x SSC and add same volume 100% formamide – see TIP)

25. Immediately put racks into prewarmed 0.1 x SSC at 55°C, wash for 30 min

26. Rinse in 0.1 x SSC for 10 min. at room temperature

All following steps are carried out at room temperature!

Incubation with anti-DIG antibodies:

27. Equilibrate sections for 10 min. in Buffer 1

28. Block in modified Buffer 2 for at least 30 min.

29. Prepare incubation chamber with filter paper soaked with Buffer 1

30. Dry area around sections with Kleenex tissue and reapply PAP-Pen

31. Immediately after removing modified Buffer 2, place slides into chamber and add anti DIG-AP antibodies, diluted in modified Buffer 2. (1.2000 to 1:4000)

32. Seal chamber with tape and incubate at 4 °C overnight

Day 4

Development of hybridization signal:

33. Wash sections 2 x 15 min. in Buffer 1

33. Apply staining solution to sections for 5 min.

34. Prepare incubation chamber with Buffer 1
    Remove staining solution and immediately reapply fresh staining solution (color substrate buffer for alkaline phosphatase)

    Developing should be carried out in the dark

35. Stop development by pouring off staining solution from the sections and placing slides into 1 x PBS

36. Coverslip slides with Elvanol

Buffers for in situ hybridization

Hybridization Mix:	Dilution	Final Concentration	Volume
100 % deionized formamide	1:2	50 %	500 µl
10 x Grundmix	1:10	1 x	100 µl
5 M NaCl	1:15	0.33 M	66.7 µl
2 M DTT	1:20	0.1 M	50 µl
DEPC-H_2O	add to final volume minus dextran sulfate		
50 % dextran sulfate	1:5	10 %	200 µl

Add probe to achieve a final concentration of 30ng/100µl.

4 % Paraformaldehyde:

Dissolve 40 g of PA in 800 ml of Millipore Water
Add a few drops of 2N NaOH
Slowly heat to 60°C
Add 100 ml of 10 x PBS
Adjust pH 7.2 with conc. HCl
Add Millipore water to final volume of 1000ml
Solution should be stored at 4°C and be can used for 2 weeks.

10 x PBS (pH 7.4):

400 g NaCl
10 g KH_2HPO_4 x 2 H_2O
10 g KCl
fill up to 5L with ddH_2O water

10 x Grundmix (all solutions must be RNase free)

2 ml 1 M Tris/HCl pH 7.5
200 µl 0.5 M EDTA
2 ml 50X Denhardt´s solution (Sigma D 9905)
2 ml tRNA 25 mg/ml (Boehringer, Yeast tRNA 109525)
1 ml poly A RNA 10 mg/ml (Sigma P 9403)
2,8 ml DEPC-H_2O
Solution should be stored at –20 °C

Buffer 1

100 mM Trizma Base
150 mM NaCl
pH 7.5

Modified Buffer 2

1 % Blocking Reagent (Roche Diagnostics, Mannheim, Germany)
0.5 % BSA, Fraction V
Dissolve first the BSA under stirring in Buffer 1 at RT and add at 60 °C the Blocking Reagent, then cool down and store at –20 °.
Can be used several times.

Staining Solution:

BCIP / NBT Staining tablets (SigmaFast, B-5655) in 10ml dest.H_2O

2.18.2 Whole Mount *in situ* Hybridization

To detect the expression patterns of mRNAs in 16-24 hpf zebrafish embryos, non-radioactive whole mount *in situ* hybridization is performed.

Day 1:

1. Fix dechorionated embryos in 4% PFA ON (or 4h at RT)

Day 2:

2. wash 4 x in PBST (PBS + 0.1% Tween) for 5 min

3. wash in 25%, 50%, 75% methanol/PBST for 5 minutes at RT

4. fix in 100% methanol at -20°C for at least 2h

5. rehydrate embryos in 75%, 50%, 25% methanol/PBST and PBST for 5 minutes at RT

6. wash 2 x with PBST

7. bleach embryos with 1% H_2O_2 in PBT for 30 min

8. wash 2 x with PBST

9. digest embryos with ProteinaseK (10µg/ml in PBT) at 28°C:
   8 min for 24hpf embryos
   20 min for 36hpf embryos
   30 min for 48hpf embryos
   60 min for 72-96hpf embryos
   90 min for 5dpf embryos

10. wash 2 x in PBT 5 min

11. postfix in 4% PFA for 15 min

12. wash 5 x in PBST for 5 min

13. prehybridize embryos in hybridization buffer at 65°C for 1-3h

14. replace with hybridization buffer + probe (1µg/ml)

15. incubate 65°C ON

Day 3:

16. 1 x 20 min hybridization buffer 65°C (preheat the buffers)

17. 2 x 20 min 50% formamide in 2x SSCT (65°C)

18. 1 x 20 min 25% formamide in 2x SSCT (65°C)

19. 3 x 20 min 2x SSCT (65°C)

20. 3 x 30 min 0.2% SSCT

Now at RT:

21. block for 1h in Boehringer/Roche blocking reagent (1% in PBST)

22. add anti-DIG alkaline phosphatase coupled fab fragments (Roche)
    in blocking solution 1: 1000 at 4°C ON

Day 4:

23. wash 8 x in PBST for 15 min

24. wash in staining solution (10 ml H_2O plus one NBT/BCIP tablet; Sigma, B-5655) 5 min

25. replace by staining solution and incubate in the dark for 30 min to overnight

26. wash in PBS to stop reaction

27. clear embryos in an ascending gradient of glycerol 30%, 50% and 70 % glycerol in PBS

28. Remove the yolk sack, prepare slides with drops of vaseline as spacers and mount the embryos in 70% glycerol

Sense probes, developed in parallel under the same conditions as the anti-sense probes, did not show any labeling.

Solutions

PBST	PBS plus 0.1% Tween	
SSCT in DEPC-H_2O	SSC pus 0.1% Tween	
Hybridization buffer	5 ml	formamide
all solutions in DEPC-H_2O	2.5 ml	20xSSC
	10 µl	Tween
	100 µl	100mg/ml yeast RNA
	2.38 ml	DEPC-H_2O
	10 µl	50mg/ml heparin

2.19 Immunohistochemistry

2.19.1 Indirect Immunofluorescence on Sections

At the appropriate time point (9 and 20 days after insertion of the morpholino soaked gelfoam) fish are anaesthetized with MS222, perfused with 4% paraformaldehyde (PFA), eyes are removed and placed in 4% PFA over night. To perform indirect immunfluorescence eyes are embedded in 6% agar and cut in 50µm sections on a vibrating blade microtome.

1. Cut specimen into 50µm sections on vibrating blade microtome and place the sections in a 24-well plate filled with 1xPBS
2. in 1xPBS for 10 min.
3. 2 x 10 min. at room temperature in Mix1:
   0.1M glycine
   0.1% Tween
   TRIS-HCL pH 3.5
   → pH 2.2 with 1M HCL
4. 3 x 10 min rinse with PBS
5. Block 30 min with appropriate preimmune-serum at RT
6. Apply Anti-Fluorescein AP-coupled antibody (1:5000) at 4°C overnight
7. Wash 4 x with 1xPBS
8. Apply Staining solution NBT/BCIP at RT and incubate in the dark
9. Stop staining by washing 4 x with 1xPBS
10. Cover slip with Elvanol

2.19.2 Tracing and Visualizing the Optic Nerve

To visualize the optic projection, optic nerves are labeled with biocytin (Sigma, B-1758, 25mg) as previously described in section 2.20.2.1 (Becker, Meyer et al. 2000). To investigate the position of misguided optical axons in adult *astray*/*robo2* mutant fish we apply the tracer biocytin onto one optic nerve, which is cut directly behind the eye. Through the anterograde transport of the tracer all axons from one eye can be made visible.
To get applicable pieces of biocytin (Sigma-Aldrich), the lyophilized biocytin is dissolved in a few microliters of distilled water while it rests on a piece of parafilm. By adding very small fragments of Gelfoam the solution will be soaked up and dry onto the Gelfoam.

Chunks of approx. the diameter of the optic nerve are suitable for tracing.

After perfusion of the labeled fish, the brain is carefully removed, embedded in agar and cut in 50µm slices with a vibrating blade microtome.
To visualize the tracing the ABC method (section 2.19.2.3) is used. After sorting the sections in the right order on slides, these slides are counterstained with neutral red.

Every section is analyzed for the appearance of traced axon fibers by microscopic methods.

2.19.2.1 Biocytin Tracing of the Optic Nerve

Fish are anaesthetized in 0,033% aminobenzoic acid ethylmethylester (MS222, Sigma-Aldrich). The tracing procedure takes place with the fish resting on a metal surface cooled by ice.
After removal of the conjunctive tissue the eye is carefully rotated out of its socket and the opaque entire optic nerve cut under visual control using watchmaker's scissors and a suitable chunk of biocytin is placed directly on the severed nerve. After carefully sliding back the eye, the fish is put back for 2.5 hours in its tank.

2.19.2.2 Fixation of Traced Animals

After 2.5 hours these traced fish are sacrificed in 0.1% MS222 and perfused with a mixture of 2%Paraformaldeyde/2%Glutaraldehyde in PBS pH 7.3.
After an overnight fixation of these fish in 4% PFA the brains are carefully removed, embedded in 6% Agar and cut in 50µm sections on the vibrating blade microtome into a 24 well plate.
It is important to leave these sections after cutting in PBS at 4° Celsius over night.

2.19.2.3 Visualizing the Tracing: The ABC-Method

To visualize the tracing the Vectastain-ABC method by Vector Labs using the Vectastain Elite ABC-Kit PK-7200 is used.
This system exploits the fact that avidin has an extraordinary high affinity to biotin.

Protocol for ABC staining

Protocol for ABC staining of 2%PA/2%GA fixed zebrafish brain vibrating blade microtome sections after an over night 4°C incubation in PBS:

1. 0.5% H_2O_2 in PBS + Triton 0.1% for **20min**
2. in my case: 166µl 30% H_2O_2 in 10ml PBSTriton 0.1%
3. **mix** complex A+B – has to incubate for **30 min** prior use
   Complex A: 1:120 in PBSTriton 0.1% (vortex after adding)
   Complex B: 1:120 in PBSTriton 0.1% (vortex after adding)
   Don't vortex again!
4. 0.1% Glycine in PBS + Triton 0.1% for **20 min**
5. in my case: 10x Glycine stock solution (380mg in 10ml PBST) filtered sterile, can be kept at 4°C for 3 weeks!
6. 300µl Complex A+B solution per well for **90 min in the dark**
7. wash 2 times with PBSTriton 0.1%
8. wash once with PBS
9. prepare DAB 1:120 from 6% stock solution in PBS
   Always add 2µl/ml of $NiCl_2$ (1%) and 2µl/ml of $CoSO_4$ (1%) just before use. Heavy metal stock solutions can be kept at 4 °C after sterile filtration.
   e.g. 15ml DAB working solution:
   125µl 6% DAB + 14,815 µl PBS + 30µl $NiCl_2$ + 30µl $CoSO_4$
10. 500µl DAB working solution each well
11. incubate for **30 min at 4°C**
12. add 50µl/well 1:1000 H_2O_2 – mix together **just** before using
13. after reaction (1 – 5 min!) wash 2 times with PBS
14. keep at 4°C in PBS

Next step is to sort these sections in their correct order on slides and counterstain them.
The adhesion of the slides to sort these sections is important.
Slides coated with chrome alum-gelatine (see section 2.19.2.4) gave the best results.

2.19.2.4 Coating Slides and Counterstaining Sections

Solutions for coating slides with chrome alum-gelatine

Washing solution:

500ml 95% EtOH + 10ml 100% acetic acid

Chrome alum-gelatine solution:

1. 2,5g gelatine in 250ml dest. H_2O – warm to 50°C but DO NOT BOIL!
2. Let it cool down until hand warm
3. Add 0,13g potassium chromium (III) sulfate dodecahydrate (carefull! poisoning)

Good for 1-2 month

Protocol for coating slides

Use normal glass slides

1. put slides in glass rack
2. add washing solution and shake for 5 min
3. dry slides at 60-65°C in oven
4. add chrome alum-gelatine solution and shake 1 min
5. dry at 60-65°C in oven
6. repeat step 4. and 5. once

Solutions for staining

Neutral Red Staining solution:
4 ml acetate buffer (pH 4.8) + 100ml 1% neutral red in H_2O

Acetate buffer:
75ml 0.1N sodium-acetate + 50ml 0.1N acetic acid

Protocol for neutral red staining

1. 1 – 2 min in dest. H_2O
2. 6 min in neutral red staining solution
3. 2 times wash briefly in dest. H_2O
4. 2 - 5 min in 70% EtOH
5. 2 - 5 min in 95% EtOH
6. 2 times 15 sec in 100% acetone
7. 2 times 5 min in xylene

8. embed with Eukitt

2.20 Zebrafish

Adult (body length > 2 cm, age > 4 months) and developing zebrafish, *Danio rerio*, are taken from our breeding colony or bought at a fish breeder and raised according to standard protocols (Westerfield 1989). Prior to surgery, adult fish are kept in groups of 10 animals at a 14 hour light and 10 hour dark cycle, a temperature of 27°C and a high salt concentration of 1300µS. After surgery, fish are kept individually in two liter tanks. Fish are fed dried fish food and live brine shrimp. All animal experiments were approved by the British Home office.

2.20.1 Zebrafish Lines

We used wild type fish and homozygous *astray* mutants, which are adult viable, crossed with Brn3c:GFP (green fluorescent protein) transgenic fish to visualize the optic projection in living larvae (Hutson and Chien 2002).
To assess the presence of an ectopic projection to the telencephalon, larvae are checked 3 to 5 days post fertilization for strong projections to the telencephalon. Larvae are anaesthetized in 0.033% MS222 (Sigma) and the presence of fibers in the telencephalon is assessed in a stereo-microscope equipped with fluorescence detection (SV8, Zeiss, Germany). Subsequently they are sorted by the presence of misprojections to the telencephalon and returned to tank water and raised to adulthood (older than 3 month of age).
12 animals with strong projection were raised in the Becker lab and 19 animals by the Chi Bin lab.

2.20.2 Zebrafish Surgeries

2.20.2.1 Optic Nerve Lesions

For lesions of the optic nerves of adult zebrafish, individuals are anaesthetized by immersion in 0.033% aminobenzoic acid ethylmethylester (MS222, Sigma-Aldrich) for 3 minutes. The left eye is gently lifted from its socket and the exposed intraorbital nerve crushed or cut behind the eyeball under visual control using watchmaker's forceps or scissors as previously described (Becker, Meyer et al. 2000). A translucent stripe across the otherwise opaque optic

nerve at the site where the forceps have been applied indicates a successful crush of the nerve. A successful cut is indicated by a visible retraction of the nerve bundle separated from the eye. For the enucleation experiments, individuals are anaesthetized as described above and the left eye is removed using fine scissors. After surgery, gills are flushed with tank water by gently pulling the fish through the water. Fish resume breathing within a few seconds.

2.20.2.2 Spinal Cord Transection

Spinal cord transections are performed as described previously (Becker, Wullimann et al. 1997). Briefly, fish are anaesthetized, scales are removed from the flanks of the fish at the level of the spinal cord, a longitudinal incision is made and the vertebral column is exposed by pushing the muscle tissue aside. Then the vertebral column is cut with micro-scissors at a level halfway between the dorsal fin and the operculum, corresponding to the eighth vertebra. The wound is sealed with a drop of histoacryl (B. Braun Melsungen, Germany). After surgery, fish are revived as described above for optic nerve lesions.

2.20.3 Perturbation of Gene Expression by Morpholinos

2.20.3.1 Injection of Morpholino into Freshly Fertilized Eggs

The zebrafish offers the possibility to analyze the functions of genes during early development in vivo by injecting reagents directly into the freshly fertilized egg. Antisense oligonucleotides are widely used to inhibit the translation of proteins in a variety of model systems. The first antisense oligonucleotides like RNA and single-stranded DNA were derived from natural origins. Later developed oligonucleotides were chemically synthesized and several modifications were added to improve stability and specificity (Summerton and Weller 1997). Morpholino phosphorodiamidates, a new generation of antisense oligonucleotides which were originally developed for therapeutic approaches (Arora, Knapp et al. 2000) are the first viable sequence specific gene inactivation method in the zebrafish. Morpholinos are synthetic DNA analogues which contain a morpholine ring in lieu of the standard ribose sugar moiety and contain a neutral backbone. Morpholinos are very resistant to a variety of nucleases, they show a low toxicity and have a high affinity to RNA (Summerton et al., 1997). Morpholino phosphorodiamidates function in a RNAse H independent manner, which makes them different from other antisense oligonucleotides. A morpholino selected against the leader sequence or nearby bases of an mRNA can bind to it

and sterically inhibit scanning of the mRNA by the 40S ribosomal subunit (Ekker and Larson 2001). The efficacy of morpholinos is restricted to target sites within the leader and sequences surrounding the start codon (Summerton 1999), a bound morpholino does not appear capable of altering activity of the ribosomal complex once translation is initiated. Thus, only a small fraction of the transcribed RNA sequences bound by morpholinos within a cell will result in a deleterious effect on gene function.

A different possibility are splice site directed morpholinos. Morpholino oligonucleotides can block nuclear processing events, pre-mRNA processing in particular. The power of high specificity and steric blocking allows one to specifically and reproducibly delete exons of choice by blocking access of the splicing machinery to the pre-mRNA. This technology, not possible with RNase-dependent or RISCdependent oligonucleotides (phosphorothioates, RNAi and others), not only allows characterizing specific exon function and creating loss-of-function deletions or insertions but it also allows researchers to eliminate a specific splice variant while leaving another splice variant of the same gene intact. Many papers have now been published using morpholinos to block splicing by targeting exon-intron or intron-exon boundaries (Draper, Morcos et al. 2001).

Since protein synthesis of specific genes is not completely inhibited by morpholino application, the effect will be referred to as a *knockdown*.

To establish morpholino use in the zebrafish, phenotypes of known mutants such as no-tail (Schulte-Merker, van Eeden et al. 1994) were copied. The morpholinos were injected into fresh fertilized eggs and shown to phenocopy the mutations (Nasevicius and Ekker 2000). Morpholinos have been used with great success in many studies to gain information of gene function (Erter, Wilm et al. 2001; Solomon and Fritz 2002). They are also useful to analyze gene function in the fruit fly *Drosophila melanogaster*, the frog *Xenopus laevis* and in cell culture systems (Heasman 2002). Unspecific effects of morpholinos were also described (Nasevicius and Ekker 2000), these effects are due to hybridization of the morpholino to sequences similar to the target or are dose dependent (Ekker and Larson 2001).

300 nmol lyophilized morpholinos specific for *robo2* (see appendix for sequences) were delivered and resuspended in 41.5 µl Danieau solution to obtain a stock solution of 65ng/nl (8mM). The stock solutions were split in 3 µl aliquots and stored at –20°C. Morpholinos were adjusted with Danieau solution to obtain a concentration of 8ng/nl and were injected into 1-4 cell staged eggs as described below.

Morpholino injection:

Freshly fertilized eggs are harvested and disinfected with autoclaved fish water containing 0.02 % methylenblue (500µl/1Liter).
Eggs are washed three times with the treated fish water and arranged in a groove in a petri dish containing 2 % agarose. Usually 0.5 µl 5% rhodamine dextran (MW = 10000) are added to a 3 µl aliquot of morpholino solution to visualize the amount of injected liquid. A glass micropipette is filled with the solution by capillary forces and held by a micromanipulator. Morpholino is injected with a Microinjector (Narishige Intracel, Japan) directly into the yolk of 1-4 cell staged eggs. Finally, injected eggs are incubated in the autoclaved fish water plus methylenblue at 28.5°C until the desired developmental stage is reached and embryos are subjected to phenotypic analysis.

2.20.3.2 Using a Gelfoam Soaked with Morpholino

To influence gene translation in adults, especially in the regeneration of the optic nerve, a new method for specific morpholino delivery is used. To transport the morpholino specifically into the RGC layer the method by Goldmann (Veldman, Bemben et al. 2007) is used, who himself adapted this method from a spinal cord lesion paradigm by the Becker lab using a morpholino soaked gelfoam.
Immediately after a transection of the optic nerve (without damaging the blood vessels supplying the eye!) directly behind the eye, a piece of Gelfoam soaked with a defined amount of morpholino is placed on the nerve stump and the eye is carefully put back into its socket. Detailed description of the operation to be found in section: 2.20.2.1

Protocol for the preparation of morpholino soaked Gelfoam pieces:

1. place a small Petri dish (35 x 10 mm) onto a piece of Parafilm and circle with a marker around the dish
2. cut a round piece of Parafilm and place it in the Petri dish
3. place a small chunk of Gelfoam into that Petri dish
4. use the watchmaker's forceps to tear pieces (one for each operation; plus one extra as a backup) off the Gelfoam chunk which have approx. the diameter of the optic nerve – chunks will shrink a bit when solution is soaked up – and remove the remaining big chunk from the Petri dish

5. prepare the morpholino dilution (in my case: 8,16 and 32µg/µl) in Danieau solution
6. pipette 1µl drops of diluted morpholino solution next to each Gelfoam piece in the Petri dish onto the Parafilm
7. carefully pull each Gelfoam piece into its morpholino drop and let it soak up the liquid (Tip: use a pen to make a small dot next to the soaked up Gelfoam – they are hard to see once they are dried up)
8. after 1 or 2 minutes the soaked Gelfoam piece dries up and is ready to be placed on the nerve stump behind the eye (they are easier to handle if they are still a bit wet)

All soaked Gelfoams were used and none stored.

2.21 Decision Criteria for Scoring Phenotypical Errors

Overall we analyzed 26 wild type and 30 mutant fish. The brains of these were cut into 50µm sections and mounted in anatomically correct order on slides. Every section was investigated starting at the very first section of the telencephalon and finishing with the beginning of the brainstem.
Appearing errors are assigned to 4 groups (A to D) and each brain was screened thoroughly for such errors.

These 4 groups are:

A) Anterior posterior errors: Ectopic optic tracts in the telencephalon and the tegmentum
B) Termination errors: Diffuse innervation of pretectal targets and increased depth of optic fiber receiving layer in the tectum
C) Crossing Errors: Crossing in posterior commissure, ipsilateral innervation of the tectum, gaps in the contralateral innervation of the tectum and ipsilateral fibers at the chiasm
D) Irregular growth into tectum: Defasciculation of dorsal optic tract and fascicles of optic fibers below optic fiber receiving layer in the tectum

Group A

Criteria of ectopic optic tracts in the telencephalon:

If optic tracts in one of the telencephalic sections could be observed, the animal was marked positive for telencephalic projection errors. No positive marking was given if one single optic fiber was observed (which was very rare).

Criteria of ectopic optic tracts in the tegmentum:

If ectopic tracts in the tegmentum could be observed, the animal was marked positive for tegmental projection errors. The error would manifest itself always with a misguided tract terminating in the optic fiber receiving layer.

Group B

Criteria of diffuse innervation of pretectal targets:

We chose to investigate the central pretectal nucleus (CPN), the periventricular pretectal nucleus (PPd) and the ventrolateral thalamic nucleus (VL) as pretectal targets. They are situated dorsal of the chiasm, below the very rostral part of the tectum. In wild type fish these targets are discrete termination zones, having a clear boundary. An error is recorded if these termination zones do not have a distinct border (see for example Figure 21). Sometimes they were even not recognizable as termination zones at all and looked like regions where lots of axons are passing through.

Criteria of increased depth of optic fiber receiving layer in the tectum:

The thickness of the fiber receiving layer was always measured at the plane of section of the oculomotorius, under a 45 degree angle from the midline, perpendicular to the innervated layers. The calculated mean thicknesses were compared between wild type (always around 48µm) and *astray* (always around 92µm) animals.

Group C

Criteria of crossing at the posterior commissure (PC):

An animal was scored if at least 2 axonal profiles were detectable in the PC per section.

Criteria of ipsilateral innervation of the tectum / gaps in the contralateral innervation:

If ocular dominance column like structures are visible, the animal will be marked as positive

for a contralateral error if a gap in the traced fiber receiving layer can be observed. Is a dark column on the otherwise untraced tectal half visible an ipsilateral error will be recorded.

Criteria for ipsilateral fibers at the optic chiasm:
All optic fibers, with the exception of one or two fibers, cross at the chiasm in zebrafish. Since one or two can be seen regularly in wild type fish, an error is scored if 3 or more fibers could be observed.

Group D
Criteria for defasciculation of the dorsal optic tract:
To reach the tectal zone at this anatomical position optic fibers normally avoid the cell dense area (represented by violet staining in Figure 25, section 3.3.2.4). A defasciculation is marked by ectopic tracts crossing through the cell dense area. It often looks as if these tracts sprout from the PPd – an extratectal termination point – sending axon fascicles directly into the tectum (see Figure 25, right panel, section 3.3.2.4).

Criteria for fascicles of optic fibers that ectopically grow below the optic fiber receiving layer in the tectum:
The optic fiber receiving layer in the tectum appears as a solid layer, the Stratum Fibrosum et Griseum Superficiale (SFGS). If fibers of passage, which run straight and parallel, were visible in the Stratum Album Centrale layer (SAC), which is below the SFGS and Stratum Griseum Centrale layer (SGC), the animal was scored as positive for this phenotype.

2.22 Micro-Array Chips

2.22.1 Chip Designs

To investigate gene regulation in a specific tissue at a specific time point we decided to use DNA microarray chips.

2.22.1.1 The “Faber Chip”

In order to study gene expression in zebrafish we started off with a 65-mer oligonucleotide DNA microarray chip printed at the Kimmel Cancer Center (www.kimmelcancercenter.org/kcc/kccnew/research/resources/zebrafish/index.htm) (Thomas

Jefferson University) comprising more than 16,000 unique transcripts from the Zebrafish oligo library from Compugen/Sigma-Genosys. Since only one Faber Chip was tested results could not be statistically verified but some results were verified through realtime PCR.

2.22.1.2 The Affymetrix Chips

By using GeneChip® microarrays from Affymetrix each of our microarray experiments could be compared with each other due to the standardized manufacturing techniques. These chips consist of small DNA fragments chemically synthesized at specific locations on a coated quartz surface.

Array manufacturing:

The photolithographic process begins by coating a 5″ x 5″ quartz wafer with a light-sensitive chemical compound that prevents coupling between the wafer and the first nucleotide of the DNA probe being created. Lithographic masks are used to either block or transmit light onto specific locations of the wafer surface. The surface is then flooded with a solution containing either adenine, thymine, cytosine, or guanine, and coupling occurs only in those regions on the glass that have been deprotected through illumination.

The coupled nucleotide also bears a light-sensitive protecting group, so the cycle can be repeated. In this way, the microarray is built as the probes are synthesized through repeated cycles of deprotection and coupling. The process is repeated until the probes reach their full length, usually 25 nucleotides.

Probe Design

Every probe on an Affymetrix microarray is designed to determine whether or not the complementary sequence of RNA or DNA is present in the sample. Usually 25 nucleotides in length (25-mer), Affymetrix probes have high specificity and are designed to reject targets that are not identical. Just as the 25-mer probe length confers high specificity, the use of multiple probes provides for high sensitivity and reproducibility; 22 probes are routinely used for each expression measurement. For each probe on the array that perfectly matches its target sequence, Affymetrix also builds a paired “mismatch” probe. The mismatch probe contains a single mismatch located directly in the middle of the 25-base probe sequence. While the perfect match probe provides measurable fluorescence when sample binds to it, the paired

mismatch probe is used to detect and eliminate any false or contaminating fluorescence within that measurement. The mismatch probe serves as an internal control for its perfect match partner because it hybridizes to nonspecific sequences about as effectively as its counterpart, allowing spurious signals, from cross hybridization for example, to be efficiently quantified and subtracted from a gene expression measurement or genotype call.

Probe Selection

For each transcript or DNA sequence to be interrogated, 16 pairs of probes are selected from the 3' end of each gene that uniquely represent that sequence or transcript.

Zebrafish GeneChip design

Approximately 14.900 transcripts can be tested with a Zebrafish GeneChip spotted with approx. 15.600 probes. Sequence information for the GeneChip Zebrafish Genome Array was selected from the following public data sources: RefSeq (July 2003), GenBank® (release 136.0, June 2003), dbEST (July 2003), and UniGene (Build 54, June 2003). Oligonucleotide probes complementary to each corresponding sequence are synthesized *in situ* on the arrays.

2.22.2 Gene Expression Profiling on Retina Tissue

To detect genes associated with successful CNS regeneration, we perform expression profiling of retinal mRNAs using Affymetrix micro-array chips covering approximately 14.900 transcripts.

After crushing the optic nerve directly behind the eye, animals are given the chance to regenerate their optic nerve for 6 hours, 12 hours and 11 days.

At each time point the retina from the lesioned eye is removed, its RNA extracted and sent off for being tested on an Affymetrix GeneChip.

For every time points post-lesion mRNA expression profiles are established. Each profile is tested with three individual chips, testing a total of 12 chips. The software "GeneSpring" is used to analyze these chips. To get statistical significant results a p-value of 0.05 is chosen and a gene regulation "fold change", which has to be at least 2 fold up or down.

It is essential to do the statistical analysis of variance (ANOVA) testing which variance is bigger, either the one between groups or the variance inside groups. To do this one can calculate a p-value. If $p = 0.05$ or less, there is a 95% chance that there is a statistical significant difference between two groups, hence a gene is significantly differently expressed

between e.g. the 0 hour and the 6 hour time point. The method of choice for filtering this data set is ANOVA. ANOVA assumes a normally distributed data set, even though it is generally quite robust to departures from normality (Ayroles and Gibson 2006). Hence, to get a more normally distributed data set, the raw intensity data from the chip had to be converted to a logarithmic scale with the base of 2.

3 Results

3.1 Micro-Arrays

3.1.1 Tissue Selection and Preparation for Chips

Retinal tissue was used for the microarray chips to investigate potential changes in gene expression in RGCs after a lesion of the optic nerve. Tissue was collected after a crush or cut of the optic nerve of adult zebrafish. For each chip, 10 retinae were extracted from anaesthetized fish - one eye per fish. The idea was to minimize potential variation between individuals by combining tissue from a large number of fish. Three different regeneration time points were chosen to collect the eyes (6 hours, 12 hours and 11 days after the lesion). The 6 hour time point was chosen to look for stress related and immediate early genes. The 12 hour time point was chosen to see, how many genes would overlap regarding their regulation between 6 and 12 hours post lesion. The 11 day time point was chosen, because axons would actively grow and pathfind, allowing us to look for growth and pathfinding related genes. In comparison to the 6 and 12 hour time point on which nothing has been published yet, there was literature available for gene profiling from 2 – 11 days (Cameron, Gentile et al. 2005; Veldman, Bemben et al. 2007) post lesion of regenerating CNS axons in fish. This gave us the possibility to compare our results with already published data to support the feasibility of the experimental approach.

Each eye was dissected at the specified time, and the retina removed and used for RNA extraction (see section 2.13.3). Then the RNA was instantly deep frozen at -80°C, and shipped with dry ice to the microarray facility (University of Pennsylvania or Rutgers University, New Jersey).

3.1.2 Trial Version with “Faber Chip”

Unsure whether we would be able to observe differences in gene expression in RGCs by taking whole retina samples, a test run with the “Faber chip” was performed. The “Faber Chip” was made at the Kimmel Cancer Center Microarray Facility, University of Pennsylvania (see supplementary list in section 5.5). Since only one Faber Chip was tested, the results could not be statistically verified. Some genes however, were verified by real time

PCR showing that by extracting the RNA from the whole retina valid results could be obtained. For example, our results confirmed previous observations of the upregulation of GAP-43 by Bormann (Bormann, Zumsteg et al. 1998) and Thy-1 by Deininger (Deininger, Rajendran et al. 2003) in RGCs with regenerating axons. GAP-43 was upregulated 16-fold and Thy-1 3-fold in the Faber chip experiment.

3.1.3 Affymetrix Microarray Chips

3.1.3.1 Chip Design and Grading

The encouraging results from the "Faber Chip" prompted the decision to perform a full experiment using microarray chips. Affymetrix microarrays for zebrafish seemed the best choice at the time, with high numbers of spotted transcripts and industrial manufacturing promising reproducible results. These chips carry approximately 15.600 probe sets equivalent to approximately 14.900 zebrafish transcripts. For each time point 3 biological replicates were prepared and tested on individual chips.
Testing such a large number of genes will, without multiplicity adjustments, lead to many false positive results. The software "GeneSpring", used to analyze our chip results, employs multiplicity adjustments such as Bonferroni or Benjamini and Hochberg. The statistical analysis of variance (ANOVA) was employed (see section 2.22.2.).

The different probe sets spotted on the Zebrafish Affymetrix chip are not all perfect matching probes. To distinguish the quality of the probe sets, Affymetrix sorts the probes on the chip in 4 categories, ranging from precisely matching probes (Grade A) to probes for which no transcript could be found and only an expressed sequence tag (EST) is known as yet (Grade E). 51% of the probe sets are Grade A compared to 32% of Grade E (see Table 2). Further sequencing efforts on the zebrafish genome will provide more accurate information transforming some E-graded probes to A-graded ones. An overview of grades on the chip is given in table 2. A short explanation of the different grades is given below, taken from an Affymetrix publication to be found on the Affymetrix website (http://www.affymetrix.com/support/technical/whitepapers/Transcript_Assignment_whitepaper.pdf).
Matching Probe (Grade A) probe sets have nine or more probes matching a transcript mRNA or gene model sequence. Genome *Target-Transcript Overlap* (Grade B) transcript assignments have a partial overlap between the transcript and the target sequence. Genome

Consensus-Transcript Overlap (Grade C) transcript assignments result when the transcript sequence overlaps the consensus, without overlapping a significant portion of the target. Overlap transcript assignments must be substantiated by a correspondence to the genome. The letter D is not used. If no transcript is found, then EST-only data described through a UniGene EST cluster are given a Grade E (EST record) assignment. If no UniGene EST cluster is built for that probe set, then the representative sequence IDs from the original design record are designated with a "minus".

While, looking at Table 2 it is obvious that only 51% of all probe sets are A-graded, it is however surprising to note that over 40% (taking E-graded and "minus"-graded together) are spots with no information so far. Taking this into account, we looked at the grading of our regulated genes ensuring they consisted of a high percentage of A-graded spots (Table 3). These numbers suggested that a high percentage of identified genes were A-graded spots and by that providing solid information for a high percentage of them, helping us to evaluate our experimental outcome. On the other hand, working on the idea to identify currently unknown genes involved in regeneration, we decided not to exclude the E-graded spots.

Letters and symbols used for grading	Probes	% of probes
Total number of letter: A	7916	50.7
Total number of letter: B	872	5.6
Total number of letter: C	319	2.0
Total number of letter: E	4989	31.9
Total number of probes marked with a: -	1521	9.7
All probes	15617	100

Table 2: Grading given to all spots on the zebrafish Affymetrix chip

Spots were filtered by an ANOVA process with p = 0.05 and a twofold cut-off. After that statistical procedure 94 genes at 6hours, 193 genes at 12 hours and 113 genes at 11days post lesion remained as regulated. The number of A-graded probes varied between 51% and 73% and none was marked with a minus, even though no UniGene EST cluster is built for nearly 10% of all probes on the chip (Table 2). Furthermore it can be seen in Table 3 that for 23% - 47% of the regulated spots only an EST is known so far, implying that a substantial amount of genes is still unknown but involved in the regeneration of the optic nerve.

	Number of probes per grade-group		
	6 hours (n = 93)	12hours (n = 193)	11days (n = 113)
Grade A	69 (73%)	99 (51%)	71 (63%)
Grade B	3 (3%)	3 (2%)	3 (3%)
Grade C	0	0	1 (1%)
Grade E	22 (23%)	91 (47%)	38 (33%)
Grade -	0	0	0

Table 3: Regulated spots split up into grade groups

The Venn Diagram

Having identified these genes as regulated, our first idea was to see how many identical genes would be regulated at different time points. By drawing a Venn diagram (see Figure 6) it became clear, that only very few genes overlap between the different time points (6 hours, 12 hours and 11 days) even though 6 hours and 12 hours are relatively close on a time scale. Only 16 genes were similarly regulated at 6 hours and 12 hours post-lesion, and only 10 genes were found to be commonly regulated comparing 12 hours and 11days post-lesion.

The 2 probes overlapping at all time points are transcribed loci in the genome but are unfortunately not yet annotated. The 16 genes overlapping at the 6 hours and 12 hours time points are not from one functional group but fall into different functional groups, such as transcription factor activity, visual perception, biosynthesis, etc.

Nothing is known about 8 of the 10 genes common to both the 12 hours and 11 days time points using the gene ontology database. The remaining 2 are found in the circadian rhythm and the visual perception group.

Due to limited information concerning these overlapping genes, only a careful interpretation of these results is possible. The observation of only so few identical genes being upregulated at 6 hours as well as at 12 hours post-lesion is somehow surprising, since the composition of functional groups being regulated is different between 6 hours and 12 hours (see Figure 7) but not as drastic compared with the overlap of single genes. One explanation could be that the function needed at these specific time points is executed by different genes, creating a minimal overlap in genes but not in functions.

Judging the two genes which are regulated at all time points is difficult, only knowing that they are transcribed loci. Further analysis using the "blast" software tool on the PubMed webpage did also not lead to satisfying results. Judging their regulation pattern, upregulated at all three time points, and knowing of the very specific actions needed for regeneration, could classify them as a byproduct of tissue damage, reflected e.g. in upregulated metabolism.
The very limited information about the 10 overlapping genes between the 12 hour and 11days time points only allows suggestions. Genes which are regulated not at 6 hours post-lesion but later might not have "immediate early" characteristics or an immediate stress response but would more likely fall into e.g. axon elongation or pathfinding.

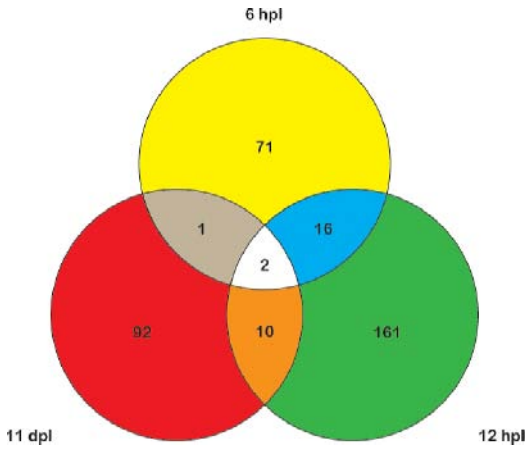

Figure 6: Venn diagram showing the minimal overlapping of regulated genes at all three time points after lesion (6 hours, 12 hours and 11 days).

3.1.4 Array Data Sorted into Functional Categories

Due to the annotation of the zebrafish genome (sixth assembly, Zv6) and computer calculated transcripts for the Affymetrix chip (with no update since July 2003), which did not always align with an annotated gene, we had to verify all of the statistically significant hits against the annotated genome to exclude artifacts. Using that information and the GO (gene ontology) annotations every identified gene could be sorted into one of the following 8 functional categories: **Transcription factors**, **signaling**, **axon guidance**, **clock/photoreceptor**, **cytoskeleton**, **differentiation**, **regulation of translation** and **stress/repair/metabolism**.
We found a significant increase in expression of 90 genes at 6 hours, 189 genes at 12 hours and 105 genes at 11 days post-lesion. The largest group of identified genes showing increased expression was related to stress at 6 hours, to signaling at 12 hours and to the cytoskeleton at 11 days post-lesion, when axons were actually growing (see Figure 7).

a) 6 hours post lesion

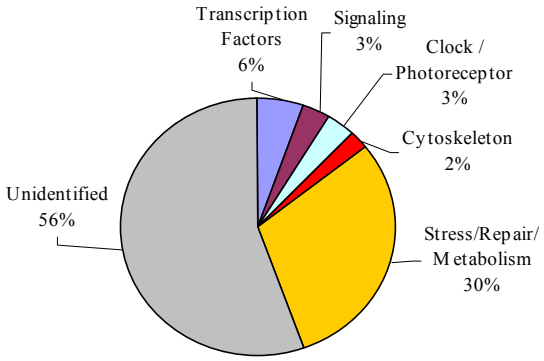

b) 12 hours post lesion

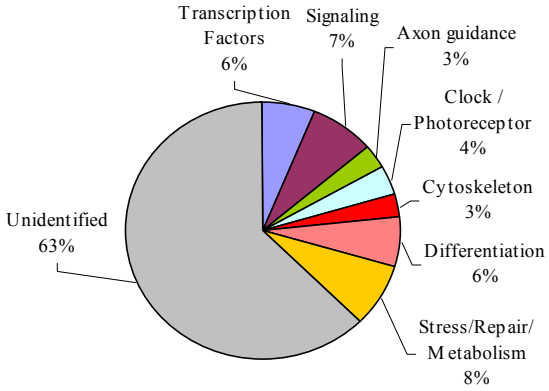

c) 11 days post lesion

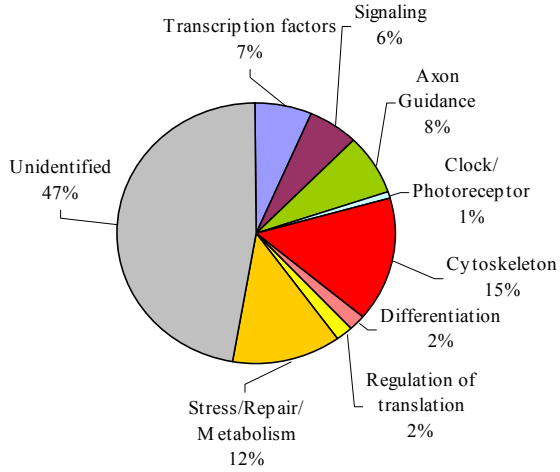

Explanations for categories:

- Transcription factor: Genes that code for proteins that bind to regulatory regions and control gene expression
- Signaling: Intra- and extracellular signaling molecules
- Axon guidance: Cell surface molecules potentially involved in axon guidance
- Clock / Photoreceptor: Molecules in photoreceptors, some of which are involved in the day/night cycle control
- Cytoskeleton: Includes cytoskeletal genes and those that interact with the cytoskeleton
- Differentiation: Genes involved in cell fate and development
- Regulation of Translation: Influence translation
- Stress/Repair/Metabolism: These genes represent acute responses to injury

Figure 7: Graphical display of regulated genes sorted in catagories after an optic nerve crush at three different time points: 6 hours, 12 hours and 11days.

Every time point had specific categories which are mainly regulated, e.g. at 6 hpl 30% of the regulated genes belong to the stress/repair/metabolism group, whereas at 12 hpl this group only represented 8% of the regulated genes.

At 12 hpl the group of axon guidance genes, which was not detectable at 6 hours at all, increased to 3%.

Looking at 11dpl the amount of axon guidance genes increased further to 8% and the group of cytoskeleton related genes reached 15%, compared to 2% at 6 hours and 3% and 12 hours. The 4 most strongly regulated functional groups, judged by the highest change in percentage (see Figure 7) comparing the 6 hour time point and the 11 days time point, were arranged graphically in Figure 8 below to show their development over the three time points.

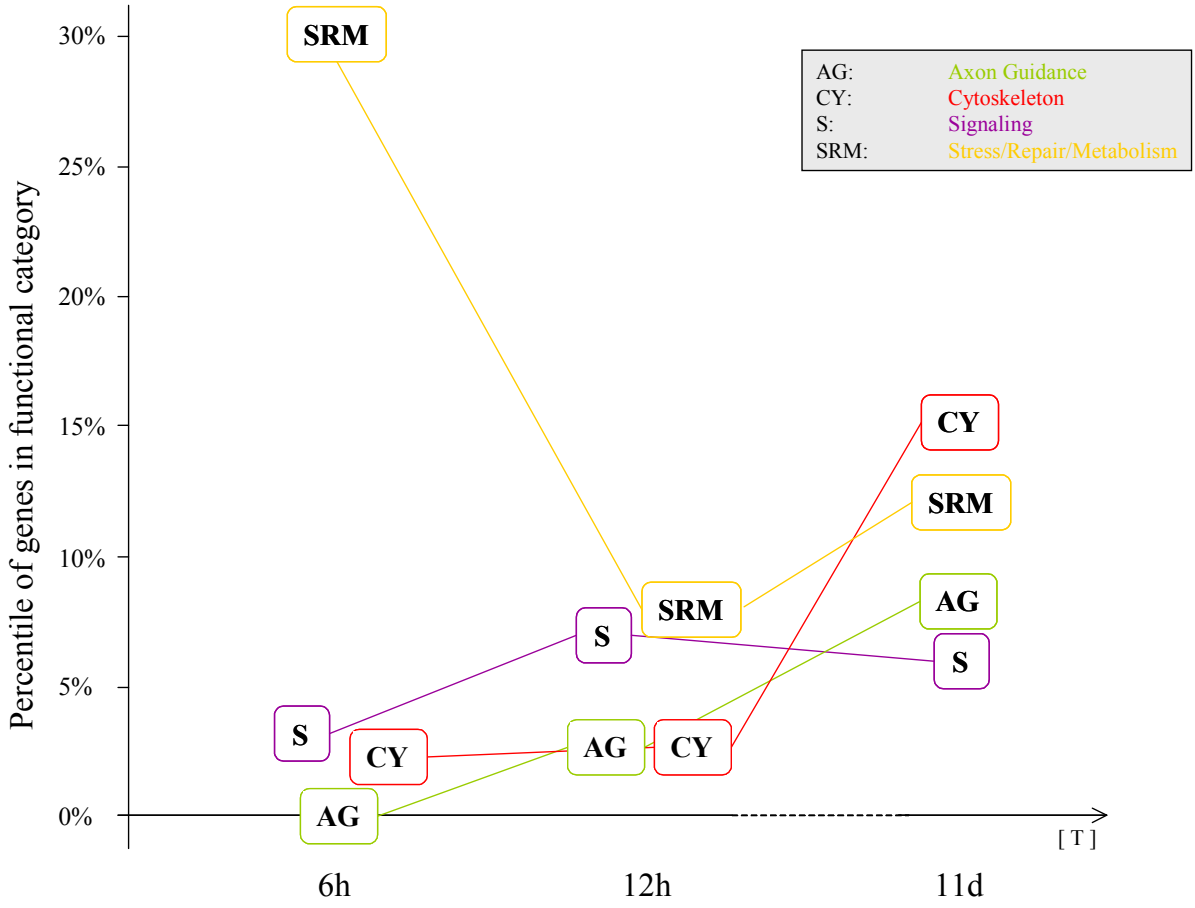

Figure 8: Changes in the percentage of genes belonging to the 4 most strongly, comparing 6 hpl and 11 dpl, regulated ontological groups (axon guidance, cytoskeleton, signaling and stress/repair/metabolism) at the three time points after the optic nerve lesions

Some of the regulated genes found to be up-regulated at the 11day post lesion time point had already been described in the literature, e.g.: Thy-1 (Deininger, Rajendran et al. 2003), Gap-43 (Bormann, Zumsteg et al. 1998) and Gefiltin (Asch, Leake et al. 1998).

Description	Gene Name	Fold Change	Previously reported in nerve injury models
Thymosin, beta	Dr.19380.1.S1_at	25,39	RGCs, zebrafish (Roth et al., 1999)
Thy-1	Dr.20019.1.S1_at	17,99	RGCs, zebrafish (Stuermer et al., 2004)
GAP 43	Dr.92.1.A1_at	14,72	RGCs, zebrafish (Bormann et al., 1998); RGCs,rat (Doster et al., 1991)
Tubulin, beta 5	Dr.4416.3.A1_at	14,43	
Sox 11b	Dr.5112.1.S3_at	8,115	RGCs, zebrafish (Goldman et al., 2007); DRGs, mouse (Tanabe et al., 2003)
Plasticin	Dr.263.2.S1_x_at	7,956	RGCs, zebrafish (Asch et al., 1998); SMNs, rat (Troy et al., 1990)
ATF 3	Dr.14282.1.S1_at	7,805	RGCs, rat (Takeda et al., 2000); DRGs, rat (Tsujino et al., 2000)
Uchl 1	Dr.8724.1.S1_at	6,112	
Sulfatase 2	Dr.12717.1.S1_at	5,196	
Tubulin, alpha 8 like 3	Dr.20214.1.A1_at	5,135	
Gefiltin	Dr.264.1.S1_at	4,873	RGCs, zebrafish (Asch et al., 1998)
Tubulin beta, III	Dr.7928.1.A1_at	4,349	
Adcyap 1b	Dr.10739.2.S1_a_at	4,126	
MARCKS	Dr.3153.1.A1_at	3,923	MNs, rat (McNamara et al., 2000)
junction plakoglobin	Dr.25119.1.S1_s_at	3,274	
Galectin 1-like 2	Dr.13015.1.S1_at	3,113	
CRMP 5a (dpysl 5a)	Dr.21550.1.S1_at	2,929	
ALCAM/Neurolin	Dr.20912.1.S2_at	2,886	RGCs, goldfish (Stuermer at al., 1992)
ICAT	Dr.1102.1.S1_at	2,763	
FABP 3	Dr.6814.1.S1_at	2,738	
jun	Dr.7608.1.A1_at	2,554	RGCs, zebrafish (Goldman et al., 2007)
Mibp 2	Dr.781.1.S1_at	2,51	
Ppia	Dr.9654.1.A1_at	2,507	
CRMP 4 (dpysl 3)	Dr.16753.2.A1_at	2,435	DRGs, chick (Yazan et al., 2007)
Caspase 3	Dr.4796.1.A1_at	2,359	
HuD	Dr.424.1.S1_at	2,321	
Tubulin, alpha 2	Dr.26381.1.A1_at	2,277	
Reticulon 1	Dr.4188.2.S1_at	2,199	
Eef2l	Dr.908.1.S1_at	2,147	
Acsl 4	Dr.16391.1.A1_at	2,125	
Selenoprotein W1	Dr.10201.1.S1_at	2,084	
Aanat 2	Dr.8142.1.S1_at	2,083	
CD9912	Dr.25120.3.S1_at	2,066	
Fibronectin 1	Dr.19965.1.S1_at	2,038	
Sox 11a	Dr.4763.3.S1_at	2,03	RGCs, zebrafish (Goldman et al., 2007)

Table 4: Table of the most strongly regulated annotated genes at 11days post lesion. DRG: Dorsal Root Ganglion; MN: Motor Neuron; RGC: Retina Ganglion Cell; SMN: Spinal Motor Neuron

The complete list of regulated genes is depicted in the appendix (section 5.6). Since no data for 6 hours and 12 hours after a CNS lesion in zebrafish has been published to date, no regulated genes for comparison with our gathered data was available.

The analysis revealed a regeneration-specific time course of gene regulation after injury in the zebrafish retina. Most interesting for this analysis were the RGCs, capable of axon regrowth in vivo, which are part of the retina. Hence, some potentially interesting genes were chosen from the list (see appendix 5.6) to be cloned and tested by *in situ* hybridizations to confirm their regulation and determine the cell type in which these genes were up-regulated.

Our main focus was axon growth, differentiation and transcription factors while still including other (internal group decisions based on literature and database research) genes with different functions. The final decisions were made, taking function, biological relevance and regulational strength into account. The list of these chosen genes is set out in Table 4.

	Name	Fold Change	Gene Name	Baseline Raw Data	Regulated Raw data	Function	Cloned in Vector	In-situ probe
6 hours post lesion	**Thra**	3,3	Dr.454.1.S1_at	64	205	TF	Yes	Yes
	Her 4.2	2,4	Dr.5372.7.A1_at	14	34	TF	Yes	Yes
	Wnt-7b	4,4	Dr.22588.1.A1_at	23	101	S	Yes	Yes
	Ndrg1l	0,4	Dr.8090.1.A1_at	251	108	S	Yes	Yes
12 hours post lesion	**Tf12**	5,3	Dr.10346.1.S1_at	14	89	TF	Yes	Yes
	Nf1	5,3	Dr.15268.1.A1_at	178	958	TF	Yes	Yes
	Lim-only	2,9	Dr.18163.2.S1_at	26	76	TF	Yes	Yes
	Sp5	2,7	Dr.23472.1.S1_at	13	22	TF	Yes	Yes
	Vsx1	2,7	Dr.558.1.S1_at	185	489	TF	Yes	Yes
	close to plexin B3	2,1	Dr.22796.1.A1_at	95	196	AG	Yes	Yes
	Aanat 2	13,6	Dr.8142.1.S1_at	37	459	CP	Yes	Yes
	Bmpr1a	8,1	Dr.8154.1.S1_at	18	150	D	Yes	Yes
	Thra	4,1	Dr.454.1.S1_at	64	282	D	Yes	Yes
	Ndrg1l	3,9	Dr.8090.1.A1_at	251	992	D	Yes	Yes
	Rx3	2,6	Dr.540.1.S1_at	48	122	D	Yes	Yes
11 days post lesion	**CRMP-5a**	2,9	Dr.21550.1.S1_at			AG	Yes	Yes
	CRMP-4	2,4	Dr.16753.2.A1_at			AG	Yes	Yes
	CRMP-5b	Not reg	Dr.11133.1.A1_at			AG	Yes	Yes
	Jun	2,6	Dr.7608.1.A1_at	56	92	TF	Yes	Yes
	T-Box1	2,2	Dr.10723.1.S1_at	13	143	TF	Yes	Yes
	Sox11b	8,1	Dr.5112.1.S3_at	204	1654	TF	Yes	Yes
	Sox11a	2,0	Dr.4763.3.S1_at	422	870	TF	Yes	Yes
	Alcam	2,9	Dr.20912.1.S2_at	40	118	AG	Yes	Yes
	Aanat	2,1	Dr.8142.1.S1_at	37	94	CP	Yes	Yes

Table 5: The list depicts the chosen candidates for in-situ probe making sorted by function; AG: Axon Guidance, CP: Clock/Photoreceptor, D: Differentiation, S: Signaling, TF: Transcription Factor

3.1.5 Cloning and *in situ* Hybridization of Candidate Genes

After extracting the desired sequence for the chosen genes using online databases, such as “Ensembl” and “NCBI”, fitting primers were designed (amplified fragments approx. 1kb in length), using the PrimerExpress Software. To amplify these genes from cDNA, these primers were used in a PCR (see section 2.14). Successful cloning resulted in purification of the desired insert (see section 2.13). The cloning of the amplified sequence was done using the pGEMT-Vector system (see section 2.12). Subsequent sequencing (see section 2.11.4) made sure the correct sequence was cloned.

Using the cloned plasmids containing the genes from the Table 4, *in situ* hybridization probes were synthesized with the Megascript Kit by Ambion (see section 2.15). The upregulation of mRNA in the RGC layer can be made visible with *in situ* hybridization technique (see section 2.18.1). In the following sections the data for the CRMP family and the c-JUN and Sox11a gene will be shown.

3.1.5.1 Collapsin Response Mediated Proteins - CRMPs

One group of genes, members of the cytoskeleton-associated collapsin response mediated proteins (CRMP) family, showed increased expression at 11 days post lesion. Since this family had not been described formerly in connection with the regeneration of the CNS, but the PNS, it was chosen as an interesting candidate to investigate.

Regarding the Affymetrix chips, only three CRMP family members were represented on the chip. The chip results identified two of these - CRMP 4 and 5a - as upregulated at 11days post lesion and one - CRMP 5b - as not regulated (see Table 4).

Consequently, to verify the chip results all known family members - including the three on the chip - were tested by *in situ* hybridization (Figure 9 and 10).

Two regions from the eye were under special focus in these *in situ* hybridization experiments: The first being the peripheral growth zone (PGZ), next to the ciliary marginal zone (CMZ), which adds new retinal cells, throughout the whole life of many fish, to the retina(Marcus, Delaney et al. 1999). Because of this feature the PGZ and CMZ can be used to identify developmentally active genes. At 3 – 5 days post fertilization (dpf), the left panel in Figure 9 and 10, the PGZ is still prominent and hence ideal to check for developmental gene expression.

The second being the retina with its retinal layers, especially the RGC layer, which harbors the somata of the optic nerve cells, displaying possible changes in mRNA levels after an optic nerve crush.

CRMP-1 was the only family member not showing any expression in the developing eye or the adult retina with unlesioned or lesioned optic axons. In comparison, CRMP-2 showed developmental expression in the PGZ of the eye, no expression in the RGC layer of the adult eye with unlesioned optic axons but strong expression 9 days after an optic nerve lesion. CRMP-3 mRNA expression was detected in the inner nuclear layer (INL) at the developmental stage (3 to 5dpf) and also “salt and pepper like” expression in the INL of the adult eye before and after a lesion of the optic axons. Furthermore no expression was detectable in the RGC layer of the adult eye without an optic nerve lesion, but strong mRNA expression was found 9 days after the optic nerve was lesioned. Similar to the expression pattern of CRMP-2, CRMP-4 was expressed in the PGZ of the larval eye but not expressed in the retina of adult fish, which did not receive an optic nerve crush. In contrast, strong expression was detectable in the RGC layer 9 days after an optic nerve crush. Similar to CRMP-4 and CRMP-2, CRMP-5a was not expressed in the RGC layer of the adult eye which did not experience an optic nerve lesion but could be detected in the one with lesioned optic

axons. The expression in the developing retina was not restricted to the PGZ but included the complete INL and the RGC layer. CRMP-5b showed broad expression in the retina at the developmental stage but was not expressed in the retina of adult fish with or without an optic nerve crush.

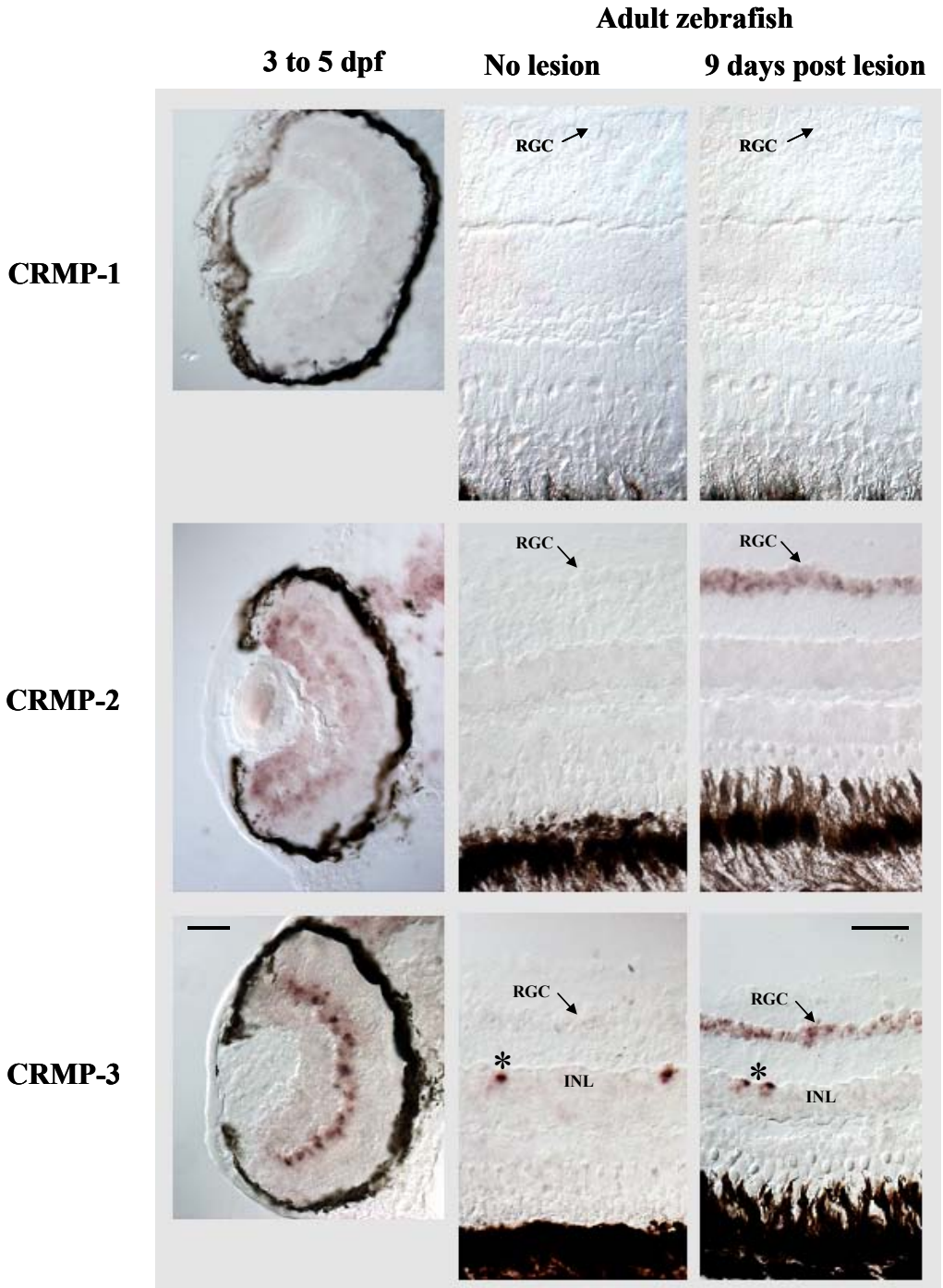

Figure 9: CRMP-2 and -3 show strong mRNA expression in the developing eye as well as in the adult eye 9 days after its optic nerve was lesioned. Cryo sections (14 µm, DIG-labeled) of the zebrafish eye were probed at 3 to 5 days post fertilization (dpf) (left column), as were sections at an adult stage of wild type animal eyes with no lesions (middle column) or 9 days post an optic nerve lesion (right column). Top row, CRMP-1: No in-situ signal is visible at development or in the unlesioned or lesioned eye. Middle row, CRMP-2: Developmental expression is observable in the peripheral growth zone. No expression is visible in the unlesioned eye but present in the lesioned eye in the RGC layer. Bottom row, CRMP-3: Expression in the inner nuclear layer at the developmental stage and "salt and pepper like" expression in the inner nuclear layer in the unlesioned and lesioned retinae is visible (see asterisks). No expression can be observed in the RGC layer in the unlesioned eye, but strong expression in the lesioned eye. Left column: vitreous side is left; middle and right column: vitreous side is up. RGC: retina ganglion cell layer; INL: inner nuclear layer. Scale bars: left column: 25 µm; right column: 20 µm.

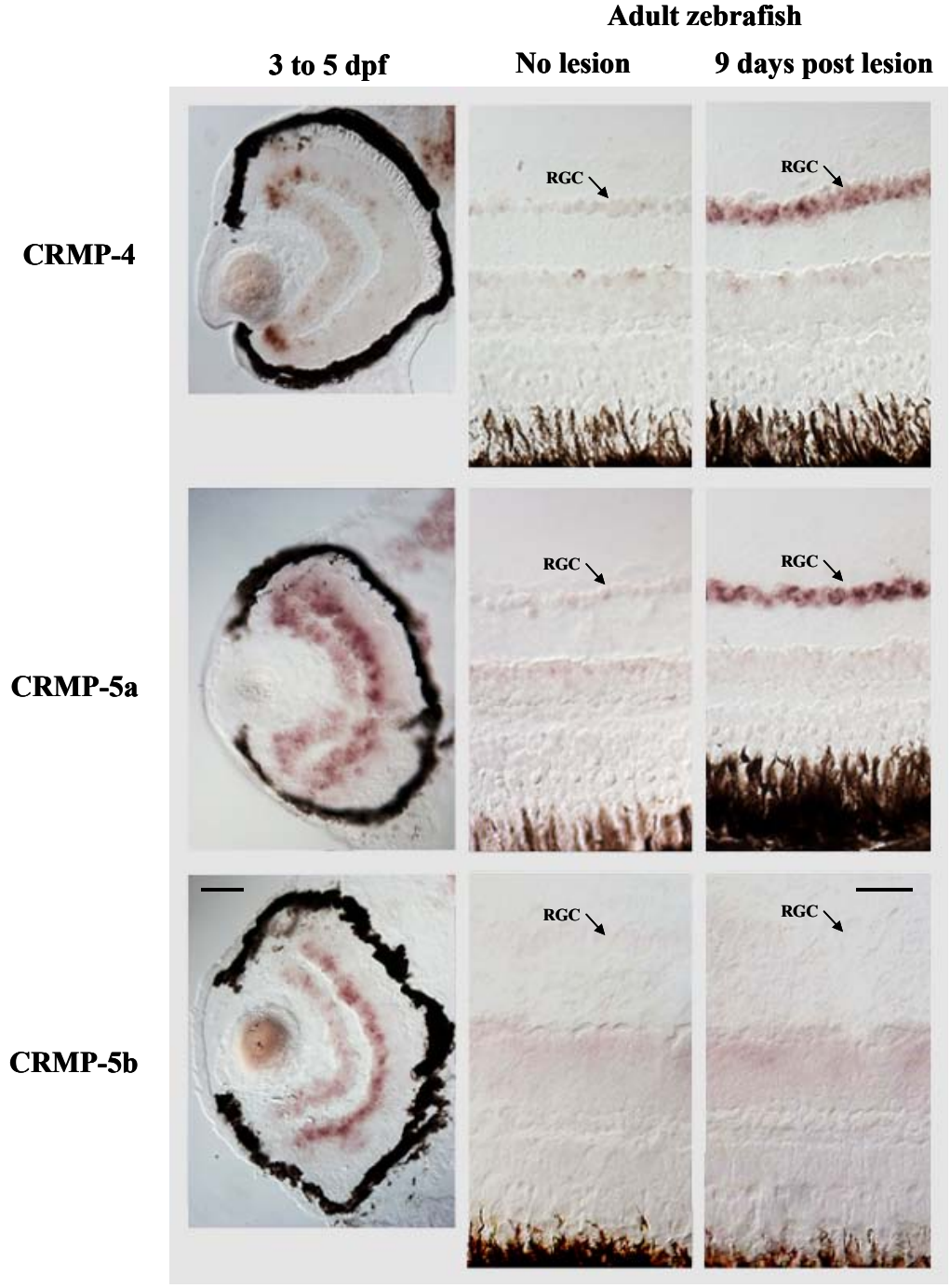

Figure 10: Crmp-4 and -5a show strong mRNA expression in the developing eye and in an adult eye 9 days after its optic nerve was lesioned. In situ hybridizations from a CRMP-4,-5a and –5b probe are shown. Cryo sections (14 µm. DIG-labeled) of the zebrafish eye were probed at 3 to 5 days post fertilization (dpf) (left column) as were sections at an adult stage of wild type animals with no lesion (middle column) or 11 days after an optic nerve lesion (right column). Top row, CRMP-4: Expression is visible in the peripheral growth zone in the larval eye. No expression can be observed in the RGC layer in the unlesioned eye, but strong expression in the lesioned eye. Middle row, CRMP-5a: Strong expression is visible in the larval eye but no expresssion in the RGC layer of the unlesioned adult eye. Strong expression can be observed in the RGC layer in the lesioned eye. Bottom row, CRMP-5b: Expression in the larval eye can be found but no expression in the unlesioned or lesioned adult eye was detectable. Left column: vitreous side is left; middle and right column: vitreous side is up. RGC: retina ganglion cell layer; INL: inner nuclear layer. Scale bars: left column: 25µm; right column: 20µm.

3.1.5.2 Sox11a and b

Sox11a and -b are transcription factors, belonging to the HMG-box superfamily of DNA-binding proteins. These two paralogues, Sox11a and Sox11b, share 75% protein sequence identity and are thought to be gene duplicates of an ancestral Sox11 gene. Studies in mice and chick show expression of Sox11 in the developing central nervous system. In comparison to that, Sox11a and b are expressed in the developing nervous system of zebrafish (de Martino, Yan et al. 2000). Additionally, Sox11 in mice is known to be involved in the regulation of neuron survival and neurite outgrowth (Jankowski, Cornuet et al. 2006). It also plays a role in events that underlie successful regeneration following peripheral nerve injury in mice (Jankowski, McIlwrath et al. 2009). *In situ* hybridizations of Sox11a (Figure 11), which was 2-fold upregulated in our microarray chip experiment, and Sox11b (Figure 12), 8-fold upregulated on the chip, showed a clear upregulation in the RGC layer after a lesion.

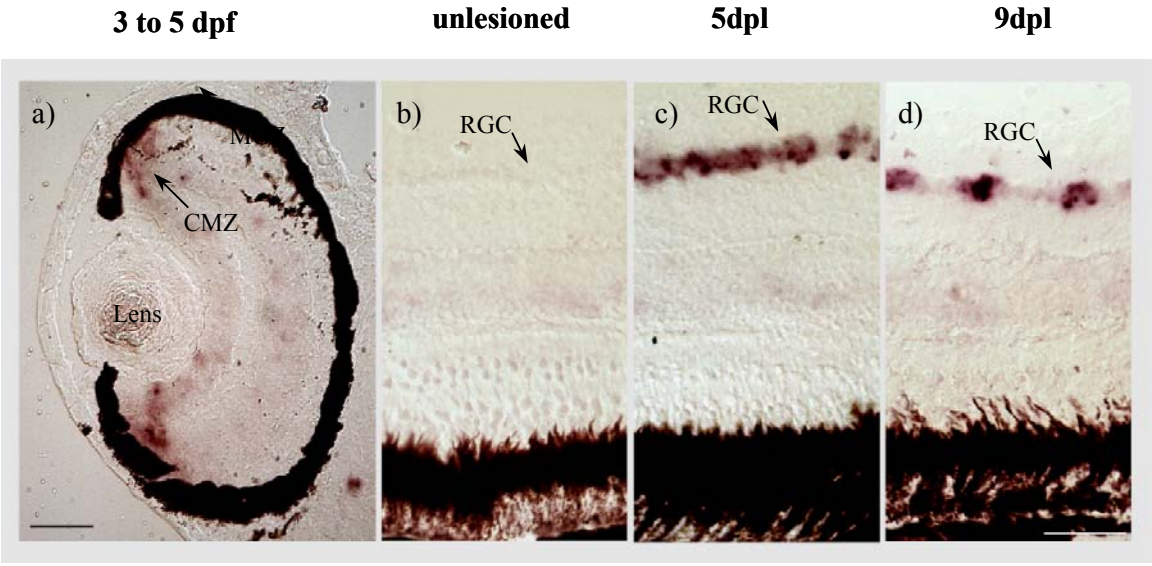

Figure 11: Sox11a was expressed in the growth zone of the retina at 3 days post fertilization (3dpf) (a). It was not expressed in adult unlesioned retinae (b), was strongly expressed at 5 days post lesion (5dpl) (c) and already declined in expression at 9 days post lesion (d). Cross sections of retinae are shown, in (b)-(d), vitreous side is up. RGC: Retina Ganglion Cell, PGZ: Peripheral Growth Zone, Scale bar: 25µm in (a) and 25µm in (b)-(d).

Similar results have been published just before the completion of this thesis by the laboratory of Goldman (Veldman, Bemben et al. 2007). Length of the probe and *in situ* primer sequences for Sox11a can be found in section 5.1. Sox11b was cloned by Dr. J. Schweitzer (Becker Laboratory).

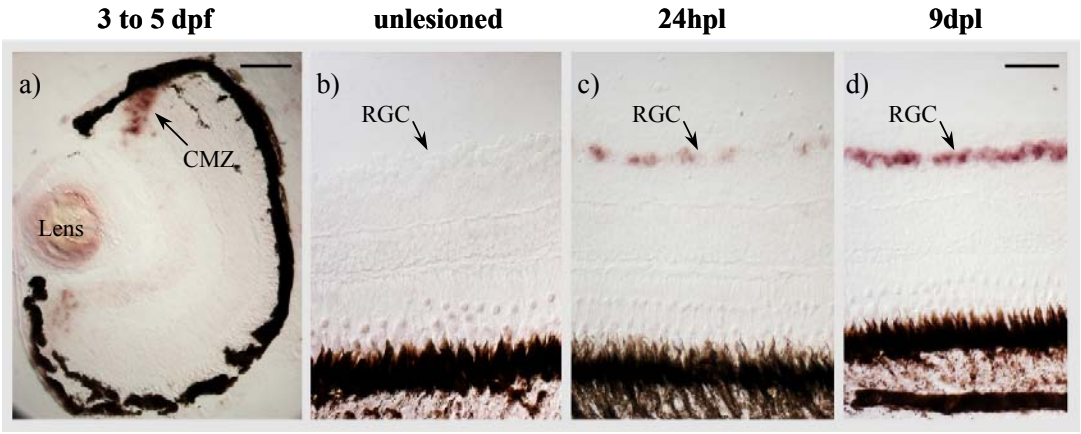

Figure 12: Sox11b was expressed in the growth zone of the retina at 3 days post fertilization (3dpf) (a). It was not expressed in adult unlesioned retinae (b), started to be expressed at 24 hours post lesion (24hpl) (c) and was strongly expressed at 9 days post lesion (d). Cross sections of retinae are shown, in (b)-(d), vitreous side is up. RGC: Retina Ganglion Cell, PGZ: Peripheral Growth Zone, Scale bar: 25µm in (a) and 20µm in (b)-(d).

3.1.5.3 Jun

The human JUN gene codes for a protein which is highly similar to a viral protein and interacts directly with specific DNA sequences to regulate gene expression. It is known to have transcription factor- and promotor binding activity (Bohmann, Bos et al. 1987; Zhang, Feng et al. 1998). Furthermore, Jun is part of a control circuit influencing the growth hormone-mediated synaptic plasticity in the mouse hippocampus (Zearfoss, Alarcon et al. 2008).

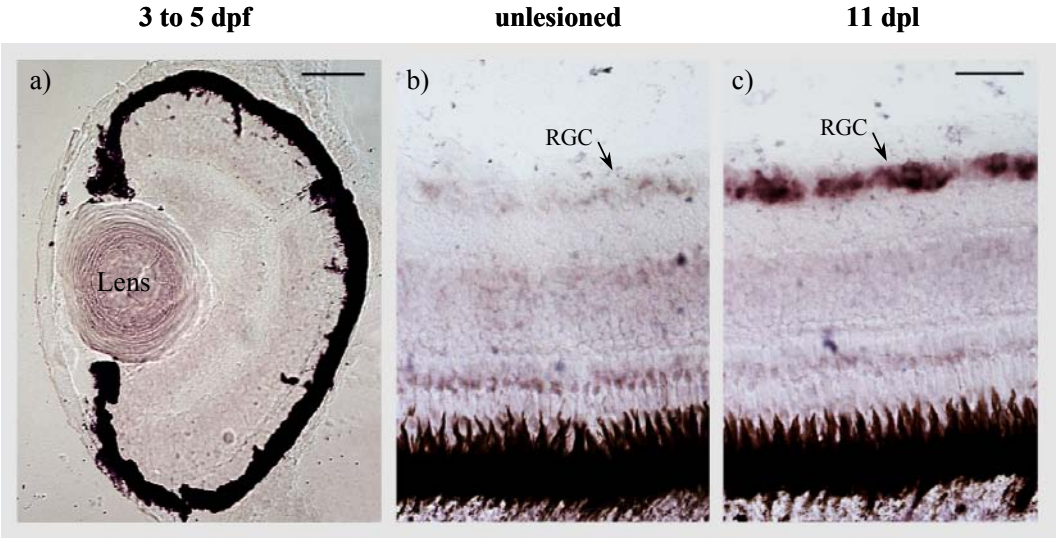

Figure 13: Jun was not expressed in the retina at 3 to 5 days post fertilization (3 to 5dpf) (a). It was also not expressed in adult unlesioned retinae (b) but strongly expressed at 11 days post lesion (c). Cross sections of retinae are shown, in (b)-(c), vitreous side is up. RGC:Retina Ganglion Cell, Scale bar: 25µm in (a) and 20µm in (b) and (c).

Activation of Jun signaling is sufficient for CNS axonal regeneration in *Drosophila*, whereas injured adult wild type fly CNS axons fail to regenerate (Ayaz, Leyssen et al. 2008). The zebrafish Jun, 2.6-fold upregulated in our microarray chip experiment, was re-expressed after optic nerve lesion specifically in the RGC layer. The length of the *in situ* probe and sequences of primers used to generate it are found in section 5.1.

3.1.5.4 Problems with the 6 Hour and 12 Hour Time Points

The *in situ* hybridizations with the genes chosen for the 6 and 12 hour post lesion time points unfortunately did not show any detectable upregulation of mRNA expression in the RGC layer. Every hybridization experiment was done at least twice. All hybridization probes were synthesized at least two times. Data collected by real time PCR for the chosen genes (see Table 5, section 3.1.4) for 6 hour and 12 hour time points did not match the mRNA regulations observed with the microarray chips for these genes and time points. These real time measurements were performed at the Keck Center by Prof. R. Hart, a collaborating laboratory at Rutgers University, New Jersey, USA.

3.2 In Vivo Application of Morpholinos

3.2.1 Morpholino Transport into the RGC Layer of the Eye

Inhibition of translation or RNA splicing by the use of morpholinos is the method of choice to influence gene expression in zebrafish. Normally, these small antisense ribonucleotides are injected into the egg and down regulate expression over a few days of development. Since this research is concerned with the regeneration of the optic nerve it was attempted to demonstrate whether gene expression could be influenced through morpholinos specifically in the RGCs which regenerate their optic axons. The goal was to deliver morpholinos specifically into axotomized adult RGCs (see chapter 2.20.3.2). This required that the optic nerve in adult fish be cut and a little gelfoam pledget, soaked in morpholino solution, be placed directly on the cut nerve stump. The morpholino was tagged with fluorescein to enable us to localize the morpholino afterwards.

We applied the morpholino, sacrificed the fish at two different time points (9 dpl and 20 dpl), perfused the fish and sectioned the dissected retinas using a vibrating blade microtome. Immunohistochemistry was performed, with an anti-fluorescein-coupled antibody tagged with alkaline phosphatase (AP) (see section 2.19.1).

Staining was clearly visible in the RGC layer at 9 days after application of morpholino to cut RGC axons. A reduction in staining intensity was clearly visible at 20 days after morpholino application (Figure 14b, c). This, the method of morpholino transport in the retina ganglion cells after lesion worked well and the amount of detectable morpholino was diminished at 20 days post lesion.

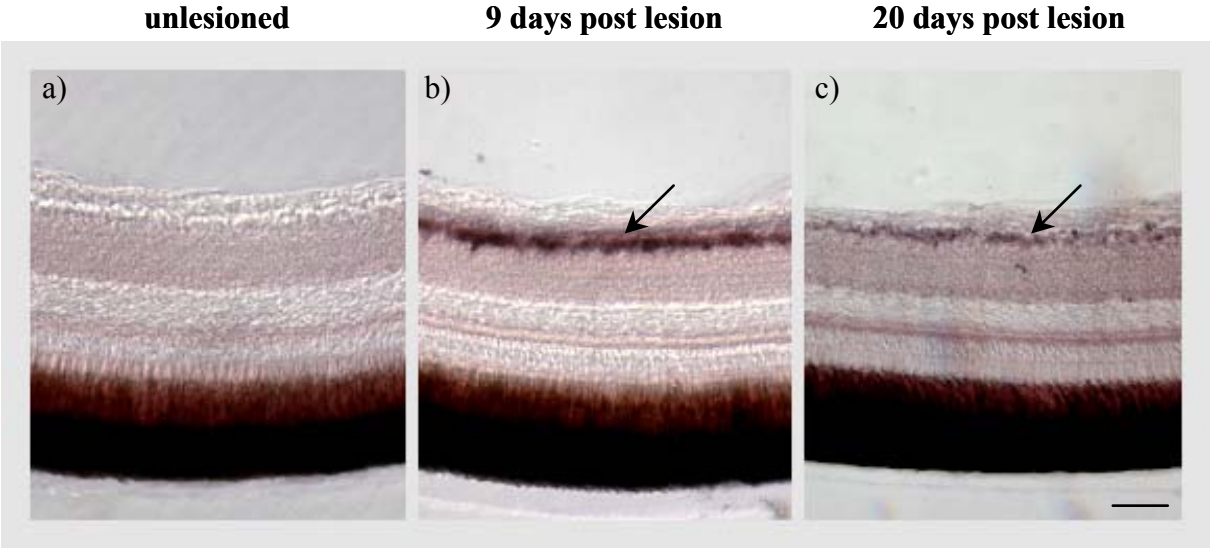

Figure 14: Morpholino has been transported specifically into the RGC layer. After an optic nerve transection, a small piece of gelfoam soaked with 400ng fluorescein-labeled morpholino was placed directly on the nerve stump. At 9 days (b) and 20 days (c) post lesion the eyes were sectioned with a vibrating blade microtome, followed by immunohistochemistry for fluorescein. A strong signal was detected after morpholino application specifically in the RGC layer at 9 dpl (arrow in b). There is still signal visible in at 20 dpl but visible reduced compared to 9 dpl. No signal could be detected in retinae of unlesioned animals (a). Scale bar: 20µm

3.2.2 Influencing Gene Expression in vivo with CRMP Morpholinos

Combining the information from the Affymetrix chip analysis and the *in situ* hybridizations for the CRMP family, both methods indicated a temporal correlation with axonal regeneration and specificity for RGCs for some family members.

Hence, two CRMP family members, CRMP-2 and -4, were chosen as candidates for in vivo perturbation experiments. Consequently CRMP-2 and CRMP-4 morpholinos were used for perturbation experiments (for morpholino sequences see section 5.4). Earlier experiments on larvae, morpholino injections in just fertilized eggs leading to optic projection errors, suggested a combination of the CRMP-2 Intron Exon morpholino 2 (called CRMP-2IE Mo2) and a CRMP-4 start codon morpholino (called CRMP-4B). A combination of CRMP-2IE2 and CRMP4B (a total of 32µg morpholino) was used on gelfoam pledget to influence gene expression in vivo. At three different time points 8 days, 16 days and 4 weeks post-lesion,

regenerated optic axons of RGCs that received morpholino were traced with biocytin, fixed and the brains were sectioned with a vibrating blade microtome.

Morpholinos	Regeneration Time		
	8 days	16 days	4 weeks
CRMP-2IE Mo2 16µg + CRMP-4B 16µg	16	9	8
Control Mo 32µg	17	4	8

Table 6: Number of animals used for each time point treated with a morpholino gelfoam

To see whether the morpholino treatment influenced regeneration of optic axons, we focused on the speed of regrowing axons and the paths they would take. Not being able to directly measure actual speed of growth in the animal, we decided to compare in control morpholino versus active morpholino treated animals, which brain regions would be repopulated by regenerated fibers at specific time points. At the same time the trajectories of regenerated optic axons were analyzed. All morpholino treated animals (Table 6; 16 at 8 days, 9 at 16 days and 8 at 4 weeks) displayed fibers at the set landmarks not distinguishable from the control morpholino treated animals. The trajectories of the morpholino treated animals were also not distinguishable from control morpholino treated animals. Landmarks were the chiasm, pretectal nuclei such as the central pretectal nucleus (CPN), the periventricular pretectal nucleus (PPd), and the tectum. Unfortunately no errors were detected either in pathfinding or in speed.

The second main part of the thesis was the morphological investigation of the *astray* mutant and the regeneration of its optic axons after a lesion (section 3.3).

3.3 Roundabout - *robo*

3.3.1 Expression of *robo2* and *slit2* During Optic Nerve Regeneration

Earlier experiments, performed by Dr. T. Becker and C. Wyatt in this laboratory (unpublished data) were designed to determine whether the *robo*/*slit* system could be involved in regeneration of the optic projection. *In situ* hybridization for *robo2* expression was performed in the retina, as well as for the potential ligands *slit1*a, *slit1*b, *slit2* and *slit3* in the brain before and after optic nerve crush of wild type animals. The retina of adult teleost fish grows continuously in an annular fashion, i.e. the central retina is older than peripheral retina (Stuermer and Easter 1984; Marcus, Delaney et al. 1999). In the juvenile zebrafish retina (4 weeks post-fertilization), *robo2* is expressed in the peripheral growth zone, next to the undifferentiated ciliary margin zone (Figure 15a). In more central, older parts of the retina, the RGCs did not show detectable levels of *robo2* mRNA expression. This is typical for genes involved in axonal growth of newly formed RGCs (Bernhardt, Tongiorgi et al. 1996).

In the unlesioned adult retina, no *robo2* mRNA expression was detected. After a lesion of the optic nerve in adult animals, *robo2* mRNA expression was up-regulated in the RGC layer of the entire retina (Figure 15b,c). Expression peaked during the active growth phase of optic axons at 2 weeks post-lesion (Becker, Meyer et al. 2000). Thus *robo2* mRNA is expressed in RGCs, when their regenerating axons navigate the brain.

Slits showed mRNA expression that was unchanged between unlesioned and lesioned animals at 2 weeks post-lesion. *Slit1a* mRNA showed the most widespread expression in the brain, including the ventral diencephalon and the tectum. In the tectum, expression was strongest in large neurons in the SFGS. The mRNA was also detectable in the outer aspect of the cell dense stratum periventriculare (SPV), but not in the ventricular layer of ependymo-radial glial cells (Fig. 15e). *Slit1b* mRNA expression was mostly restricted to specific brain midline zones, such as at the medial aspect of the habenula and at the level of the posterior commissure (Figure 15f,g). Low levels of expression were detected in the ventral telencephalon, rostral to the chiasm. *Slit2* showed strong and highly localized mRNA expression in the habenula and the ventral diencephalon at the chiasm (Figure 15d). *Slit3* mRNA showed low levels of expression in the ventral diencephalon and in the A/VL region of the diencephalon (Figure 15h). A strong *slit3* mRNA signal was found in the tegmental midline, which did not coincide with the trajectories of optic axons (data not shown).

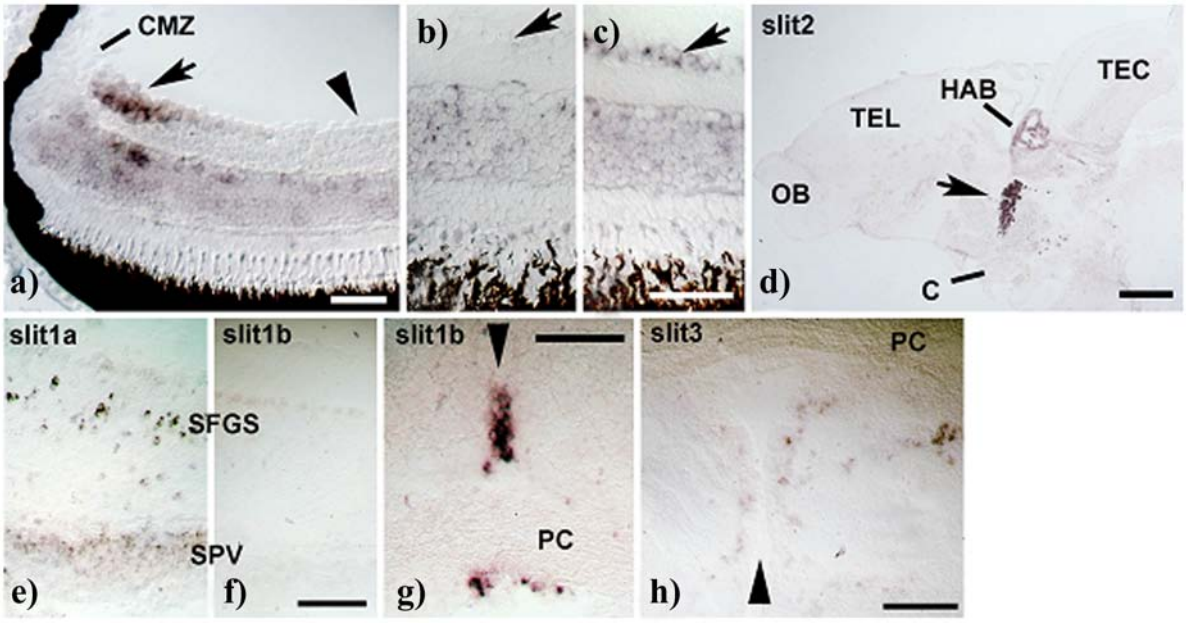

Figure 15: *Robo2* and *slits* are expressed during regeneration of the adult optic projection. Cross sections are shown, except for d). a) In the retina of unlesioned juvenile, 4-week-old animals, *robo2* mRNA is expressed in recently differentiated RGCs in the peripheral growth zone of the retina (arrow) next to the ciliary margin zone (CMZ). Older, more central RGCs (arrowhead) do not express detectable levels of *robo2* mRNA. b) and c) In the adult (> 3 months of age) central retina, *robo2* mRNA is re-expressed in the RGC layer at 2 weeks post-lesion (arrow in c) compared to the RGC layer in unlesioned controls (arrow in b). d) A sagittal section is shown (rostral left, dorsal up). Conspicuous expression of *slit2* mRNA is found in the habenula (HAB) and in the ventral diencephalon (arrow) at the level of the optic chiasm (C) in a sagittal section of the brain (rostral is left, OB = olfactory bulb, TEL = telenencephalon, TEC = tectum mesencephali). e) and f) *Slit1a*, but not *slit1b* is expressed in the deafferented tectum at one week post-lesion. g) Strong local expression of *slit1b* mRNA is found at the level of the posterior commissure (PC) in cross sections of the brain. h) Low levels of *slit3* mRNA expression are found in the pretectum. Arrowheads in g) and h) indicate the brain midline. Bars in a, c, g = 50 µm; bar in d = 200 µm; bar in e, f = 100 µm; bar in h = 100 µm. The *in situ* hybridizations were kindly contributed by Dr. T. Becker and C. Wyatt.

Targeting errors of regenerating axons in *astray* mutants correlate with *slit* expression domains. The rostral tectum, in which defasciculated growth of axons occurs and abnormal deep innervation of the tectum originates is bordered by *slit2* and *slit1b* mRNA expression in the habenula. The posterior commissure, through with regenerating fibers aberrantly cross, is bordered by *slit1b* mRNA expression in the midline. Aberrantly large terminal fields in the pretectum correlated with *slit1a* and *slit3* expression and expanded termination layers of optic axons in the tectum correlated with *slit1a* mRNA expression in the tectum.

To estimate the potential contribution of developmentally altered brain morphology to targeting errors of regenerating axons in adult *astray* mutants, we analyzed the laminated architecture of the denervated tectum. This is because expansion of tectal termination layers is a phenotype that is found in all of the *astray* mutants with a regenerated optic projection. We found that the layered expression of Tenascin-R (Becker, Schweitzer et al. 2004), another extracellular matrix protein, as well as Tyrosine Hydroxylase and serotonin immuno-positive afferents (Kaslin and Panula 2001) was comparable between *astray* mutants and wild type animals in the tectum at 1 week post-lesion. At this time point, the tectum is denervated and the first optic axons begin to grow back onto the tectum (Becker, Meyer et al. 2000). However, Tenascin-R immunoreactivity and innervation by Tyrosine Hydroxylase immuno-positive axons, but not serotoninergic axons, was increased (Figure 16). Since basic layering of extracellular matrix and afferent systems is retained in *astray* mutants, it is unlikely that the massive laminar termination errors of regenerating optic axons are solely secondary to developmentally altered tectal cytoarchitecture.

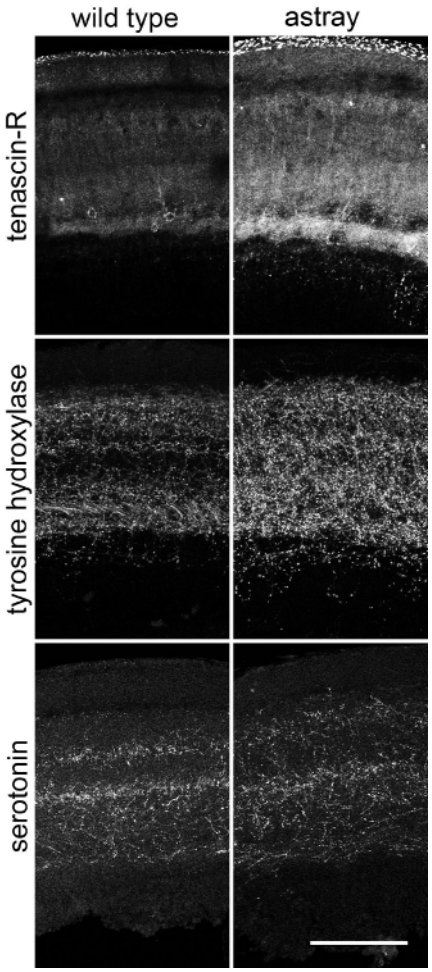

Figure 16: Comparison of laminar distribution of different markers in the denervated tectum at 1 week post-lesion. Tenascin-R shows a comparable distribution in wild type and *astray* animals. However, labeling intensity in *astray* mutants, as measured by mean pixel brightness (ImageJ), was increased by 41% (n = 3, mean pixel brightness was 96.2 ± 6.65 in *astray* and 68.0 ± 5.53 in wild type, Mann-Whitney U-test, $P < 0.05$). Tyrosine Hydroxylase was distributed in similar layers. However, labeling intensity was increased by 94% (n = 3, mean pixel brightness was 48.0 ± 3.11 in *astray* and 24.8 ± 1.98 in wild type, Mann-Whitney U-test, $P < 0.05$). No measurable changes were observed in serotonin immunohistochemistry (mean pixel brightness was 37.4 ± 12.02 in *astray* and 37.0 ± 11.99 in wild type). Scale bar = 100 µm. Pictures were kindly contributed by Dr. T. Becker and C. Wyatt.

Thus *robo2* receptor expression in RGCs and expression of *slit* ligands in the brain, where they could interact with growth cones of regenerating optic axons, correlates with optic axon regeneration. Based on these results, the decision was made to investigate the *astray* mutant, deficient for the *robo2* gene, with regard to the positions of its optic axons in adulthood and after regeneration.

3.3.2 Pathfinding Errors in the Adult Optic Projection of *astray*/*robo2* Mutants

This chapter is divided into two main sections, section 3.3.2 and 3.3.4. The first one determines the relative consequences of *robo2* deficiency for the patterning of the adult optic projection. The second section identifies the contribution of *robo2* to the regeneration of the optic projection in adult *astray*/*robo2* mutants. It ascertains whether guidance errors seen in the first section are recommitted and which ones they are. In either case, only those specimens were raised to adulthood that had developed a strong telencephalic projection as 4-5-days-old larvae. This was judged based on the presence of an ectopic telencephalic projection, which was detected in 66.9% ± 7.10% (n = 92 larvae) of the larvae (Figure 17). The telencephalic projection was determined in living larvae by virtue of green fluorescence of optic axons (Figure 18).

The fact that a third of the mutants did not have a telencephalic projection suggests that tract formation in the telencephalon is an indirect event, rather than optic axons following directly secondary cues directly in the absence of *robo2* signaling.

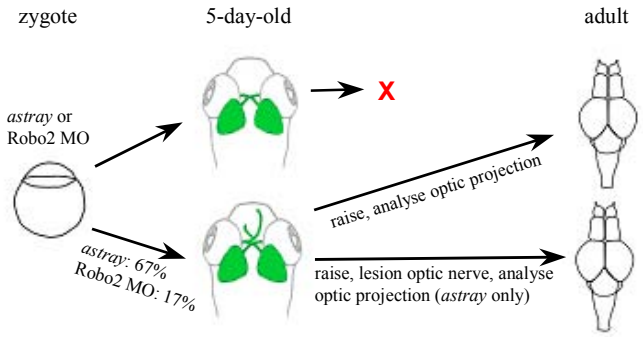

Figure 17: Schematic representation of experimental paradigm. Living 5-day-old larvae were pre-selected for the presence of an aberrant telencephalic optic projection and raised for adult experiments as indicated. Figure was kindly contributed by Dr. T. Becker.

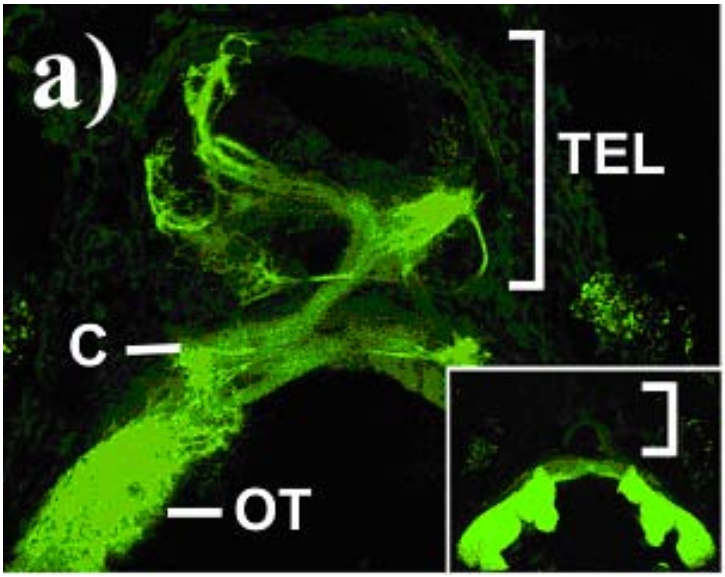

Figure 18: Larval assessment and morpholino induction of *astray* phenotypes. a) Dorsal views are shown (rostral is up). Living *astray* larvae were selected according to the presence of GFP positive optic fibers in the telencephalon (TEL). Inset shows a wild type projection without telencephalic tracts. (C = chiasm; OT= optic tectum). Figure was kindly contributed by Dr. T. Becker.

In contrast to the live investigation of the *astray* phenotype in the transparent larvae, a different approach had to be taken in non-transparent adult fish. To investigate the adult optic projection, tracing had to be performed in adult *astray*/*robo2* mutants and in wild type fish as controls. Optic axons from one eye were visualized by a unilateral whole nerve tracing with biocytin, followed by fixation through perfusion and vibrating blade microtome sectioning. Then, the entire zebrafish brain was examined for misguided axons.

The observed pathfinding errors can be summarized in 4 groups:

1) Irregular growth into the telencephalon and tegmentum (Section 3.3.2.1)	Ectopic optic tracts in the telencephalon and the tegmentum
2) Termination errors in pretectal targets and tectal termination fields (Section 3.3.2.2)	Diffuse innervation of pretectal targets and increased depth of optic fiber receiving layer in the tectum
3) Midline crossing errors of optic fibers (Section 3.3.2.3)	Crossing in posterior commissure, ipsilateral innervation of the tectum and gaps in the contralateral innervation of the tectum
4) Irregular growth of optic fibers into tectum (Section 3.3.2.4)	Defasciculation of dorsal optic tract and growth of fascicles of optic fibers below optic fiber receiving layer

In the following sections all observed errors will be documented by pictures and analyzed statistically.

3.3.2.1 Irregular Growth into the Telencephalon and Tegmentum

Telencephalon 

We commenced by observing ectopic fibers in the telencephalon. Optic fibers in wild type zebrafish (n = 12) project to a variety of extratectal targets, but never to the telencephalon (Figure 19a). They do, however, in *astray* mutants (n = 15) as shown below by labeling one optic nerve with biocytin (Figure 19b). Fifteen *astray*/*robo2* mutants were raised with an ectopic telencephalic projection. Fourteen of these animals retained ectopic optic tracts in the telencephalon as adults, as determined by unilateral optic nerve tracing. Tracts entered the telencephalon ventrally, rostral to the chiasm. Fascicles of optic axons often recrossed the midline in the ventral telencephalon. At the end of fascicles dense arborization fields were found, particularly in the dorsal telencephalon. Expressed as percentages, 0% of wild type animals and 93% of *astray* mutants displayed optic tracts in the telencephalon (highly significant, Fisher's Exact Test, $P < 0.001$). Thus, *astray*/*robo2* mutants that had ectopic telencephalic tracts as larvae retained these in adulthood. For a summary see Figure 38.

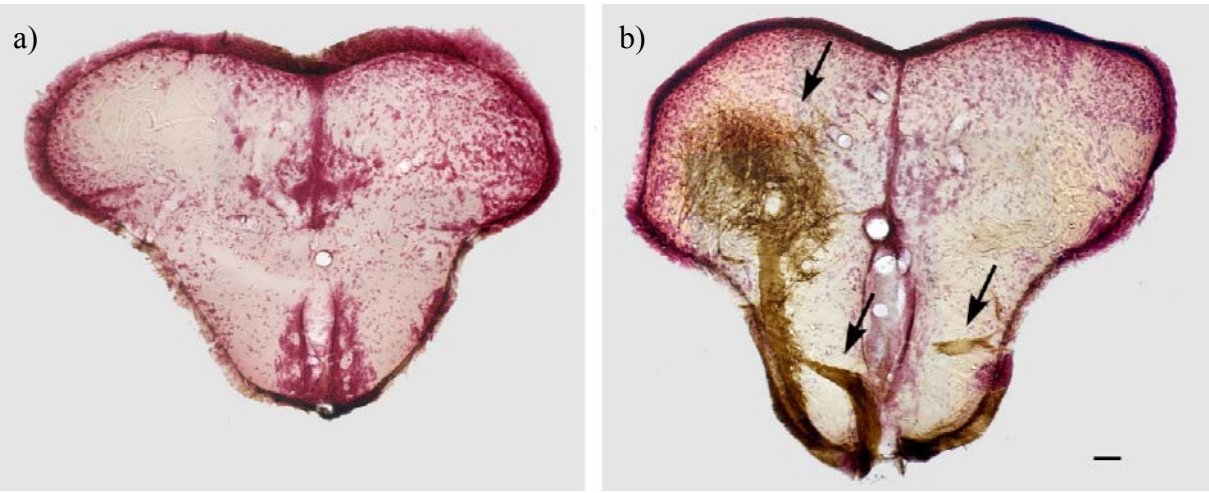

Figure 19: Targeting errors displayed in the optic projection in *astray* fish. No ectopic optic tracts are seen in the wild type telencephalon (a). *Astray* mutants (b) exhibited ectopic fibers in the telencephalic region. All sections are transverse and counterstained with neutral red. Dorsal is up. Black arrow indicates ectopic axons. Scale bar: 100µm

Tegmentum

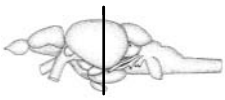

The most caudal ectopic optic fibers are found in the tegmentum at the level of the caudal tectum (4 out of 15). These fibers cross the midline in the tegmentum and grow dorsally to terminate in the optic fiber receiving layer of the tectum. Shown here are two examples of tegmental fibers (Figure 20b to d) observable in *astray* mutant fish, but never in wild type fish (Figure 20a). Expressed as percentages, 0% of wild types and 27% of *astray* mutants display optic tracts in the tegmentum (difference not significant, Fisher's Exact Test, P = 0.106). We discovered them at the plane of section with the oculomotor nucleus (ON). The arrows in Figure 20b and c indicate how axon tracts emerge on the contralateral side (arrow 1, Figure 20b) of the brain, cross over the midline (arrows 2 and 3, Figure 20b) and terminate in the ipsilateral half of the tectum (arrow 4, Figure 20c). Figure 20d shows a close up of these termination fields. In wild type animals crossing events of the optic tract always occur at the chiasm whereas, as seen here, in *astray* mutants sometimes these crossing events happen at the tegmentum. For a summary see Figure 39.

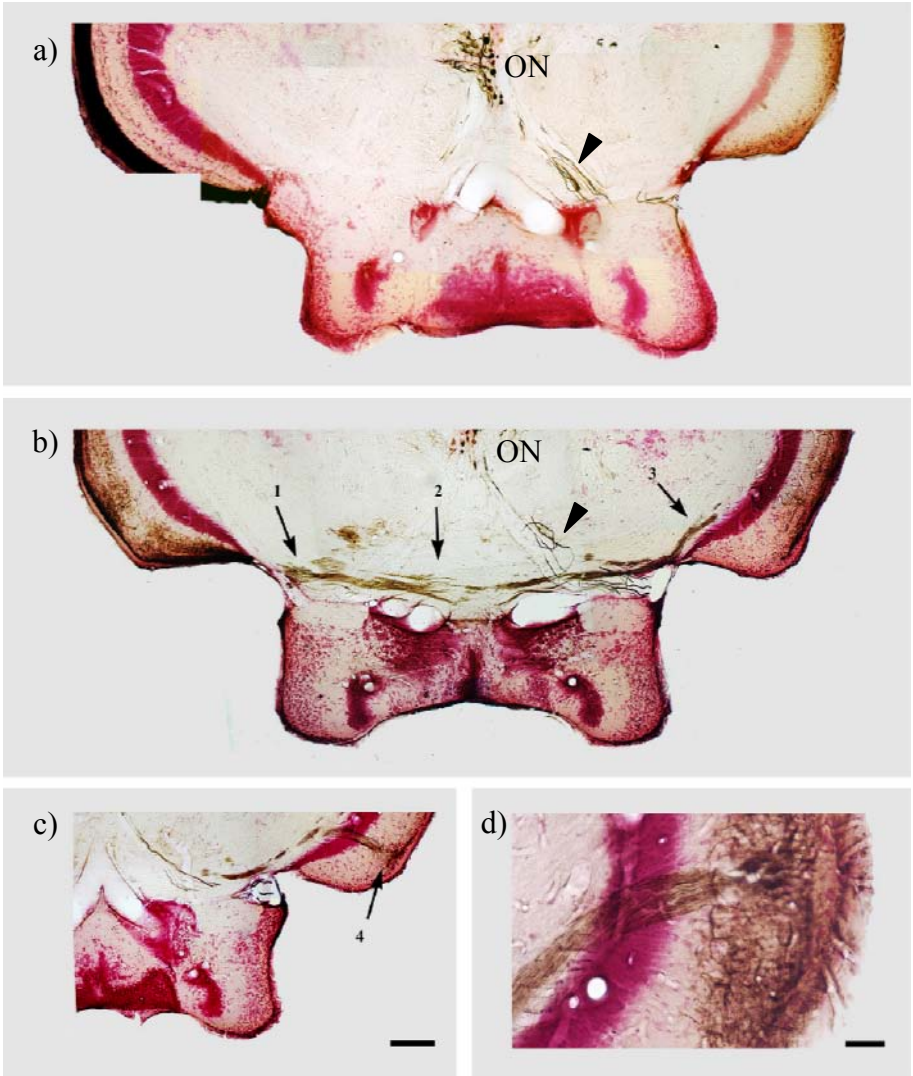

Figure 20: Ectopic optic tracts in the tegmentum. a) No ectopic tracts were found in wild type animals. b) *Astray* animals exhibited ectopic fibers (arrows) in the tegmentum, starting at the contralateral tectal side (arrow 1) and cross the midline (arrows 2 and 3). Fibers terminated in the ipsilateral tectum (c, arrow 4). b) and c) are consecutive sections from the same fish. d) Shown is a close up of the termination field (*astray* mutant, but different fish compared to c). Fibers indicated by black arrow heads in (a) and (b) are not optic axons. Dorsal is up. All sections have been counterstained with neutral red. Scale bar in a-c = 50µm; scale bar in d = 25µm.

3.3.2.2 Termination Errors at Pretectal Targets and Tectal Termination Fields

Retino-Recipient Pretectal Targets

Expanded target innervation can be observed at retino-recipient pretectal targets, from which the central pretectal nucleus (CPN), periventricular pretectal nucleus (PPd), anterior thalamus (A) and ventrolateral thalamic nucleus (VL) are strongly affected in the *astray* mutant. In wild type fish (n = 12) these termination fields are distinct (Figure 21a), meaning easily recognizable as a dot or elliptoid shape. The very opposite is the case in *astray* mutants (n = 15), which no longer showed clearly defined termination fields but rather expanded innervation fields with more diffuse borders (Figure 21b and c). Expressed as percentages, 0% in wild type animals and 100% in *astray* mutants displayed disrupted termination fields (highly significant, Fisher's Exact Test, $P < 0.001$). The missing *robo2* gene seems to have an important impact on discrete termination in zebrafish in the area of the pretectal nuclei.

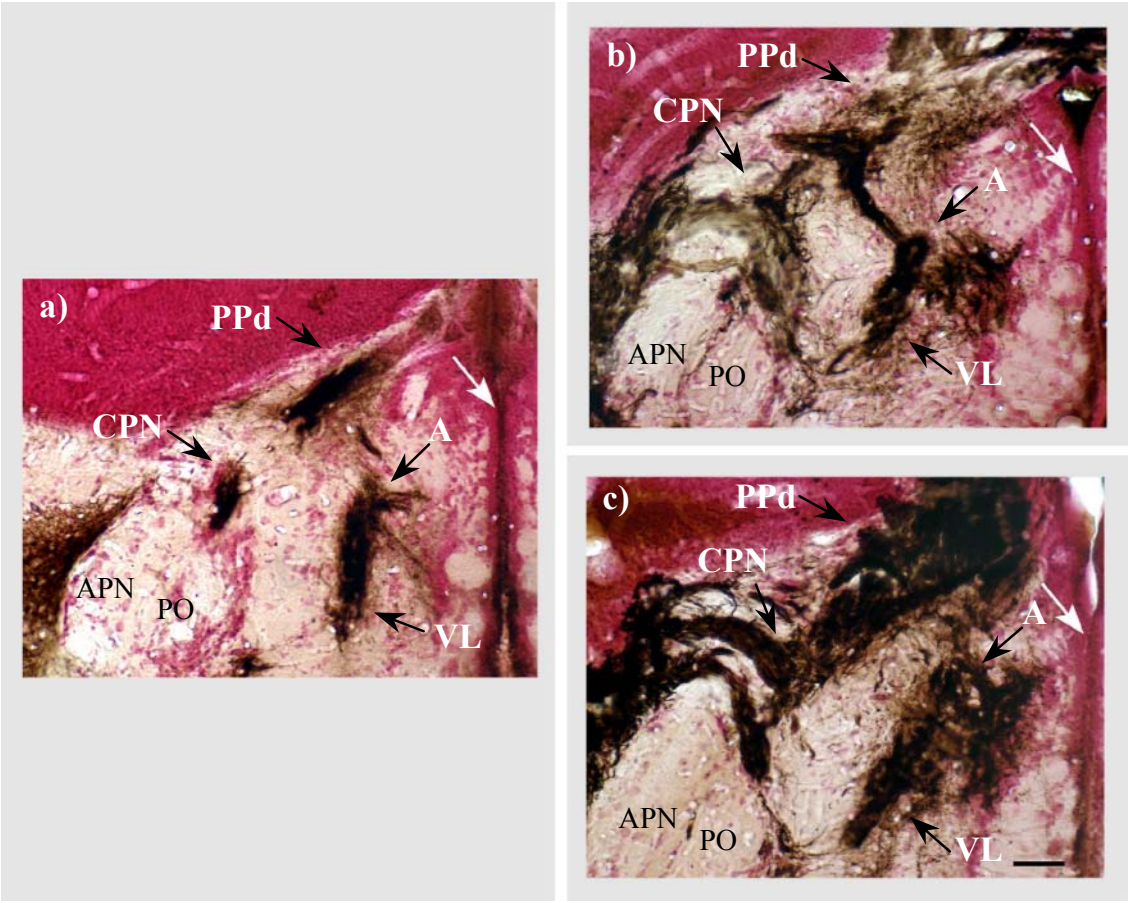

Figure 21: Expanded retino-recipient pretectal nuclei in the *astray* mutant. The clearly defined regions of four extratectal targets, the central pretectal nucleus (CPN), the periventricular pretectal nucleus (PPd), the anterior (A) and ventrolateral thalamic nucleus (VL) are expanded in the *astray* mutant (b and c). The termination fields of these three targets are highly disrupted (black arrows). Discrete termination fields are visible in the wild type animals (a). The accessory pretectal nucleus (APN) and the posterior pretectal nucleus (PO) are in all cases avoided by axons. Dorsal is up. All sections were counterstained with neutral red. White arrows indicate midline. Scale bar in c = 50µm.

For a summary see Figure 40. We were able to quantify the lateral extent of the A/VL terminal field at the level of the CPN, which was significantly enlarged in *astray* mutants (203. 2 ± 18.35 µm SEM) compared to wild type animals (124.67 ± 6.67 µm; Mann-Whitney U-test, P = 0.0005). However, the cytoarchitecture of the pretectal area appeared unaltered in neutral red counter-stain of *astray* mutants. For example the distance between the CPN and the dorsal aspect of the ventricle was comparable between *astray* (333.5 ± 13.38 µm) and wild type animals (323.3 ± 14.11; P = 0.6). This suggests that optic axons terminated beyond their normal boundaries (data for A/VL field measurements kindly contributed by Dr. T. Becker).

Thickness of Tectal Termination Fields

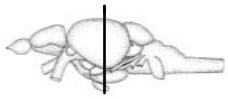

The innervation of the tectal layers in *astray* fish deviated strongly from that of wild type fish. The structural architecture of the teleost tectum, described in detail for wild type fish by Stuermer et al. (Stuermer and Easter 1984) and Diaz et al. (Diaz, Becerra et al. 2002), seemed to be unaffected when comparing wild type with *astray* fish. Three main layers were marked in Figure 22, starting dorsal with the Stratum Fibrosum et Griseum Superficiale (SFGS), followed by the Stratum Griseum Centrale (SGC) and marking the ventral part with the Stratum Album Centrale (SAC).

In wild type animals (Figure 22a) very few retinal axons were visible in the SGC and SAC layer. By comparison the *astray* mutants showed strong innervation in the SGC layer. Some fibers were even visible in the SAC layer (Figure 22b). Measurements showed that the thickness of the optic fiber receiving layers identified by intense solid labeling, were significantly increased in mutants (15 of 15 animals, Figure 22b). The mean thickness of the optic fiber receiving layers of *astray* mutants was 92.4 ± 3.7µm (SEM) compared to 48.8 ± 1.7µm in wild type animals (ANOVA, $P < 0.001$). The total thickness of the tectum was unchanged in *astray* mutants (185.1 ± 4.31µm), compared to wild type animals (198.3 ± 10.21µm, Mann-Whitney U-test, P = 0.4). This suggests that expanded thickness of termination layers of optic axons was not a consequence of increased thickness of tectal target layers (data for the total thickness of the tectum was kindly contributed by Dr. T. Becker). For a summary see Figure 41.

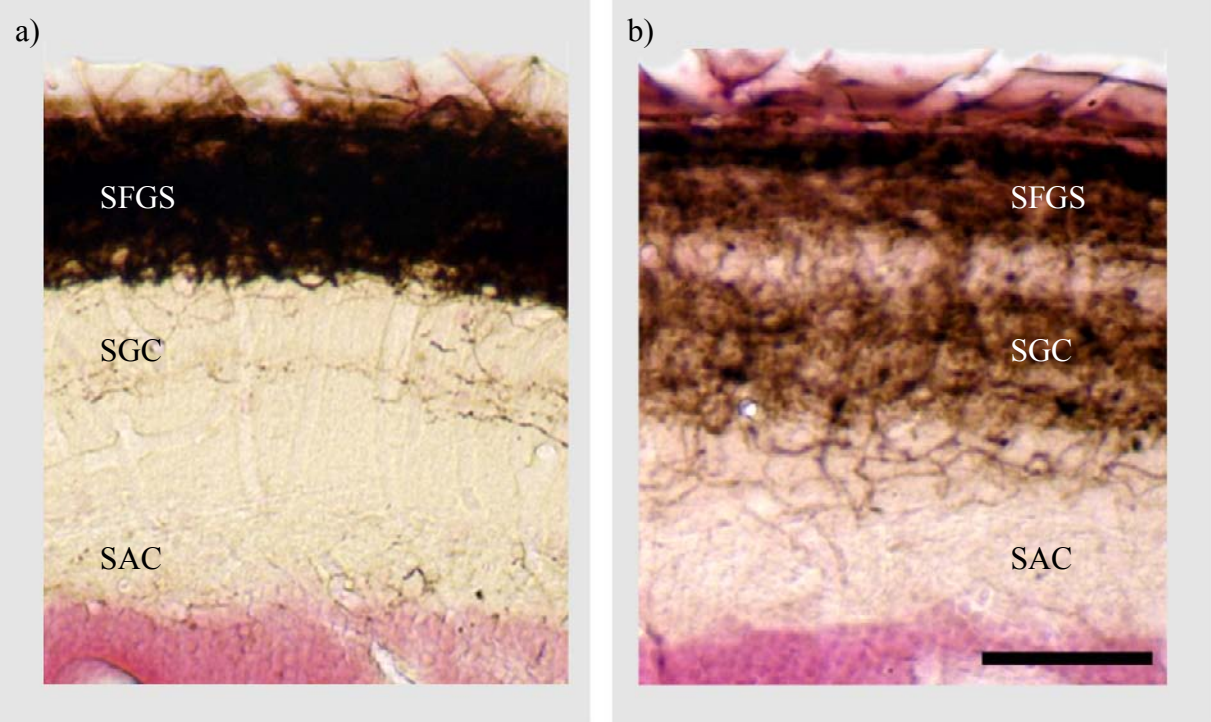

Figure 22: Increased thickness of tectal termination fields in *astray* mutants. Tectal termination fields are nearly twice as thick in *astray* (b) compared to wild type (a) animals. Dorsal is up. All sectioned are counterstained with neutral red. Scale bar in b = 50µm.

3.3.2.3 Midline Crossing Errors of Optic Fibers

Fibers Crossing at the Posterior Commissure

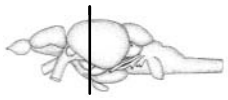

Compared to wild type animals (Figure 23a, 0 out of 12 animals) *astray* fish showed significant aberrant midline crossing (black arrow) of optical axon fibers at the posterior commissure (PC) (Figure 23b, 12 out of 15 animals). Expressed as percentages, 0% in wild types animals and 73% in *astray* mutants crossed the midline at the PC (difference highly significant, Fisher's Exact Test, $P < 0.001$). Many of the misguided axons re-cross at the PC additionally to the chiasm where they are supposed to cross. Some fibers coming from the contralateral side of the brain project towards the PC and then into the tectum (Figure 23b, black arrow head). A possible reason for these wrong crossing events of the optic projection could be only partially guided axon growth at the morphological area of the pretectal nuclei due to the missing *robo2* gene in *astray* mutants. For a summary see Figure 42.

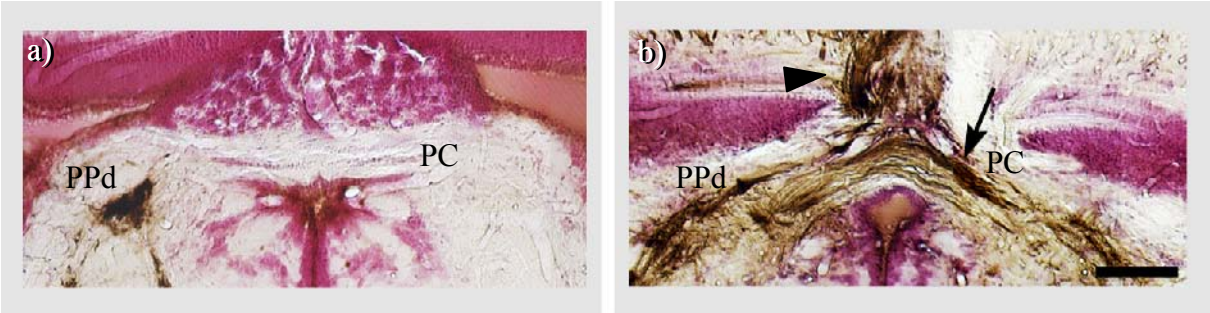

Figure 23: Optic fibers crossing at the posterior commissure in *astray* mutants. In *astray* fish (b) many fibers (arrow) cross at the posterior commissure, which is never the case in wild type animals (a). The periventricular pretectal nucleus (PPd) is indicated for orientation. Dorsal is up. All sections were counterstained with neutral red. Scale bars = 100µm.

Ipsi- and Contralateral Innervation of the Tectum

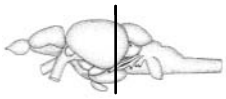

The following phenotype is visible as blocks or gaps in the tectal innervation. These blocks and gaps are called "ocular dominance column-like" (ODC-like) structures. ODCs represent groups of cells on one tectal half that receive input only from one eye, whereas adjacent groups of cells receive input only from the other eye. This is the case in the lateral geniculate of mammals (Kandel 2000), contrary to fish and amphibians where nearly all optic axons cross to the contralateral side at the chiasm. Hence, no ODC-like structures are established (Figure 24a, 12 out of 12 animals) in wild type zebrafish. ODC-like structures in the ipsilateral tectal half of *astray* mutants (right arrow Figure 24b, 15 out of 15 animals) are never seen in wild type animals (Figure 24a, 12 out of 12 animals). ODC-like structures in the tectal termination layers on the contralateral side which can be found in *astray* mutants (left arrow Figure 24b, 13 out of 15 animals) are also never seen in wild type animals. Expressed as percentages, 0% of wild types and 100% of *astray* mutants exhibit ipsilateral ODC-like structures (Figure 24d) and 87% of *astray* mutants show contralateral ODC-like structures of missing innervation (Figure 24c). According to Fisher's Exact Test both occurrences are highly significant ($P < 0.001$). For a summary see Figure 43 and 44. The ODC-like structures which are found in *astray* mutants are probably a consequence of axons re-crossing the midline after the chiasm. Thus, having optic axons from both eyes on one tectal half leads to the occurrence of ODC-like structures. A similar pattern can be induced by forcing axons from both retinas onto one tectal half which is achieved by crushing both optic nerves and ablation of one tectal half (unpublished observations).

These data suggest that ODC-like structures in the innervation pattern in *astray*/*robo2* mutants result from axon-axon competition. Tracing of one optic nerve visualizes these structures very clearly in *astray* mutants (Figure 24b, c, d).

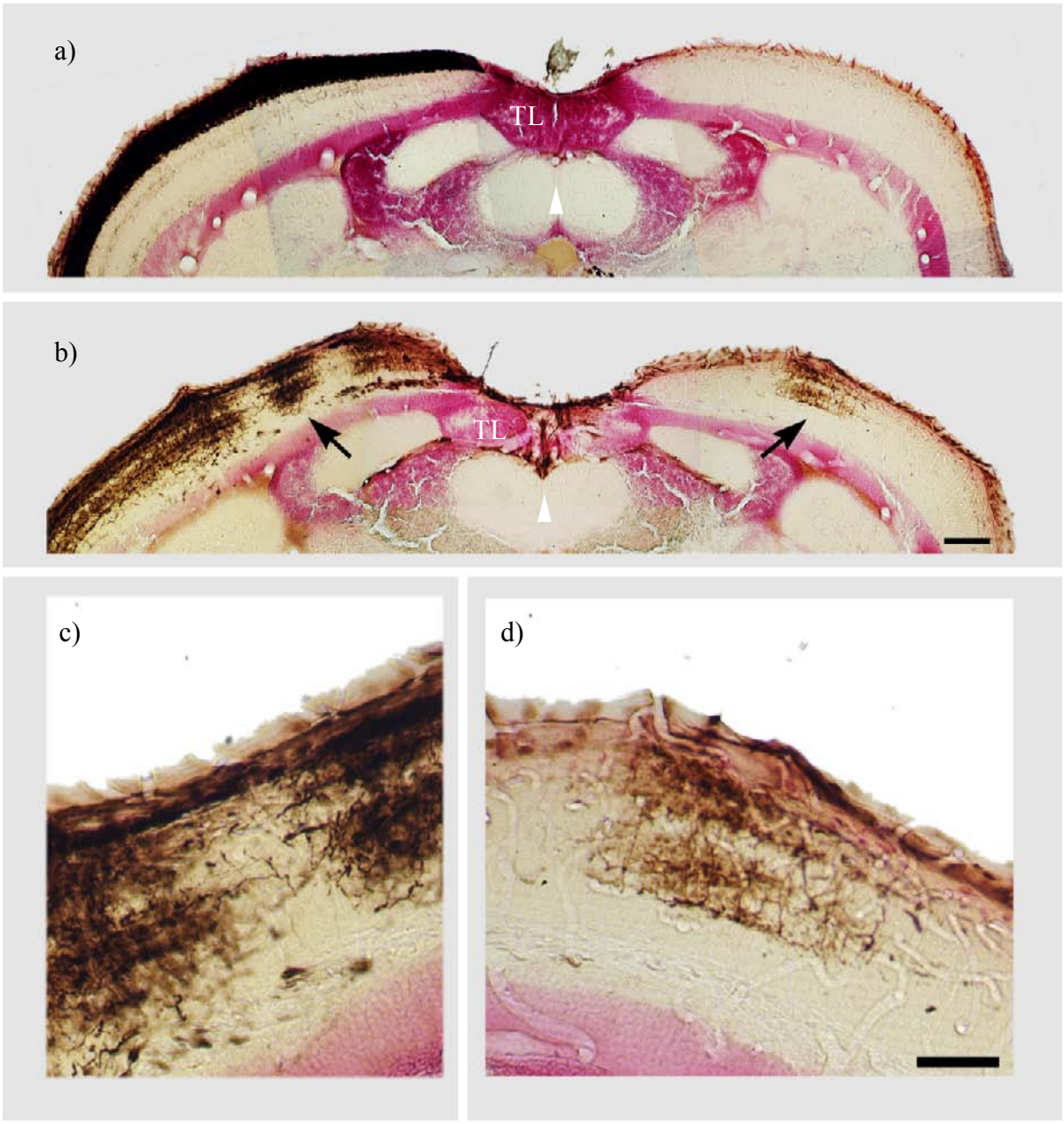

Figure 24: Ocular dominance columns (ODCs) appear in the tectum of *astray* mutants. In wild type fish (a) all optical axons from one eye cross to the contralateral side so there are no ODC-like columns visible when tracing an optic nerve with biocytin unilaterally. Aberrant crossing events in *astray* mutants during development lead to ODCs (b, black arrows). c and d: Magnifications of the ODCs from the *astray* fish; c = contralateral side, d = ipsilateral side. Torus longitudinalis (TL) is indicated for orientation. Dorsal is up. All sections were counterstained with neutral red. Scale bar in b = 100µm; d = 50µm.

3.3.2.4 Irregular Growth of Optic Fibers into Tectum

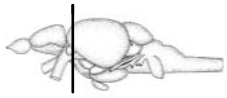

Defasciculation of the Optic Tract

A strong phenotype is visible for *astray* mutants at the caudal end of the chiasm and rostral part of the tectum. In wild type animals, the optic axons are clearly restricted to the surface layers of the tectum. A border can be readily observed between areas of termination (visible as a solid dark stain) and deeper tectal layers where normally only few optic axons terminate (Figure 25 a). The cell-dense region (counterstained in red) is avoided by the optic axons. The opposite was observed in the *astray* mutants. The dorsal brachium of the optic tract entered the tectum in an abnormally broad front of individual fascicles (15 out of 15 animals, Figure 25b, arrow), but never in wild type animals, indicating defasciculation of the optic tract in *astray* mutants (Figure 25b). Expressed as percentages, 0% of wild type animals and 93% of *astray* mutants exhibited defasciculation of the optic tract (difference highly significant, Fisher's Exact Test, $P < 0.001$). At the dorsal brachium the optic projection in *astray* mutants splits up into individual fascicles as if pathway cues are strongly reduced even though these fascicles still seem to aim for their target structure (tectum). For a summary see Figure 45.

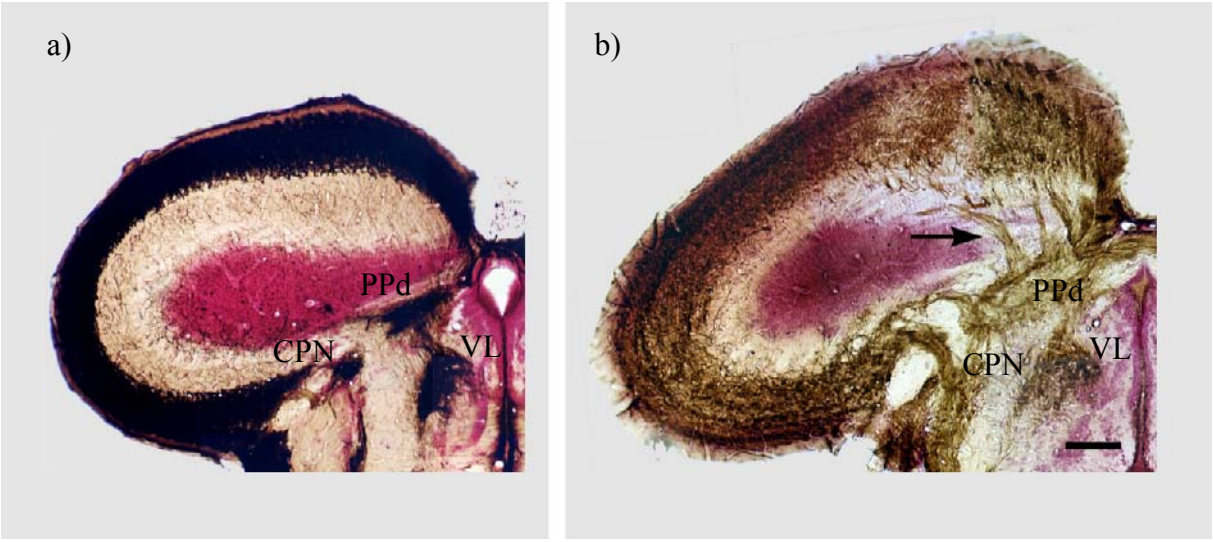

Figure 25: Strong defasciculation of the optic tract in *astray* mutants (b). a) Wild type fish show no defasciculation. b) *astray* fish displayed strong defasciculation (black arrow) at the rostral end of the tectum. CPN (central pretectal nucleus), PPd (periventricular pretectal nucleus) and VL (ventrolateral thalamic nucleus) are indicated for orientation. All sections were counterstained with neutral red. Dorsal is up. Scale bar = 100µm.

Fascicles of Optic Fibers Below Fiber Receiving Layers in the Tectum

Fascicles are thick bundles of fibers growing in a straight fashion, compared to terminals which are thinner and strongly branched out. Fascicles of optic fibers are visible below the optic fiber receiving layer in *astray* fish (13 out of 15 animals) (Figure 26b, arrow). Further caudally they seem to project into the optic fiber receiving layer. This was never observed in wild type fish (0 out of 12 animals) (Figure 26a). Expressed as percentages, 0% of wild types and 87% of *astray* mutants exhibit fascicles of optic fibers below the tectum (difference highly significant, Fisher's Exact Test, $P < 0.001$). Some fascicles of the optic projection in *astray* mutants can be found to transvers a layer below the fiber receiving layer, possibly due to a slight additional or missing guidance cue radiating from adjacent structures to their tectal termination goal. For a summary see Figure 46.

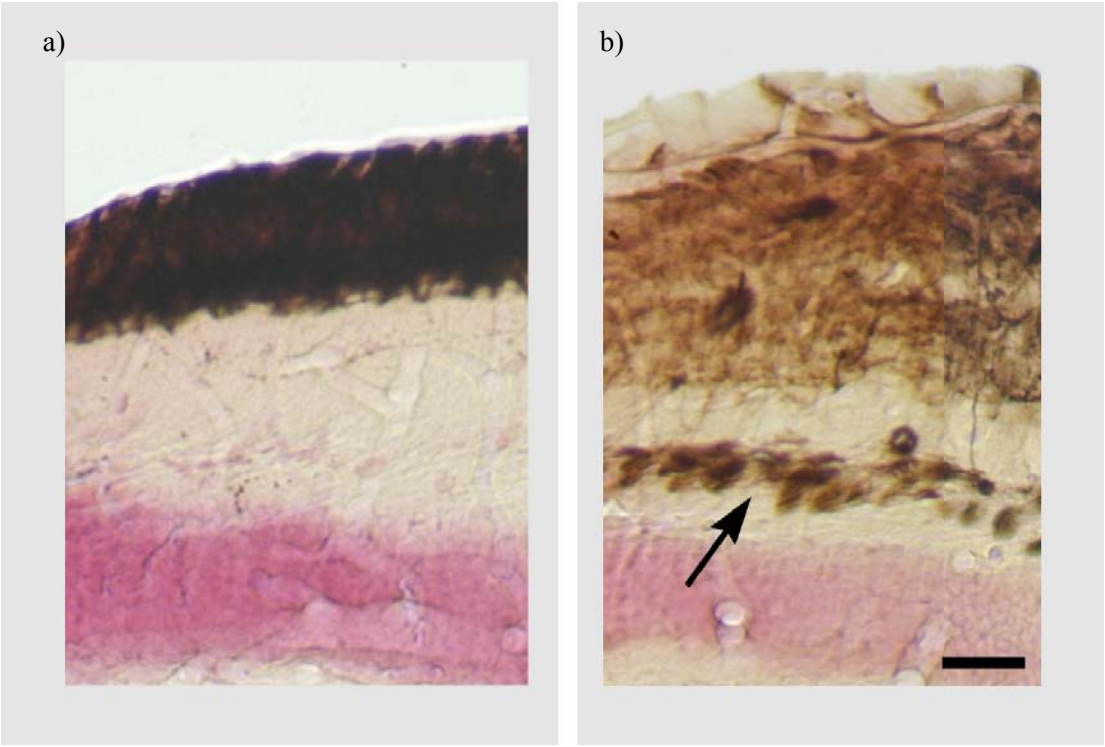

Figure 26: Fascicles of optic fibers below the optic fiber receiving layer in *astray* mutants. Fascicles of optic fibers are visible below the optic fiber receiving layer in *astray* fish (b, arrow). No fascicles can be observed in the wild type (a). All sections were counterstained with neutral red. Dorsal is up. Scale bar in b = 25 µm.

The Optic Chiasm

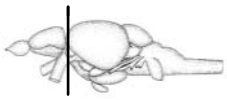

At the optic chiasm, where optic axons cross to the contralateral side, the numbers of aberrant misguided axons in *astray* fish were similar to those in wild type fish. 7% of *astray* fish (Figure 27b and d) and 17% of wild type fish (Figure 27a and c) exhibited ipsilateral fibers in the optic chiasm. According to Fisher's Exact Test this difference is not significant, expressing that wrong crossing events at the chiasm happen as often in *astray* mutants as in wild type fish. Thus, *robo2* seems not to have any influence on the crossing events at the chiasm of the optic projection in zebrafish.

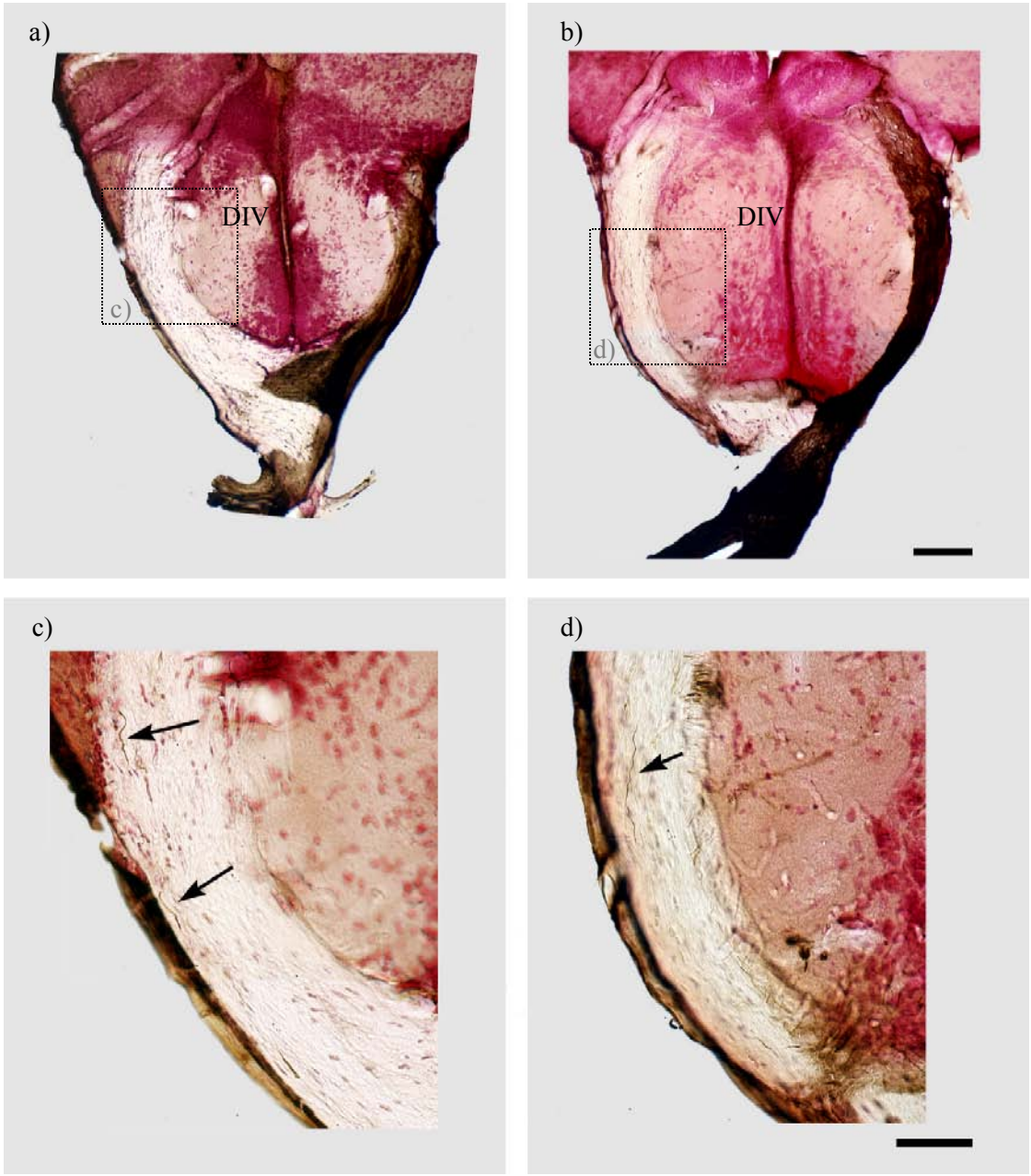

Figure 27: Ipsilateral fibers at the optic chiasm. No significant difference in ipsilateral fibers at the optic chiasm could be observed comparing wild type (a, c) and *astray* (b, d) fish. Diencephalic ventricle (DIV) is indicated for orientation. All sections were counterstained with neutral red. Dorsal is up. Scale bar in b = 100µm; scale bar in d = 50µm.

3.3.3 Conditional Knock Down of *robo2* During Early Development

We aimed to determine whether continuous absence of *robo2* during development is required for adult mis-projections to be maintained or whether interference with *robo2* expression during early establishment of the optic projection is sufficient to induce mis-projections that are maintained in adult animals. Therefore, we injected a splice-site-directed morpholino against *robo2* into eggs from a zebrafish line carrying the Brn3c:GFP transgene.
Morpholinos are active approximately 1-3 days after injection (Sumanas and Larson 2002). PCR analysis of mRNA extracts from injected larvae indicated a specific knock down of *robo2* mRNA that diminished with increasing age (Figure 28a). Analysis of the optic projection at three days of development by DiI tracing showed a phenocopy of the *astray* phenotype including telencephalic projections in 4 out of 5 larvae (Figure 28c). This was never observed in control morpholino injected larvae (Figure 28b). Thus, *robo2* morpholino specifically mimics the *astray* mutant phenotype in larvae.

Brn3c:GFP embryos were injected with a *robo2* morpholino and sorted for strong telencephalic projections and raised to adulthood. Since telencephalic labeling in larvae often appeared to be unilateral we traced optic axons from both eyes in adults, such that a potential unilateral aberration of the projection would not be missed. All (n = 5) animals raised to adulthood showed telencephalic fiber tracts. In addition we labeled four fish unilaterally to assess crossing events that would be occluded by bilateral tracing. One of these fish showed traced axons in the telencephalon and two fish showed ectopic myelinated tracts in the telencephalon that were not traced. This suggested that telencephalic mis-projections originated from the untraced eye in these animals. Thus, overall 8 out of 9 morpholino-injected embryos retained a telencephalic mis-projection in adults. This indicates that errors in the optic projection that are induced by knock down of *robo2* during a short period in early development are not corrected in the majority of cases.

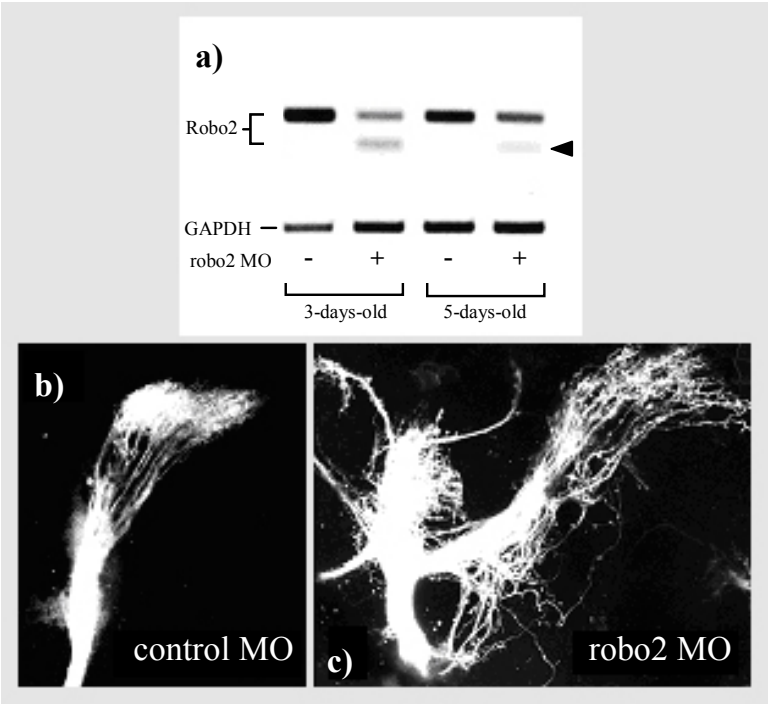

Figure 28: a) PCR analysis of *robo2* mRNA expression with and without *robo2* splice site directed morpholino (MO). The morpholino reduces the abundance of the wild type transcript and an erroneous transcript (arrowhead) becomes detectable. The morpholino effect is weaker in 5-day-old than in 3-day-old larvae. GAPDH is used as an internal standard. b) and c) Lateral views of DiI-traced optic projections (rostral is left) indicate *astray*-like pathfinding errors in *robo2* morpholino-injected, but not in control morpholino-injected 3- to 4-day-old larvae. Pictures were kindly contributed by Dr. T. Becker.

Other errors in the optic projection found in *astray* mutants were not observed in morpholino-injected animals, except for ODC-like innervation of the ipsilateral tectum in 1 of 4 unilaterally traced animals. Specifically, the tectal optic fiber layer was not thicker in any of the 9 animals (mean thickness: 47.8 ± 1.41 µm; $p<0.671$) than in uninjected wild type animals. Thus early morpholino injection leads to permanent telencephalic projections (Figure 29), but other errors might be corrected due to the highly dynamic structures of terminal arbors in adult teleost fish (Stuermer and Easter 1984).

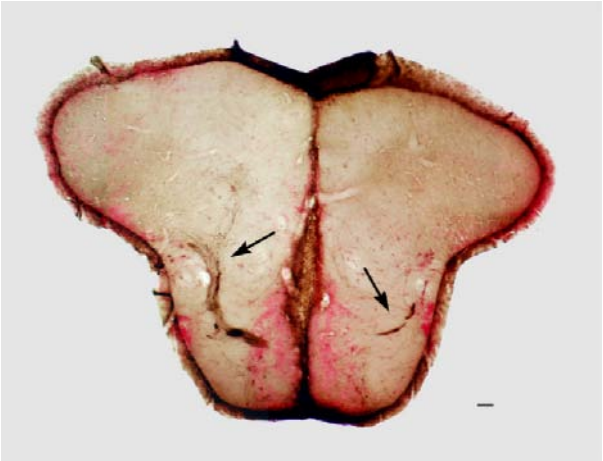

Figure 29: *Robo2* morpholino injection in early development leads in most cases (89%) to permanent telencephalic projections (arrows). Dorsal is up. Section is counterstained with neutral red. Scale bar = 50µm.

3.3.4 Pathfinding Errors in the Regenerated Optic Projection of *astray*/*robo2* Mutants

Having already mapped and analyzed whether developmental mis-projections are retained in adult *astray* mutants, a subsequent research questions could be approached:

Do optic axons regenerate along non-specific guidance cues such as ectopic degenerated optic tracts?

If this was the case, regenerating optic axons in *astray* mutants should have faithfully re-populated not only the tracts also found in wild type animals but also ectopic tracts, such that the regenerated projection in *astray* fish looks similar to the unlesioned projection in *astray* animals. Alternatively, if axons use specific pathfinding cues, ectopic tracts, which do not provide these, should be randomly entered at a lower frequency.

To answer this question, unlesioned *astray* mutants were compared to 4 week post lesion *astray* mutants with a regenerated optic projection to examine possible reoccurring pathfinding errors in these fish. We determined whether regenerating optic axons projected to the telencephalon in *astray* mutants that were pre-selected as larvae for the presence of ectopic telencephalic tracts (see Figure 17). These animals were raised, received an optic nerve lesion and the regenerated projection was traced from one eye at 4 weeks post-lesion.

All the phenotypes described so far for the unlesioned *astray* mutant fish, introduced in Chapter 3.3.2 were investigated in *robo2* mutants with a regenerated optic projection.

3.3.4.1 Irregular Growth into Telencephalon and Tegmentum in *astray* Mutants with a Regenerated Optic Projection

Telencephalon

Ectopic tracts in the telencephalon in regenerating *astray* mutants were observed in 1 of 15 animals (Figure 30b). No ectopic tracts could ever be observed in regenerated wild type fish (0 out of 13 animals) (Figure 30a). Expressed in percentage, 0% of wild type animals and 7% of *astray* mutants, both with a regenerated optic projection displayed ectopic telencephalic tracts. The occurrence of ectopic telencephalic fibers in unlesioned (found in 14 out of 15 animals) *astray* mutants compared with *astray* mutants with a regenerated optic projection is significantly different (Fisher's Exact test, $P < 0.001$). Expressed as percentages, 93% of unlesioned *astray* mutants and only 7% of *astray* mutants with a regenerated optic projection displayed ectopic telencephalic fibers. For a summary see Figure 38. If regenerating optic axons followed degenerated tracts, we should be able to observe ectopic telencephalic tracts in *astray* mutants with a regenerated optic projection. Since this could only be observed in one case, this suggests that ectopic degenerating tracts that are present in unlesioned adult *astray* mutants are not used as a guidance cue.

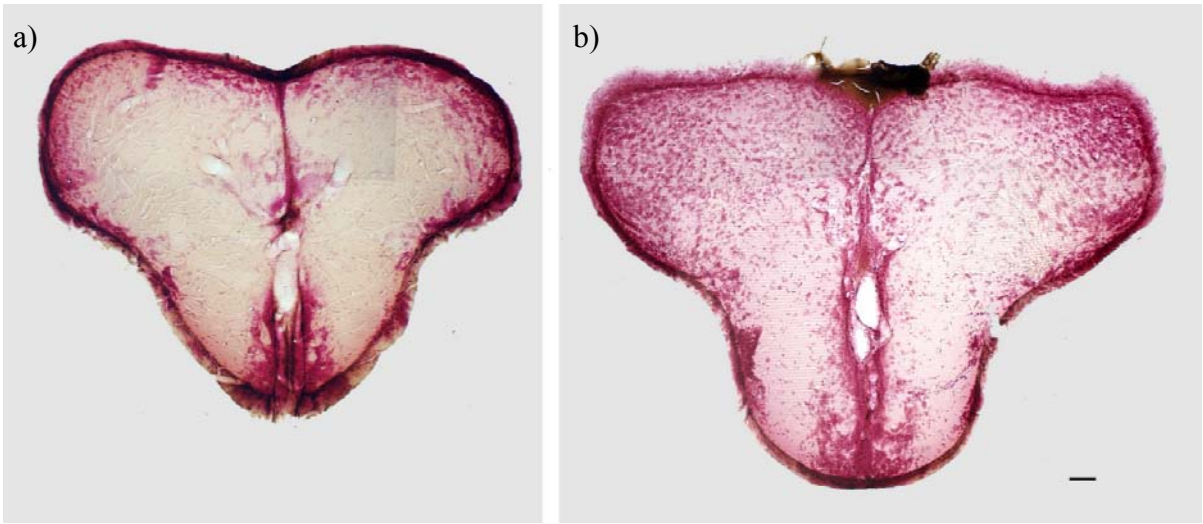

Figure 30: No ectopic optic tracts in the telencephalon of animals with a regenerated optic projection. No optic tracts could be seen in the telencephalon of wild type fish (a) or *astray* animals (b) both with regenerated optic projections. Dorsal is up. All sections are counterstained with neutral red. Scale bar in b = 100µm.

Tegmentum

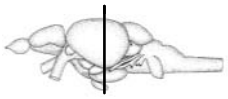

In the tegmentum, optic fibers were present in 1 of 15 *astray* mutants with a regenerated optic projection, which was not significantly different from observations in unlesioned animals (4 out of 15 animals). Expressed as percentages, 0% of wild types (13 out of 13 animals) and 7% of *astray* mutants (1 out of 15 animals), both with a regenerated optic projection, exhibited optic fibers in the tegmentum (difference not significant, Fisher's Exact Test, P = 0.33). Comparing unlesioned *astray* mutants versus *astray* mutants with a regenerated optic projection, 27% of unlesioned and only 7% of the *astray* mutants with a regenerated optic projection displayed fibers in the tegmentum. The reduced percentage of optic fibers in the tegmentum of animals with a regenerated optic projection reflects the similar finding seen in the telencephalon, giving a hint that degenerating tracts are not used as guidance cues for regeneration of the optic projection. No pictures were taken for the *astray* mutants with a regenerated projection because it looked very similar to the *astray* mutant, which did not receive a lesion to the optic nerve (see Figure 20 for comparison). For a summary see Figure 39.

3.3.4.2 Termination Errors in a Regenerated Optic Projection

Retino-Recipient Pretectal Targets

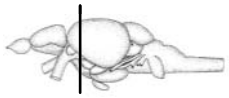

Retino-recipient pretectal nuclei, the central pretectal nucleus (CPN), the periventricular pretectal nucleus (PPd), the anterior thalamus (A) and the ventrolateral thalamic nucleus (VL), were expanded and diffusely re-innervated in 14 out of 15 *astray* mutants with a regenerated optic projection (Figure 31b,c), resembling the innervation pattern in unlesioned *astray* mutants. The regenerated innervation of pretectal nuclei in wild type animals (0 out of 13 animals, Figure 31a) was highly precise and undistinguishable from unlesioned wild type fish (see section 3.3.2.2, Figure 21a).

In *astray* mutants, these expanded termination fields have lost their discrete borders and are hard to recognize. Expressed as percentages, 15% of wild type animals and 93% of *astray* mutants, both with a regenerated optic projection, displayed termination errors in the pretectal nuclei (highly significant, Fisher's Exact Test, P < 0.001). Comparing unlesioned and lesioned *astray* mutants, 100% of the unlesioned and 93% of the *astray* mutants with a regenerated optic projection exhibited termination errors. Frequency of the reoccurence of

these termination errors is different from errors described in section 3.3.4.1 and discussed at the end of section 3.3.4.2. For a summary see Figure 40.

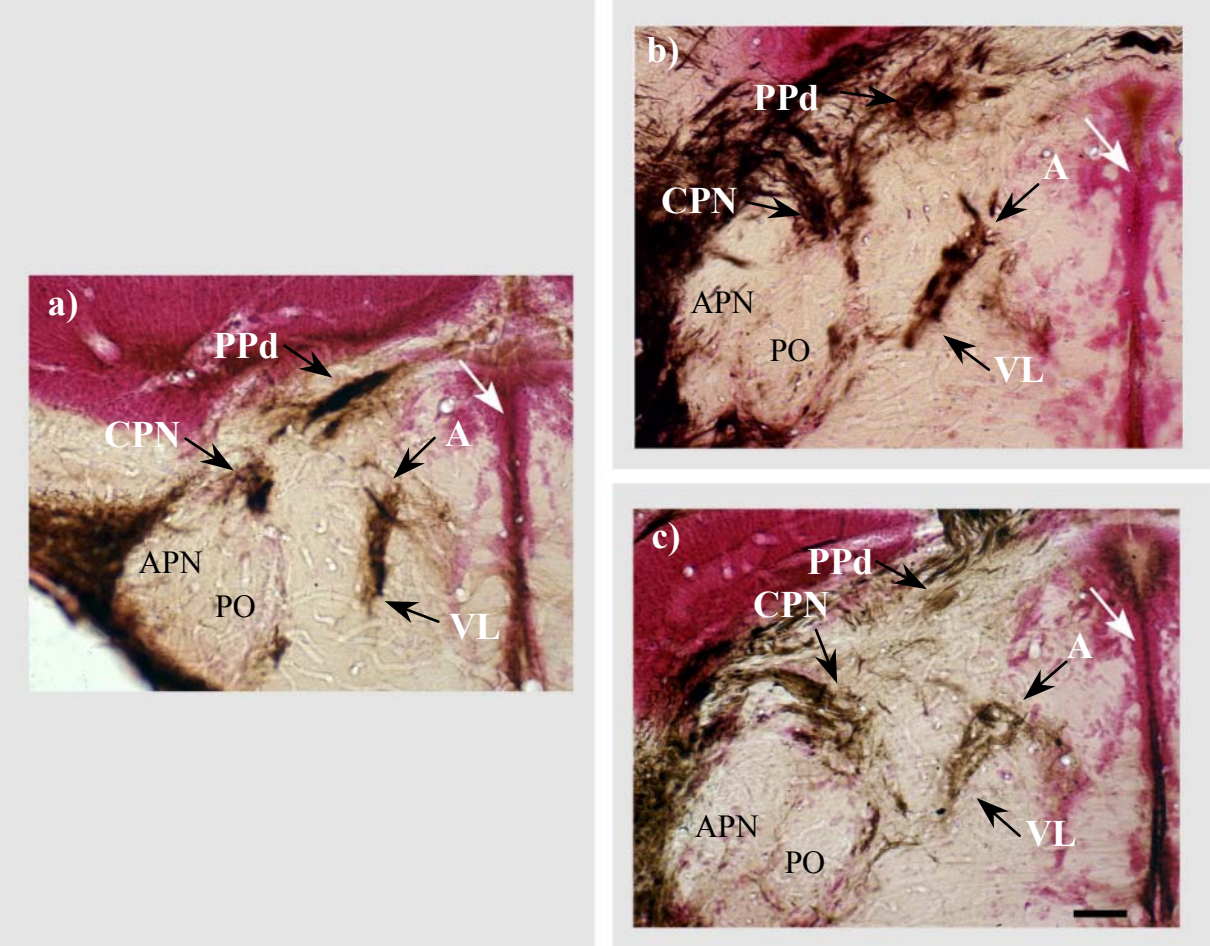

Figure 31: Expanded retino-recipient pretectal nuclei in *astray* with a regenerated optic projection. After a left optic nerve lesion pretectal nuclei such as the central pretectal nucleus (CPN), the periventricular pretectal nucleus (PPd), the anterior- (A) and the ventrolateral thalamic nucleus (VL) were diffusely re-innervated in 14 out of 15 *astray* mutants (b and c, black arrows), resembling the innervation pattern in unlesioned *astray* mutants. The regenerated innervation of pretectal nuclei in wild type animals (a) was always highly precise. The accessory pretectal nucleus (APN) and the posterior pretectal nucleus (PO) are avoided by axon fibers in all cases. Dorsal is up. All sections have been counterstained with neutral red. White arrows indicate midline. Scale bar in F = 50µm.

Thickness of Tectal Termination Fields

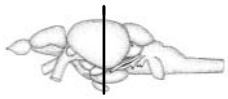

The thickness of the optic fiber receiving layer in *astray* mutants with a regenerated optic projection, mean thickness: 89.6 ± 2.62µm (SEM, standard error of the mean), was comparable to that in unlesioned *astray* mutants, mean thickness: 92.4 ± 3.7µm (SEM) and significantly thicker ($P < 0.001$) than in wild type animals with a regenerated optic projection with a mean thickness of 48.5 ± 1.9µm (SEM) (Figure 32a,b). The thickness of the tectal termination zone is between 37.8 µm and 61.6 µm in wild type fish and in the astray mutant thickness always lies between 74.2 µm and 102.2 µm. Contrary to the results from chapter 3.3.4.1, where the frequency of reoccurring errors concerning irregular growth into a wrong region diminishes, termination errors in the regenerating optic projection are not (thickness) or only marginally (pretectal nuclei) reduced compared to unlesioned *astray* mutants. This suggests that regenerating fibers from the optic projection are as strongly influenced in their termination behavior as those seen in *astray* mutants with an unlesioned optic projection. For a summary see Figure 41.

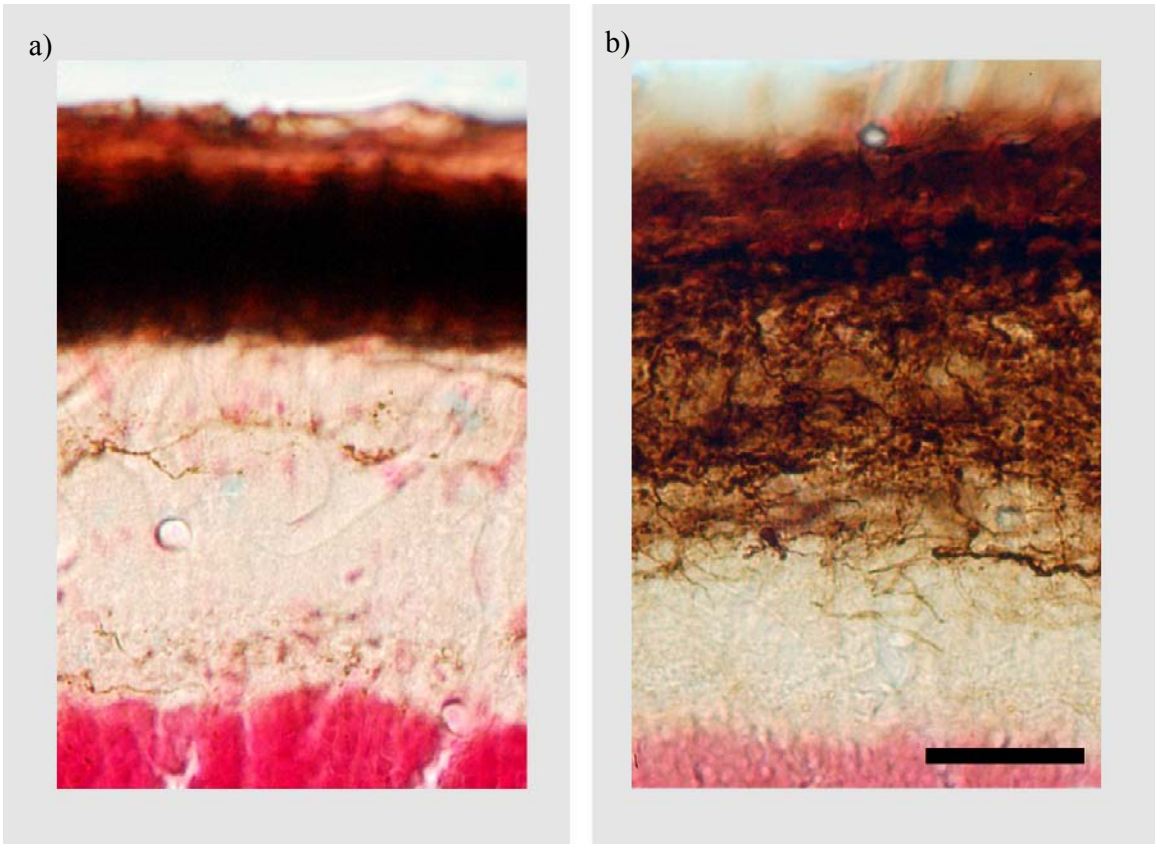

Figure 32: The thickness of the tectal termination layers is nearly doubled in *astray* mutants with a regenerated optic projection(b) compared to wild type animals with a regenerated optic projection(a). These observations are very similar to the unlesioned wild type and unlesioned *astray* phenotypes. Measurements were taken at the plane of section where the rostral part of the oculomotor nucleus appears. Dorsal is up. All sectioned are counterstained with neutral red. Scale bar in b = 50µm.

3.3.4.3 Midline Crossing Errors in a Regenerated Optic Projection

Crossing at the Posterior Commissure

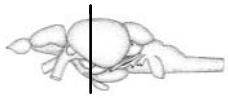

In the posterior commissure, regenerated fibers were present in 6 out of 15 *astray* animals with a regenerated optic projection (Figure 33c), compared to 12 out of 15 in unlesioned *astray* animals (see Figure 23). This corresponds to 73% of the unlesioned group displaying the phenotype compared to only 40% of the group with a regenerated optic projection. Comparing unlesioned *astray* mutants and *astray* mutants with a regenerated optic projection there is no significant difference in the occurrence of fibers in the posterior commissure according to Fisher's Exact Test (P = 0.139). Hence, 60% of *astray* mutants with a regenerated optic projection show no aberrant crossing of fibers (Figure 33b). No crossing fibers could be observed in wild type fish (n = 13) with a regenerated optic projection (Figure 33a). Even though not significant, a reduction in crossing events in the *astray* mutant with a regenerated optic projection can be observed, mirroring the results of section 3.3.4.1. It thus seems improbable that the regenerating optic tracts in *astray* mutants use degenerating tracts as guidance cues. For a summary see Figure 42. Qualitative inspection of *astray* fish with aberrant crossings suggested that the numbers of crossing fibers were reduced in the animals with a regenerated optic projection compared to the unlesioned ones (data not shown).

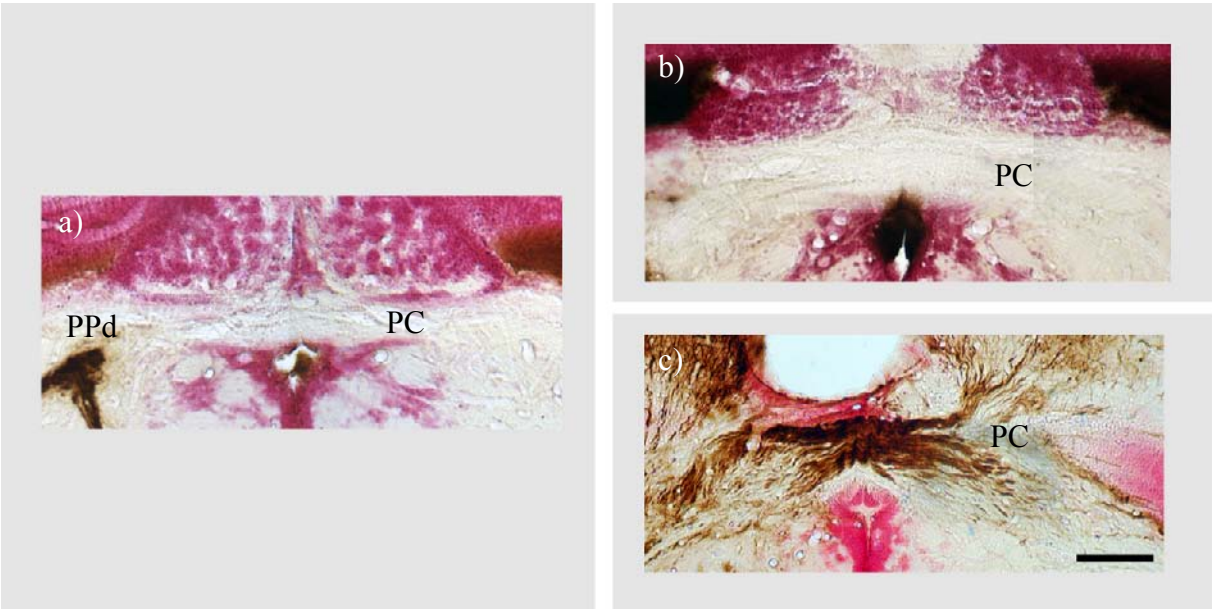

Figure 33: Wild type animals with a regenerated optic projection do not display crossing fibers at the PC (a). The number of crossing fibers in the posterior commissure (PC) is reduced in *astray* mutants with a regenerated optic projection (b) compared to unlesioned *astray* mutants. Strong crossing events in *astray* mutants with a regenerated optic projection (c) could rarely be observed. Wild type animals with a regenerated optic projection never showed any crossing in the PC. Sections are counterstained with neutral red. The periventricular pretectal nucleus (PPd) is given for orientation. Dorsal is up. Scale bar in c = 50µm

Ipsi- and Contralateral Innervation of the Tectum

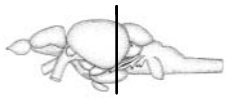

In the tectum, only 2 out of 15 (13%) *astray* animals with a regenerated optic projection showed ipsilateral tectal innervation (Figure 34b), compared to 15 out of 15 (100%) unlesioned *astray* mutants. In the contralateral tectum, the occurrence of ocular dominance-like gaps could only be observed in 8 out of 15 (53%) *astray* animals with a regenerated optic projection (Figure 34b), compared to 13 out of 15 (87%) animals in unlesioned *astray* mutants. In the *astray* mutants with a regenerated optic projection, the appearance of ipsilateral ODC-like structures is compared to unlesioned *astray* mutants significantly reduced (Fisher's Exact Test, $P < 0.001$). The occurrence of contralateral ODC-like structures is similar between unlesioned *astray* mutants and *astray* mutants with a regenerated optic projection (difference not significant, Fisher's Exact Test, $P = 0.109$). Neither ipsilateral blocks nor contralateral gaps of innervation in the tectum can be found in wild type fish (n = 13, Figure 34a). The difference in occurrence of ipsilateral structures between wild type animals and *astray* mutants, both with a regenerated optic projection, is not significant (Fisher's Exact Test, $P = 0.484$). In contrast, when comparing the occurrence of contralateral gaps in wild type animals and *astray* mutants, both with a regenerated optic projection, it was significant (Fisher's Exact Test, $P = 0.002$).

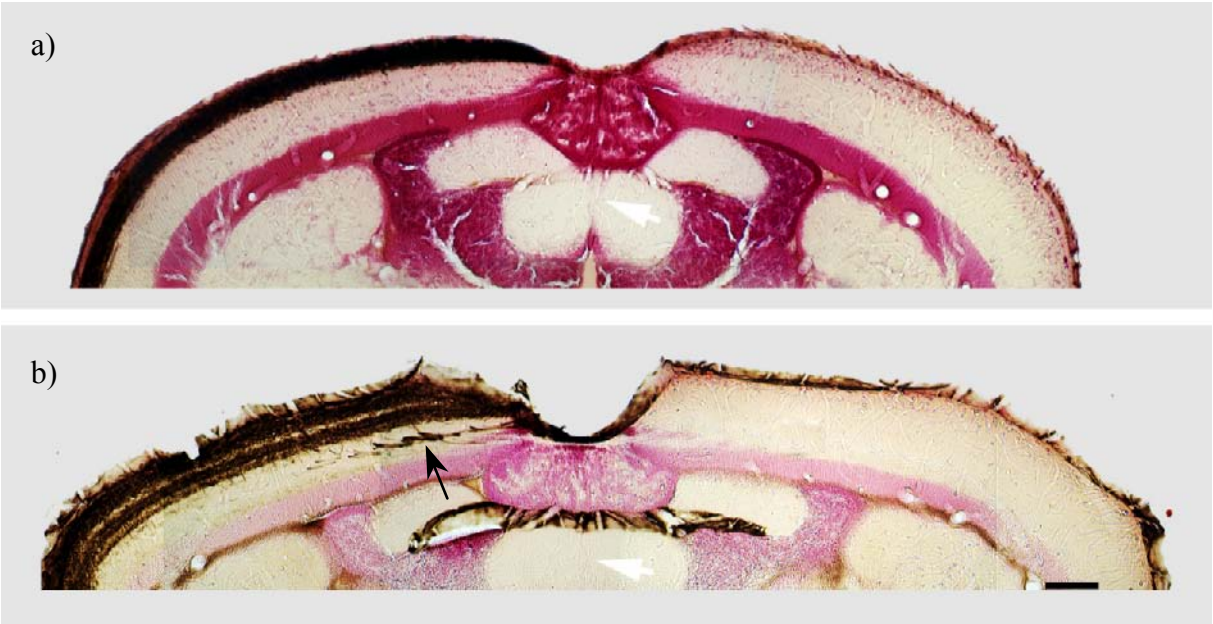

Figure 34: No ODCs could be observed in wild type fish with a regenerated optic projection (a), and the occurrence of ODCs in *astray* mutants with a regenerated optic projection is strongly reduced (b) compared to unlesioned *astray* mutants. The black arrow indicates deep fibers below the optic fiber receiving layer – see section 3.3.4.4. Sections are counterstained with neutral red. Dorsal is up. Scale bar in b = 100µm.

The frequency of occurrence of erroneous ipsilateral and contralateral structures, comparing *astray* mutants and *astray* mutants with a regenerating optic projection, is different. A possible reason could be changed parameters for fiber competition comparing the ipsi- and the contralateral tectal half. The regeneration paradigm stops the activity of the erroneous ipsilateral fibers in the tectum. Thus, allowing the remaining fibers to invade these regions. For a summary see Figure 43 and 44.

3.3.4.4 Irregular Growth into Tectum in a Regenerated Optic Projection

Defasciculation of the Dorsal Optic Tract

Defasciculation of the dorsal brachium of the optic tract entering the tectum in an abnormally broad front of individual fascicles (Figure 35b, arrow) was observed in all *astray* mutants with a regenerated optic projection (15 out of 15 animals) (Figure 35b), comparable to the unlesioned *astray* mutants (15 of 15). Wild type animals with regenerated optic projections never displayed this phenotype (0 out of 13 animals, Figure 35a), implying that *robo2* is necessary for correctly entering the tectum during regeneration. The degenerating optic tracts could theoretically also be a guidance factor, but knowing that other *astray* phenotypes like the telencephalic fibers (see section 3.3.4.1) or ODC-like structures (see section 3.3.4.3) are significantly reduced in the *astray* mutants with a regenerated optic projection, this possibility is regarded as unlikely. 0% of wild type animals and 100% of *astray* mutants, both with a regenerated optic projection displayed defasciculation of the dorsal optic tract (difference highly significant, Fisher's Exact Test, $P < 0.001$). Comparing unlesioned *astray* mutants and *astray* mutants with a regenerated optic projection, 100% of the unlesioned and 100% of the *astray* mutants with a regenerated optic projection exhibited defasciculation of the dorsal brachium. Thus, *robo2* seems to have major impact in development as well as in regeneration regarding the fasciculation of the dorsal brachium. For a summary see Figure 45.

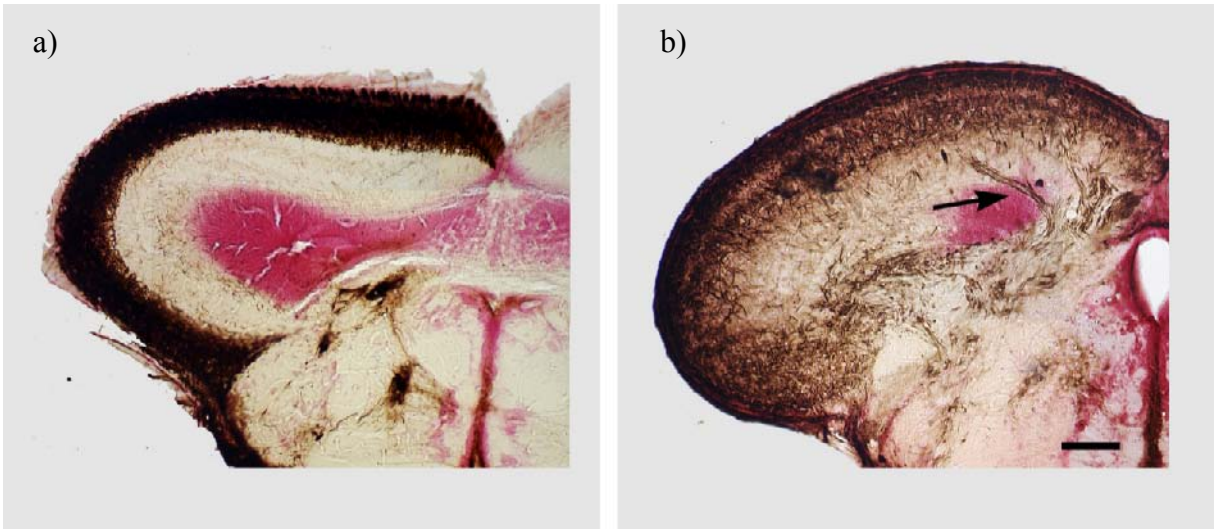

Figure 35: Individual fascicles enter the tectum of the *astray* mutant with the regenerated optic projection in an abnormal fashion (b, arrow). Defasciculation of the optic tract could be observed in all *astray* mutants with a regenerated optic projection (b) but never in wild type animals with a regenerated optic projection (a). The *astray* mutants with a regenerated optic projection showed a similar degree of defasciculation as the unlesioned *astray* mutants. Sections are counterstained with neutral red. Dorsal is up. Scale bar in b = 100µm.

Fascicles of Optic Fibers Below Fiber Receiving Layer in the Tectum

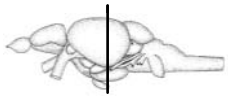

Astray mutants with a regenerated optic projection (10 out of 15 animals) (Figure 36b) display fascicles (see section 3.3.2.4) of optic fibers running below the optic fiber termination layers, as do the unlesioned *astray* mutants (13 out of 15 animals). This never occurs in wild type animals with a regenerated optic projection (0 out of 13 animals) (Figure 36a). 0% of wild type animals and 67% of *astray* mutants, both with a regenerated optic projection, displayed fascicles of optic fibers below the fiber receiving layer (difference significantly different, Fisher's Exact Test, $P < 0.001$). Comparing unlesioned *astray* mutants and *astray* mutants with a regenerated optic projection, 87% of the unlesioned and 67% of the regenerated *astray* mutants exhibited fascicles below the fiber receiving layer in the tectum (difference not significant, Fisher's Exact Test, $P = 0.39$). Fibers of these fascicles leave this area dorsally and terminate in the fiber receiving layers. For a summary see Figure 46.

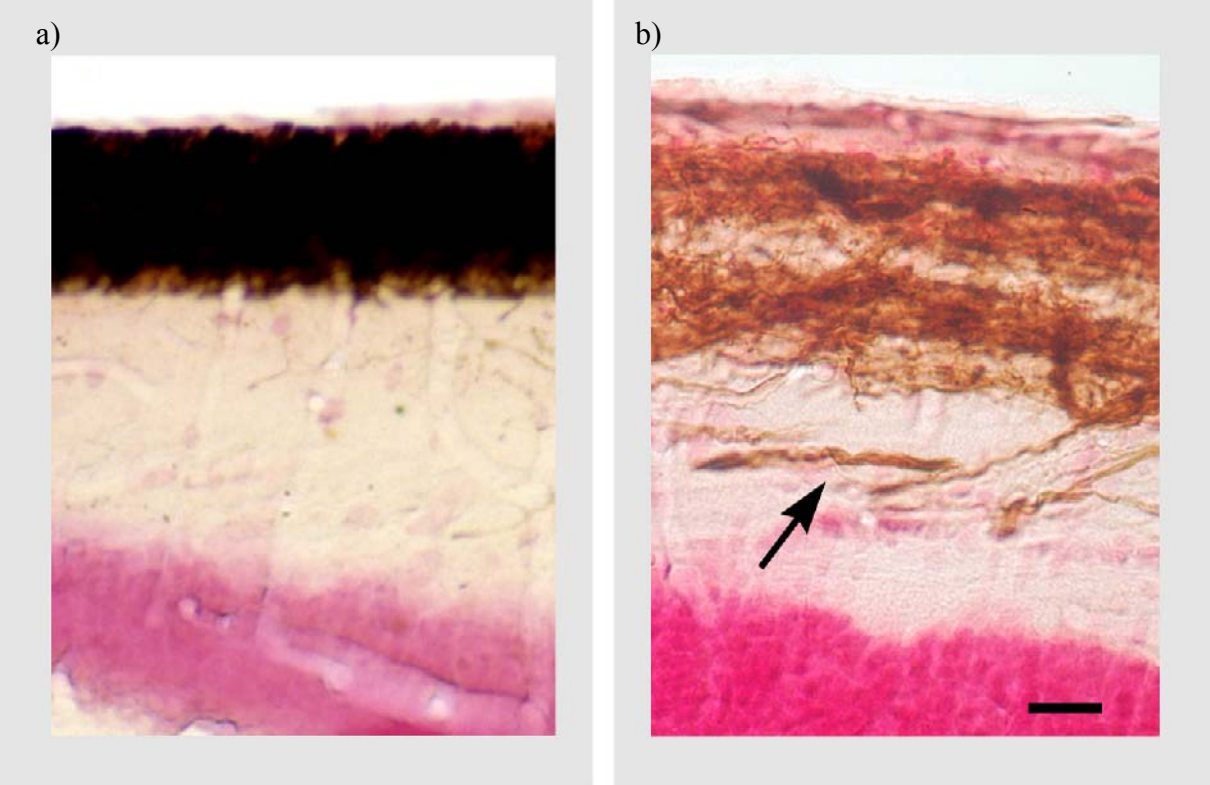

Figure 36: ***Astray*** **mutants with a regenerated optic projection (b) show fascicles of optic fibers running below the optic fiber termination layers in the tectum. These fibers leave this area dorsally and terminate in the optic fiber receiving layers. This never occurs in wild type animals with a regenerated optic projection (a) where axons run superficially. Sections are counterstained with neutral red. Dorsal is up. Scale bar in b = 25µm.**

The Optic Chiasm in Fish with a Regenerated Optic Projection

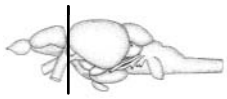

Even though ipsilateral fibers were observed in *astray* mutants with a regenerated optic projection (Figure 37b, 8 of 15 animals) at a higher frequency than in unlesioned *astray* mutants (1 out of 15 animals, difference significant, Fisher's exact test, P = 0.014), this proportion still matched that of wild type animals with a regenerated optic projection (Figure 37a, 6 out of 13 animals). This confirms our earlier observation that regenerating optic axons show an elevated rate of ipsilateral growth during regeneration even in wild type animals (Becker, Meyer et al. 2000). This indicates that *robo2* deficiency does not influence the frequency of erroneous ipsilateral axon growth in the chiasm during optic nerve regeneration.

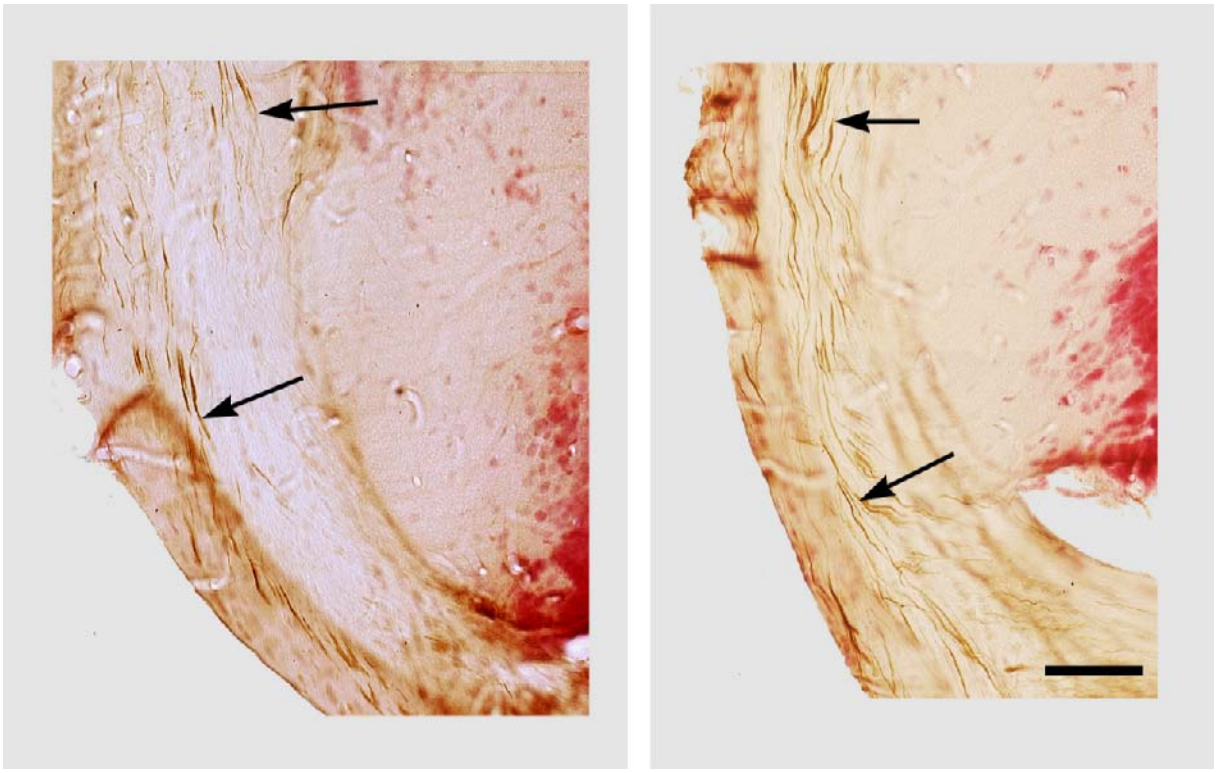

Figure 37: In animals with a regenerated optic projection, wild type fish (a) and astray mutants (b), an increased amount of ipsilateral fibers in the optic tract can be observed. Sections are counterstained with neutral red. Dorsal is up. Scale bar in b = 50µm.

A summary of the results from section 3.3.4 suggests that many pathfinding errors of optic axons (rostro-caudal pathfinding error, ectopic midline crossing) occur much less frequently whereas other phenotypical errors such as irregular growth into the tectum and termination errors in the pretectum and tectum are repeated during regeneration in *astray* mutants. Repetition of errors could have occurred because *robo2* is required for pathfinding and correct termination of regenerating axons. Judging by the reduced frequency of rostro-caudal pathfinding errors and ectopic midline crossing errors in regenerating axons, degenerating tracts do not seem to guide regenerating tracts in *astray* mutants significantly.

3.3.4.5 Graphical Summary of Phenotypical Errors and Occurrence in Lesioned and Unlesioned *astray* Fish

Accompanying each phenotypical error as investigated in section 3.3 the following graphs display an overview of animal test groups and their phenotypical error frequency.
The following two graphs are a summary of irregular growth into the telencephalon and the tegmentum (section 3.3.2.1 and 3.3.4.1).

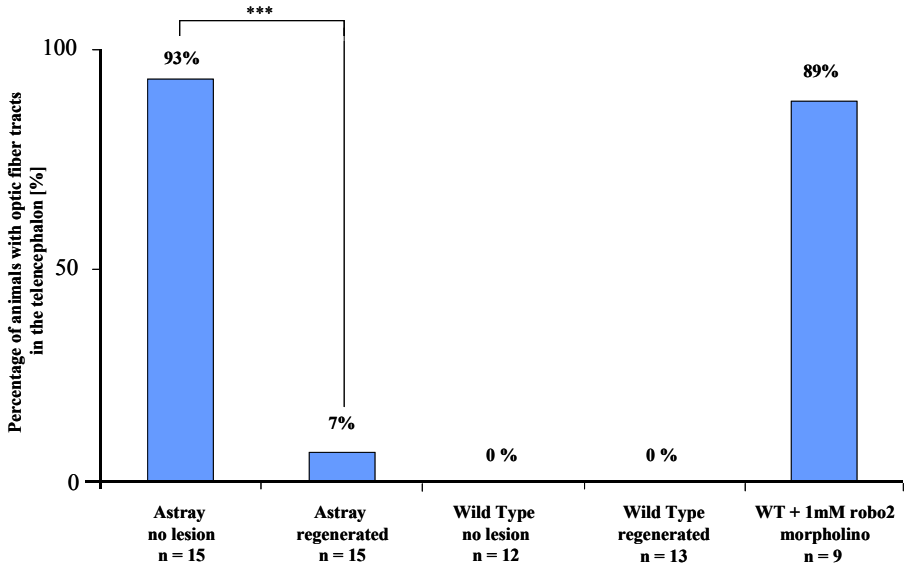

Figure 38: Animals with optic fiber tracts in the telencephalon. A significant difference between the unlesioned *astray* and *astray* with a regenerated optic projection was observed. Since nearly no ectopic optic fibers could be found in the *astray* mutants with a regenerated optic projection, it seems that degenerated tracts are not a good guidance cue. Furthermore, these results imply that *robo* is not involved in the process of avoiding the telencephalon during the regeneration of the optic projection. The *robo2* morpholino injected wild type kept telencephalic fibers until adulthood which were induced in early development, showing that pathfinding errors of the optic projection in development are not corrected until adulthood. *** = p < 0.001

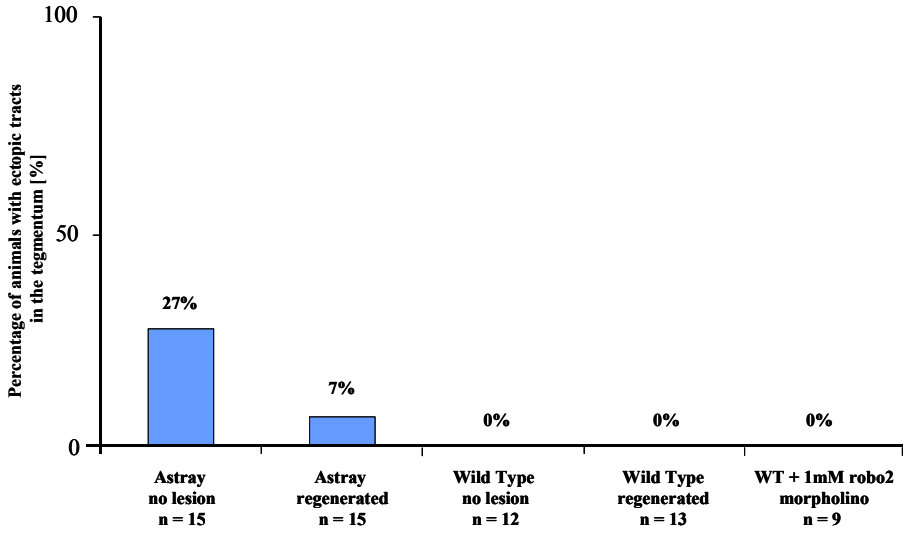

Figure 39: Animals with ectopic tracts in the tegmentum. No significant difference between unlesioned *astray* and *astray* with a regenerated optic projection was found. However, a tendency is observable hinting at the idea that more pathfinding cues beside *robo* are used for the regeneration of the optic projection.

The following two graphs are a summary of termination errors (section 3.3.2.2 and 3.3.4.2).

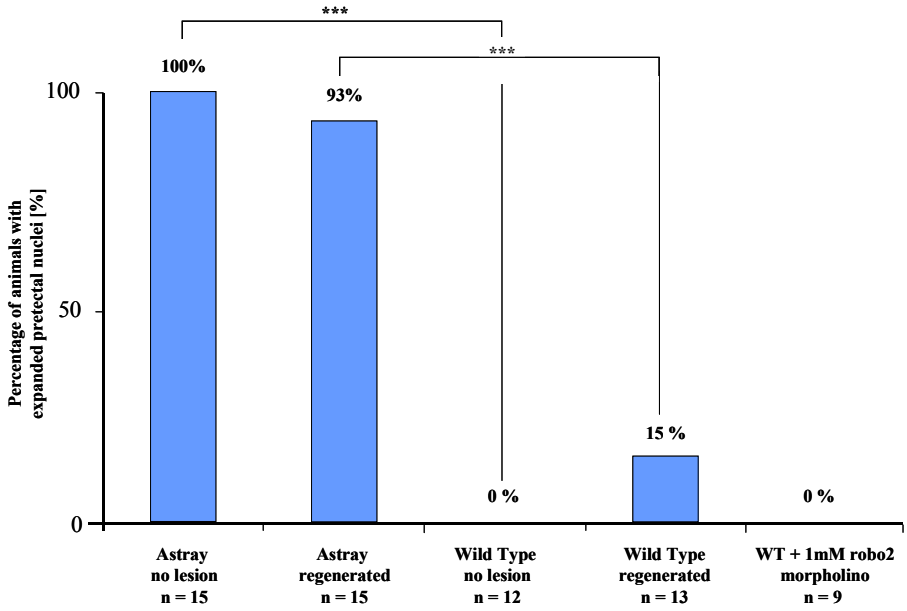

Figure 40: Animals with expanded pretectal nuclei. A significant difference between unlesioned animals and animals with a regenerated optic projection in *astray* mutants and wild types can be observed. *Robo* seems to have an influence on the correct pretectal target re-innervation after a lesion, since the percentage of expanded pretectal nuclei in the astray with the regenerated optic projection is nearly as high as in unlesioned *astray* mutants; *** = p < 0.001

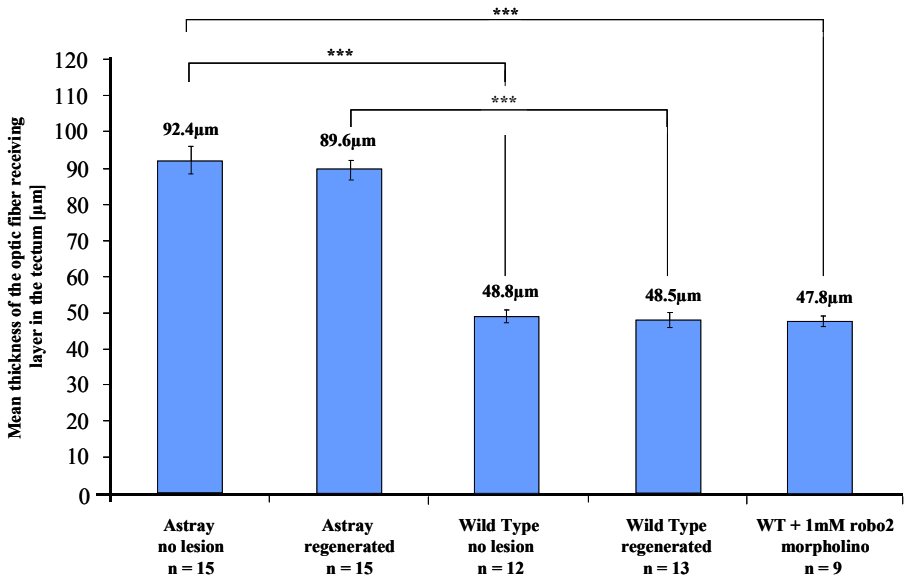

Figure 41: Mean thickness of the optic fiber receiving layer in the tectum. A significant difference between *astray* mutants and wild types can be observed. The thickness of the tectal layers in *astray* mutants with a regenerated optic projection is equivalent to the unlesioned *astray* in contrary to the wild types or the morpholino injected animals. *Robo* seems to have a strong impact on the thickness of the optic fiber receiving layers not only in development but also while regeneration of the optic projection; *** = p < 0.001

The following three graphs are a summary of midline crossing errors (section 3.3.2.3 and 3.3.4.3).

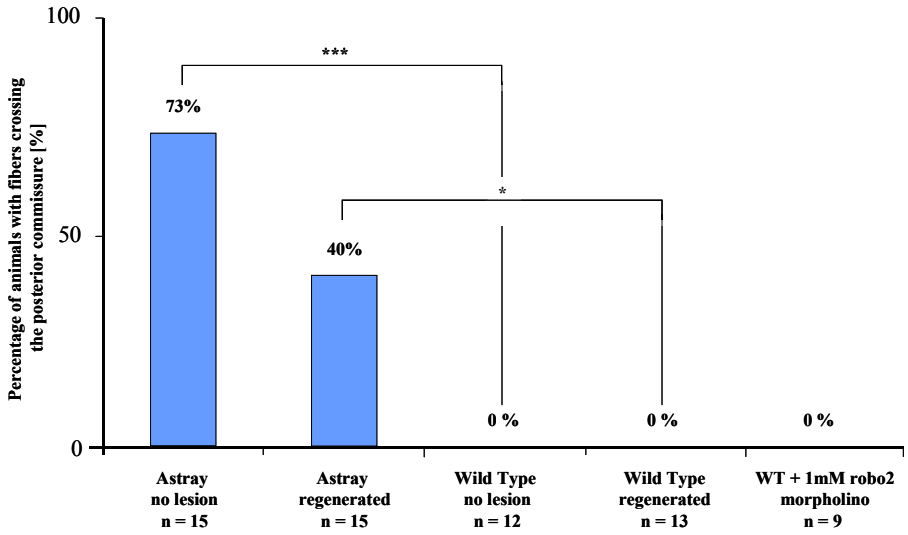

Figure 42: Animals with fibers crossing the posterior commissure; a significant difference between the *astray* and wild type in the unlesioned and regenerated case. Also a tendency is observable between unlesioned *astray* and *astray* with a regenerated optic projection. The missing *robo* seems to have a significant effect on crossing events in the PC of optic fibers during development and a slight but clearly observable trend on regenerating optic fibers; *** = p < 0.001 and * = p < 0.05

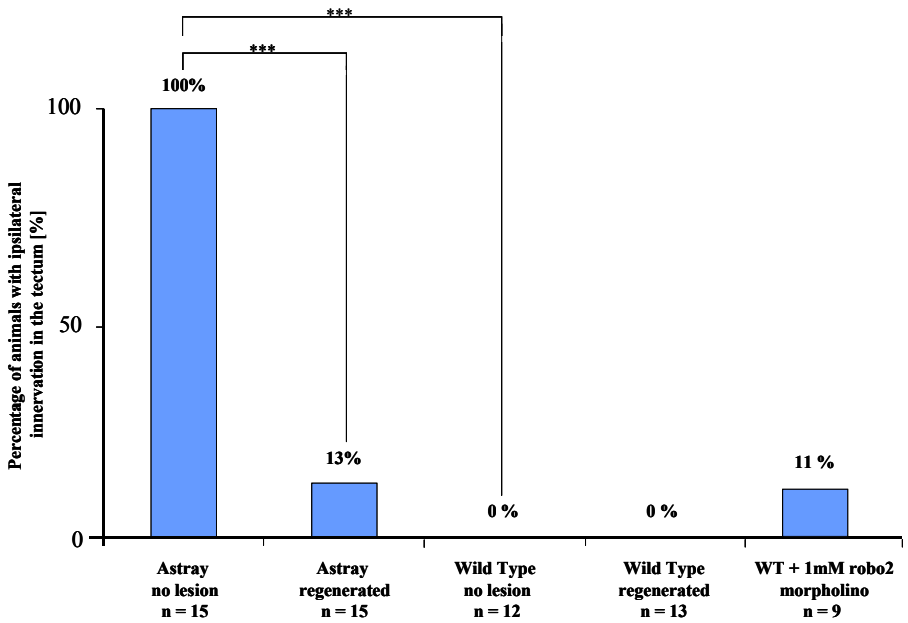

Figure 43: Animals with ipsilateral innervation in the tectum. A significant reduction from the unlesioned *astray* to the *astray* with a regenerated optic projection as well as from the unlesioned *astray* to the wild type can be observed. The regenerating optic fibers in adults seem significantly less influenced by the missing *robo* than the optic fibers growing throughout development. One of the morpholino injected animals showed ipsilateral innervation as an adult (but 4 of the 9 animals were traced bilaterally, occluding observations); *** = p < 0.001

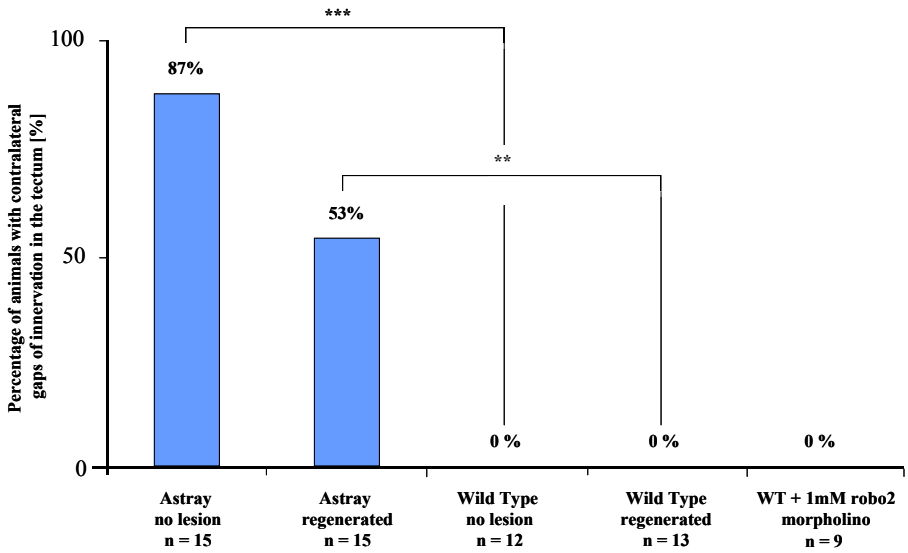

Figure 44: Animals with contralateral gaps of innervation in the tectum. A significant reduction between unlesioned animals and animals with a regenerated optic projection could be observed. In comparison to the erroneous ipsilateral innervation (see Figure 43) the difference between unlesioned *astray* mutants and *astray* mutants with a regenerated optic projection is not significant, but a tendency is observable; *** = p < 0.001 and ** = p < 0.01

The following two graphs are a summary of irregular growth into the tectum (section 3.3.2.4 and 3.3.4.4).

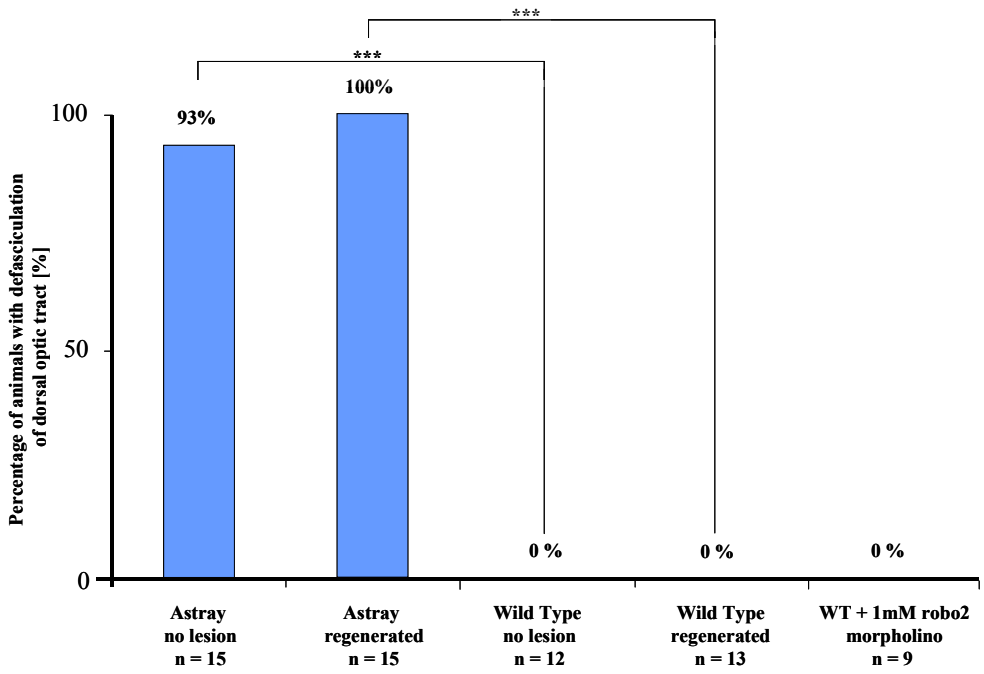

Figure 45: Animals with defasciculation of the dorsal optic tract. A significant difference between *astray* mutants and wild types in both, the unlesioned animals and those with a regenerated optic projection, can be observed. *Robo* seems to have a strong impact on the regenerating optic axons reaching the dorsal brachium, since the animals with the regenerated optic projection show even more defasciculation errors at that morphological position than the unlesioned *astray* mutants; *** = p < 0.001

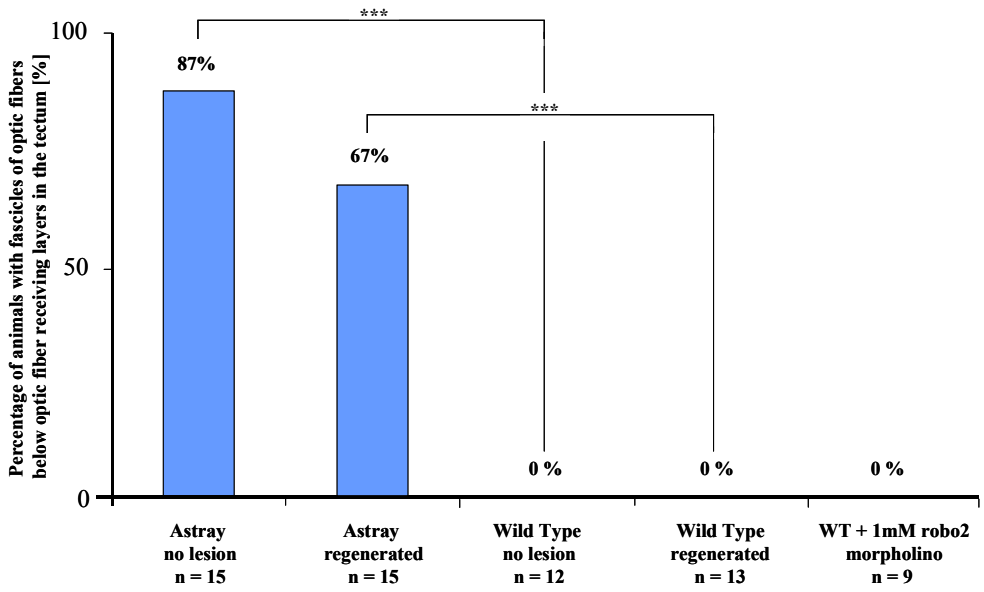

Figure 46: Animals with fascicles of optic fibers below optic fiber receiving layers in the tectum. A significant difference between *astray* mutants and wild types in both, the unlesioned animals and those with a regenerated optic projection can be seen. A slight tendency of reduction between unlesioned *astray* mutants and lesioned *astray* mutants is observable; *** = $p < 0.001$

3.3.5 Influencing Gene Expression in vivo with *robo* Morpholinos

The next step included using a developmentally active splice site directed *robo2* morpholino and trying to influence regeneration of the optic nerve in an adult fish after a full transection of the optic nerve. First to test the efficiency of the morpholino we placed gelfoams soaked with different morpholino concentrations: 16µg, 8µg and 8µg L1.1 5mismatch (a non-active controle morpholino) behind the eye on the transected nerve. 7 days post lesion these fish were sacrificed, their retinae removed, RNA extracted, transcribed into cDNA and tested in a semi-quantitative PCR for their amount of *robo* mRNA. 5 retinae were pooled for every preparation. As an internal control, actin was amplified as well. The amount of *robo* mRNA was clearly decreased with an increase of the morpholino concentration (Figure 47).

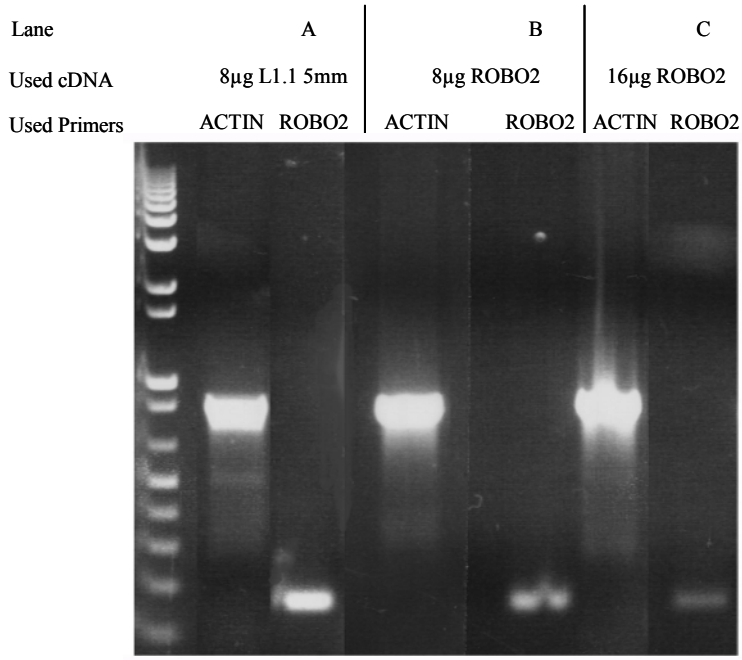

Figure 47: Changes in mRNA expression of *robo* influenced by a splice directed *Robo*2 morpholino 7 days after an optic nerve transection. The *robo* mRNA expression is drastically reduced, comparing control morpholino (Lane A) with 8µg (Lane B = moderate reduction) or 16µg (Lane C = strong reduction) of *Robo*2 morpholino. Actin was used as an internal control.

The next step was to determine whether morpholino treatment induced pathfinding errors. Different morpholino concentrations were tested and all animals were sacrificed after 4 weeks post lesion, but none induced ectopic fibers in the optic projection of treated animals. No pictures are shown, since they all looked like wild types.

Morpholino concentrations in the latter animals with sectioned brains were: 8µg (8 animals), 16µg (4 animals) and 32µg (5 animals) of the splice site directed *robo2* morpholino. Control morpholino experiments were done with a L1.1 5 mismatch (5 animals 8µg of morpholino) and a Plexin 5 mismatch (8 animals 32 µg of morpholino) morpholino (see Table 7).

Morpholinos		Morpholino in µg and number of animals (4 weeks post lesion)		
		8µg	16µg	32µg
robo2 IE Morpholino	Numbers of sectioned animals analyzed	8	4	4
5mm Plexin Morpholino				8
5mm L1.1 Morpholino		5		

Table 7: The table depicts used morpholino concentrations and numbers of sectioned animals analyzed

4 Discussion

Novel genes involved in CNS regeneration were identified microarray assays combined with an optic axon regeneration paradigm. The collapsin response mediator protein (CRMP) family, identified with the Affymetrix microarray assay, was investigated further to determine its expression pattern (section 4.1). We focused on the molecular approach of identifying new genes by microarray techniques and also observed growth pathways of regenerating optic axons in vivo. For the in vivo observations we performed a morphological dissection of unlesioned adult *astray* mutants and *astray* mutants with a regenerated optic projection (section 4.2), known to establish pathfinding errors in the optic projection during development. Our results revealed that degenerating tracts are not a strong guidance cue for regenerating CNS axons (section 4.2.3). Furthermore, we could show that *robo2* may contribute to pathfinding and termination errors of regenerating optic axons. Some specific pathfinding aberrations are drastically reduced in *astray* mutants with a regenerated optic projection, e.g. the optic fibers in the telencephalon. Hence, other pathfinding aberrations reoccur, e.g. the thickness of the fiber receiving layer in the tectum. The in vivo perturbation of regenerating optic tracts by using CRMP or ROBO morpholinos in adult fish did not show any results, albeit a reduction of expression levels using the ROBO morpholino could be achieved, showing that the experimental paradigm worked (section 4.3).

4.1 Genes Regulated After a CNS Lesion Identified by Affymetrix MicroArray Chips

As demonstrated previously, successful axonal regeneration in the CNS is accompanied by changes in gene expression (Watson 1974; Smith and Skene 1997; Plunet, Kwon et al. 2002). However the specific genes driving this regeneration process have only partially been identified. To discover additional genes that are regulated during optic nerve regeneration, we compared the gene expression profiles of retinae from unlesioned animals and retinae from fish that had received an optic nerve lesion using microarray chips. To obtain best possible results and to minimize the number of false positive spots among the chip results, 3 biological replicates per time point were performed and specific statistical limits applied. Spots were analyzed with the “GeneSpring” software, filtered by an ANOVA (analysis of variance) process with $p \leq 0.05$ and only 2-fold regulated spots were taken into consideration. The

analyzing methods and statistical limits are standard and considered by scientists working with similar methods as reliable (Irizarry, Hobbs et al. 2003; Woo, Affourtit et al. 2004; Veldman, Bemben et al. 2007). Gene ontology analysis of most strongly regulated genes identified by the microarray chip experiments suggested that RGCs with regenerating axons switch on immediate early and stress related genes until 6 hours post lesion. From 6 hours to 12 hours post lesion differentiation and signaling genes are active, reaching at 11 days a state where axon guidance, microtubuli association and growth genes are expressed (see section 3.1.4). From 100 regulated genes at the 6 hour time point and 189 regulated genes at the 12 hour time point only 16 genes are similarly regulated at both time points (see Figure 6). Considering the closeness of the 6 and 12 hour time points it is surprising to see how few genes are similarly regulated. This suggests that in the short time period between 6 and 12 hours post lesion a change from one phase of regeneration to another takes place. This is further corroborated by the observation of a reduction of the 30% segment of the stress/repair/metabolism group at the 6 hour time point to 8% at the 12 hour time point. Also the 3% segment of signaling at 6 hours changes to 7% at 12 hours, whereas the 6% segment of the transcription group remains unchanged. From 105 regulated genes at 11 days post lesion, only a few were similarly regulated as at the 6 and 12 hours post lesion time points. This was to be expected, due to the considerable time difference after lesion (see section 3.1.4). At 11 days the acute response to the injury is replaced by growth and pathfinding of axons.

The cellular localization of regulated genes in the retina cannot be determined by analyzing expression profiles from whole retinae using microarray chips. To verify the acquired chips results and to determine whether changes of mRNA expression occurred in axotomized RGCs we performed *in situ* hybridizations on retinal sections. To narrow down the number of regulated genes from the chip for in situ hybridization experiments, we started out by sorting them by their regulational strength. We excluded those which had already been described regarding regeneration of the optic projection in zebrafish. After this step, our main focus was on specific function such as axon growth, pathfinding, differentiation and coordinating transcriptional events. The final decision regarding candidates for *in situ* hybridizations were made by taking regulational strength, function, biological relevance and internal group discussions based on literature as well as database research into account. Twenty four candidates out of the group of regulated genes identified by the chip experiments were finally selected for *in situ* hybridization.

While genes selected from the gene list (see section 3.1.4, Table 5) of the 11 day time point confirmed most of our chip results, the two early time points, 6 hours and 12 hours post lesion, did not show any *in situ* signals in retina sections. Unexpectedly, no confirmation of the chip results for the 6 hour and 12 hour time point could be obtained by *in situ* technique. Although, as stated above, the recommended number of biological replicates and statistical limits concerning the chip data were applied. One possible reason for the lack of an *in situ* hybridization signal could be the low sensitivity of the technique, which might not have been high enough to pick up the low amount of mRNA produced in 6 or 12 hours post lesion. Incidentally, no data from *in situ* hybridization experiments concerning CNS regeneration in zebrafish have been published for these early time points, hinting at possible difficulties for *in situ* hybridization techniques. In contrast to the early time points, the 11 day post lesion time point revealed the interesting CRMP gene family discussed in detail in section 4.1.1. Additionally, genes already described in literature, such as Jun (Herdegen, Brecht et al. 1993; Veldman, Bemben et al. 2007) or Sox11a and b (Veldman, Bemben et al. 2007) could be confirmed as upregulated after an optic nerve lesion by *in situ* hybridizations. Because Jun is upregulated in central nervous system axons (RGCs) in zebrafish as seen in this thesis and also in CNS (Yang, Quigley et al. 2007) and PNS (Parkinson, Bhaskaran et al. 2008) axons in rats, its upregulation could be important for CNS regeneration in mammals.

4.1.1 Expression of the CRMP Family

As stated above, three members (CRMP-4, 5a and 5b) of the CRMP family were identified by the microarray chip experiment, which lead to the analysis of the mRNA expression of 6 CRMP family members (Table 7) by *in situ* hybridization in the developing retina, the unlesioned adult retina, and the adult retina 11 days after an optic nerve lesion (see section 3.1.5.1, Figure 9 and 10). Judging by the strong and specific expression of some CRMP family members after lesion, they seem to play a crucial role in the regeneration of CNS axons in zebrafish. Since the neuronal tissue which shows prominent regeneration capacity in mammals is the PNS, a comparison of the observed CRMP regulation patterns of the CNS in zebrafish and already published CRMP expression data for the PNS/CNS in mammals is given.

In zebrafish CRMP-1 was not detectably expressed in the developing eye, neither in the unlesioned adult eye or at 11 days after an optic nerve lesion. Thus, CRMP-1 is unlikely to play a major role in RGCs for axonal regeneration in zebrafish. However, CRMP-1 is weakly

expressed in the hypoglossal motor nerve of rats and increases significantly after a nerve lesion (Suzuki, Nakagomi et al. 2003).

CRMP-2 mRNA is weakly expressed in the motor nerves of rats and not detectably expressed in the RGCs of zebrafish. After a lesion either of the hypoglossal nerves (PNS) in rats (Suzuki, Nakagomi et al. 2003) or of the RGCs in zebrafish, CRMP-2 mRNA is strongly upregulated, confirming that CRMP-2 plays an important role in regeneration. Furthermore, CRMP-2 counteracts the inhibitory effects of myelin associated glycoprotein (MAG) in mammals. Correspondingly, an inhibition of CRMP-2 mimics the effects of MAG (Mimura, Yamagishi et al. 2006). CRMP-2 was also shown to interact with the Sra1/WAVE1 complex, a regulator of actin cytoskeleton. CRMP-2 transports the Sra1/WAVE1 complex to axons in a kinesin-1-dependent manner and thereby regulates axon outgrowth and formation (Kawano, Yoshimura et al. 2005). CRMP-2 is also known to enhance the advance of growth cones and Numb-mediated endocytosis regulated by Rho-kinase (Arimura, Menager et al. 2005). Additionally, Ca2+/calmodulin-dependent protein kinase II may target CRMP-2 to mediate neuronal death or survival (Hou, Jiang et al. 2008). Following these findings, an upregulation of CRMP-2 mRNA expression after a CNS lesion in mammals might have a beneficial impact.

CRMP-3 is not expressed in the motor nerve of rats (Suzuki, Nakagomi et al. 2003) and is not detectably expressed in the RGCs of zebrafish (but in a “salt and pepper”-like distribution in the inner nuclear layer of the zebrafish retina). A very different picture is given after a lesion, where CRMP-3 is strongly upregulated in the CNS of zebrafish contrary to rats where no expression in the lesioned PNS could be found. CRMP-3 is considered to play a potential role in modulating axonal damage and neuronal death (Hou, Jiang et al. 2006).

In unlesioned animals CRMP-4 is moderately expressed in the hypoglossal motor nerve of rats but is not detectably expressed in the RGCs of zebrafish. After a lesion the CRMP-4 mRNA levels remained the same in the motor nerve of rats (Suzuki, Nakagomi et al. 2003) whereas a strong upregulation of CRMP-4 mRNA could be observed in zebrafish. CRMP-4 is thought to act as a survival factor for mammalian neurons in ischemic brains (Kee, Preston et al. 2001). Furthermore, CRMP-4 is known to regulates F-actin bundling, possibly influencing the actin cytoskeleton system necessary for axon elongation (Rosslenbroich, Dai et al. 2005).

Thus, it can be stated that the mRNA expression of CRMP-3 and CRMP-4 are not upregulated after a PNS lesion in mammals in contrast to a CNS lesion in zebrafish. Additionally, the overexpression of calpain-truncated versions of CRMP-3 and -4, which can be found at the site of neuronal injury, induce neuronal apoptosis (Liu, Zhou et al. 2009).

Hence, an extensive upregulation of CRMP-3 and -4 mRNA, as observed in zebrafish, could also be beneficial for the regeneration capabilities of mammals.
In zebrafish CRMP-5a is strongly upregulated after a lesion of the optic projection. However, no data of comparison is available for CRMP-5a and b.
Especially CRMP-3, -4 and -5a might be good candidates for follow-up studies, due to their specific upregulation after lesion, not seen in mammals. This may further better the understanding of the regenerative properties of the CNS in fish versus mammals and the possible induction of regenerative processes (see Table 8).

Expression	Unlesioned		After lesion	
Organism and tissue	Fish CNS (eye)	Rat PNS	Fish CNS (eye)	Rat PNS
CRMP-1	no	weak	No	strong
CRMP-2	no	weak	Strong	strong
CRMP-3	no	no	Strong	no
CRMP-4	no	moderate	Strong	moderate
CRMP-5a	no	no data	Strong	no data
CRMP-5b	no	no data	No	no data

Table 8: The expression of the CRMP family members before and after a lesion is listed, comparing the CNS of fish and the PNS of rats.

The mRNA regulation patterns of the CRMP family before and after a lesion of the optic nerve corroborate the assumption that regeneration is not a mere recapitulation of development but has its unique regulation features (Becker and Becker 2007). CRMP-3 shows no expression in the RGCs during development but strong expression after a lesion in contrast to CRMP-5b which exhibits expression during development but no re-expression after lesion in the RGCs. CRMP-2, -4 and -5a show expression both during development and after lesion in that tissue (see Table 9).

mRNA expression of CRMP-genes in the PGZ (development) and in the RGCs (adult)	Development (3 to 5 days post fertilization)	Adult, unlesioned optic nerve	Adult, 11days post optic nerve lesion
CRMP-1	no	No	no
CRMP-2	yes	No	yes
CRMP-3	no	No	yes
CRMP-4	yes	No	yes
CRMP-5a	yes	No	yes
CRMP-5b	yes	No	no

Table 9: mRNA expression of CRMP-genes as observed in *in situ* hybridizations. Expression is marked as positive (yes) if seen in the peripheral growth zone of the retina (PGZ) in developing larvae or in the RGC layer of unlesioned and 11 days post lesion adult retinas.

Since no data can be gathered for regenerating CNS axons in mammals, because they do not regenerate, one possible "workaround" might be to look at stress response without physical injury rather than at axotomy of neurons in the CNS. Fujisawa et al. induced stress in the CNS (hyperalgesia) and measured the regulation of CRMP-2 and –4. Interestingly, CRMP-2 and –4 mRNA is not upregulated after hyperalgesia in mammals. Nevertheless, due to post translational modifications after induction of hyperalgesia truncations of the CRMP-2 molecules and a dephosphorylation of CRMP-4 molecules can be observed (Fujisawa, Ohtani-Kaneko et al. 2008). Findings of a different research group show, that truncated molecules of CRMP-3 and –4 induce neuronal apoptosis, whereas truncated CRMP-2 does not (Liu, Zhou et al. 2009). Interestingly, induced stress (hyperalgesia) was sufficient to induce truncation of CRMP-2 molecules. Hyperalgesia also induced phosphorylation of CRMP-4. The role of CRMPs in axonal guidance has been shown to be regulated by upstream kinases through increasing/decreasing phosphorylation, e.g. glycogen synthase kinase-3β (GSK-3β) regulates neuronal polarity through the phosphorylation of CRMP-2 (Arimura, Menager et al. 2005; Yoshimura, Kawano et al. 2005) and the Rho-dependent phosphorylation of CRMP-2 is important for growth cone collapse in mammals (Arimura, Menager et al. 2005).

4.2 The *astray* Mutant

4.2.1 Errors in the Adult Optic Projection Caused by *robo2* Deficiency

The errors observed in the unlesioned adult projection of *astray* mutants are similar to those reported for larvae, which also show rostro-caudal projection errors and aberrant midline crossing (Fricke, Lee et al. 2001). Enlarged terminal arbors observed for single optic axons in larval *astray* mutants (Campbell, Stringham et al. 2007) may be related to more extensive innervation of pretectal targets and termination layers in the tectum of adults (for exact percentages of error occurrence see Table 10, section 4.3.2). Finding similar errors in the two different stages of life, development and adulthood, is proof that no correction of these specific errors happens during adulthood. The very opposite is true for wild type fish where during development optic axons regularly commit pathfinding errors (especially while crossing the midline), but these are always corrected (Hutson and Chien 2002).

The lack of *robo2* is unlikely to be involved in the inability of *astray* mutants to correct these errors. This is because even in wild type animals, rostral projection errors caused by a brief conditional knock down of *robo2* during early development are not corrected at later stages, when normal levels of *robo2* expression are recovered. Interestingly, morpholino treated animals that were analyzed as adults did not exhibit enlarged termination zones of optic axons as seen in adult *astray* fish. It is possible that developmental branching phenotypes, probably induced by the morpholino, are corrected, because terminal arbors of optic axons are highly dynamic structures that are constantly remodeled even in adult teleost fish (Stuermer and Easter 1984). Thus, terminal arbors could have been corrected by normal arbor remodeling when the morpholino ceased to be active. Another explanation could be, that the morpholino was not active long enough to induce branching, which is a late developmental event.

In contrast to our observations in the CNS of the *astray* mutant, a naturally occurring transient ipsilateral optic projection in amniotes appears to be eliminated by cell death due to limited trophic factor availability (Isenmann, Engel et al. 1999) and activity dependent pruning mechanisms involving NMDA receptors (Ernst, Gallo et al. 2000). Activity dependent mechanisms are unlikely to be defective in *astray* mutants, because in tecta innervated by both eyes, segregation of axons into ocular dominance column-like patches still occurs. This form of axon pruning depends on activity (Meyer, Phillips et al. 1982) and likely involves NMDA function (Schmidt, Buzzard et al. 2000) in fish. It is, however, possible that the mis-projections in adult *astray* mutants have been stabilized by target-derived trophic support.

This could derive from the tectum, reached in all cases by caudally mis-projecting axons, or from the extensive dorsal telencephalic arborization field, reached by rostrally mis-projecting axons. The telencephalic termination field is ectopic and it is unclear which factors allow optic axons to terminate in this position.

In other mutants for axon guidance molecules, the extent of error correction of axonal pathfinding varies: In contrast to optic axons in *astray*, severe projection errors of peripheral nerves in sema3A deficient mice are corrected during development by an unknown mechanism (White and Behar 2000). However, ephA4 deficient mice retain developmental mis-wiring in the spinal cord in adults, leading to a severely abnormal gait (Kullander, Butt et al. 2003).

The functional consequences of mis-projections of optic axons in adult *astray* mutants are unknown, however, larval *astray* mutants exhibit surprisingly normal optokinetic and optomotor responses (Neuhauss, Biehlmaier et al. 1999).

4.2.2 Possible Contribution of *robo2* to Correct Pathfinding of the Regenerating Optic Projection

Optic axons re-commit *astray*-specific errors during regeneration, showing that *robo2* plays a role for axonal regeneration. Many aberrant projections established during development are not corrected in adult *astray* mutants, suggesting a low propensity for correction of erroneous optic projections in zebrafish.

The errors committed by regenerating *robo2* deficient axons indicate that *robo2* is necessary for correct rostro-caudal pathfinding, avoidance of ectopic midline crossing, precise target zone termination of optic axons and fasciculated growth of regenerating optic axons into the tectum. Regulation patterns of *robo2* and *slit* ligands correlate with this function: *robo2* is expressed in the retinal growth zone of juvenile zebrafish, and re-expressed in all retinal ganglion cells after optic nerve crush in wild type animals. This is typical for receptors implicated in axon targeting during development and regeneration of the optic projection (Bernhardt, Tongiorgi et al. 1996).

*Slit*s expressed in the brain and surrounding the optic chiasm appear to signal through *robo2* to prevent and correct pathfinding errors, shaping e.g. the chiasm by surround repulsion (Hutson and Chien 2002; Plump, Erskine et al. 2002) representing the corresponding guidance cue. Recently, *slit*/*robo* signaling was shown to play a role in inhibiting RGC arborization and synaptogenesis in the CNS in vivo (Campbell, Stringham et al. 2007).

Slits are likely the relevant guidance cues, and their expression patterns correlate with targeting errors observed in the regenerated optic projection of *astray* mutants: the rostral tectum, in which defasciculated growth of axons occurs and abnormal deep innervation of the tectum originates, is bordered by *slit2* and *slit1b* mRNA expression in the habenula. The posterior commissure, through which regenerating axons aberrantly cross, is bisected by midline *slit1b* mRNA expression. Aberrantly large terminal fields in the pretectum correlate with *slit1a* and *slit3* expression, and expanded termination zones of optic axons in the tectum correlate with *slit1a* mRNA expression there. However, the strong expression of *slit2* in the vicinity of the chiasm cannot easily be correlated with guidance of regenerating optic axons, because regeneration through the chiasm and the ventral diencephalon is comparable between wild type and *astray* animals (see section 3.3.1; Figure 15).

Interestingly, rostro-caudal pathfinding errors and aberrant midline crossing occur significantly less frequently in *astray* animals with a regenerated optic projection than in unlesioned *astray* animals that retained these aberrations from development. In contrast, termination errors in the tectum and defasciculated growth of optic axons into the tectum are found in all mutants with a regenerated optic projection. The increased thickness of the tectal termination layer stays exactly the same after a lesion suggesting an important role for *robo2* regarding correct tectal termination (see Table 10 which summarizes all observed phenotypical errors). Correlated with this observation, tectal expression of *slit1a*, which regulates arbor growth and synapse formation of developing optic axons (Campbell, Stringham et al. 2007), is maintained in the adult. Regarding pathfinding and termination errors, *robo2* does play a role in regeneration, but not in the same manner at all pathfinding decision points. As seen in the results, regenerating fibers which create optic axon bundles, while growing towards their targets, are not as strongly prone to errors as they are in their refinement state terminating at a specific spot when they recommit heavy mistakes. Termination errors do not seem random but restricted to specific areas and recurrently appear in the same manner, e.g. the thickness of the tectal termination zone is always between 37.8 µm and 61.6 µm in wild type fish whereas in the astray mutant thickness always lay between 74.2 µm and 102.2 µm. This indicates that the tectal termination zone in every mutant animal was consistently thicker than in the wild type. Also, the tectal termination zone of mutants is confined to a specific thickness, underlining that committed errors are not random and seem restricted by molecules so far not known to regulate thickness of termination.

Phenotypical errors	Astray unlesioned	Wild type unlesioned	Astray with regenerated optic projection	Wild type with regenerated optic projection
Irregular growth into telencephalon	93%	0%	7%	0%
Irregular growth into tegmentum	27%	0%	7%	0%
Termination errors at pretectal targets	100%	0%	93%	15%
Termination errors in the tectum (thickness)	92.4µm	48.8µm	89.6µm	48.5µm
Crossing errors at the posterior commissure	73%	0%	40%	0%
Ipsilateral blocks of innervations	100%	0%	13%	0%
Gaps in the contralateral innervations	87%	0%	53%	0%
Defasciculation of the dorsal optic tract	93%	0%	100%	0%
Fascicles of optic fibers below the optic layers in the tectum	87%	0%	67%	0%
Errors at the optic chiasm	7%	17%	53%	46%

Table 10: Summary of all phenotypical errors observed in astray mutants and wild types. Column 1 and 2 show unlesioned animals, column 3 and 4 display animals with a regenerated optic projection 4 weeks after an optic nerve lesion.

The different optic projection error phenotypes (see Table 10) observable for unlesioned *astray* mutants and *astray* mutants with a regenerated optic projection might be due to different expression of pathfinding genes. During pathfinding of regenerating optic axons, the relative importance of cues for some aspects of guidance may have changed, compared to axon guidance during development. Observing the expression of RGCs regeneration-associated molecules - specifically receptors for guidance cues - such as the actin-interacting protein gelsolin (Roth, Bormann et al. 1999), the recognition molecules zfNLRR (Bormann, Roth et al. 1999) and contactin1a (Schweitzer, Gimnopoulos et al. 2007), it becomes clear that these molecules are expressed at much higher levels during axon regrowth than during development. Conversely, the polysialic acid modification of NCAM is present on newly growing axons and not on regenerating axons (Harman, Rodger et al. 2003).

In fact, several guidance cues in addition to *slit*s, such as chondroitin sulfates (Becker and Becker 2002), tenascin-R (Becker, Schweitzer et al. 2004), semaphorins (Becker and Becker

2007; Feldner, Reimer et al. 2007), Netrin-1 (Charron, Stein et al. 2003) and Ephrins (Becker, Meyer et al. 2000) are present along the adult optic pathway and may guide regenerating optic axons in a combinatorial manner.

4.2.3 Guidance of Regenerating CNS Axons by Degenerating Tracts

The results of this investigation suggest that regenerating CNS axons are not guided by degenerating tracts and *robo2* might contribute to pathfinding of regenerating optic axons. Furthermore, it can be shown that correction of developmental pathfinding and targeting errors of optic axons is inefficient in *robo2* deficient zebrafish.

The adult *astray* mutant uniquely enabled us to test whether degenerating CNS tracts are a strong guidance cue for regenerating axons. This is because the mutant contains ectopic optic tracts that develop stochastically in two thirds of the animals and are mostly retained in adults. We pre-selected larvae for the presence of an ectopic telencephalic tract for adult regeneration experiments. This procedure was efficient, judged by the presence of ectopic telencephalic tracts in 14 out of 15 unlesioned, pre-selected adult animals. If degenerating tracts were an attractive guidance cue, we would expect regenerating optic axons to re-enter these tracts in almost all cases. However, growth of regenerating optic axons into the telencephalon was extremely rare following an optic nerve crush in *astray* mutants that were pre-selected for the presence of a telencephalic projection (1 of 15 animals). Furthermore, evidence from previous enucleation experiments (Schweitzer, Becker et al. 2003; Schweitzer, Gimnopoulos et al. 2007) indicates that optic tracts are unchanged in diameter through at least 4 weeks post-lesion, when regeneration is complete (Becker, Meyer et al. 2000) suggesting that degenerating ectopic tracts are available to regenerating axons, but are not re-entered. Thus, regenerating optic axons do not simply follow mechanical or non-specific molecular cues present in degenerating tracts. This differs from observations in the peripheral nervous system in mice. In this system, repeated imaging of regenerating motor axons suggested that axons re-traced their former trajectories within remaining Schwann cell tubes due to mechanical constraints and possibly interactions with Schwann cell and basal lamina derived growth-promoting molecules (Nguyen, Sanes et al. 2002). Similarly, it has been suggested from electron-microscopic observations of the optic nerve of salamanders that regenerating optic axons use degenerating fibers as guidance cues (Turner and Singer 1974). Even though fish oligodendrocytes, the myelinating cells of the CNS, up-regulate growth-promoting molecules, such as L1-related proteins (Bernhardt, Tongiorgi et al. 1996; Ankerhold, Leppert et al. 1998), P0 (Schweitzer, Becker et al. 2003) and contactin1a (Schweitzer, Gimnopoulos et al. 2007)

after a tract lesion, regenerating axons are not enticed to enter the degenerating ectopic telencephalic optic tract. This indicates that regenerating optic axons show active, target-oriented navigation during regeneration. Our results suggest that ectopic tracts were not re-innervated, even though they contain growth-promoting glial cells. This alludes that presenting axons in the non-regenerating CNS of mammals with growth-promoting glial cells (Barnett and Riddell 2007) may not be sufficient to induce directed growth of axons, if specific navigational cues are not provided at the same time.

4.3 *In vivo* Application of CRMP and *ROBO* Morpholino

The in vivo perturbation did not show any phenotypes with the three morpholinos (CRMP-2/4 and *robo2*) we used. Taking the results of the efficacy tests into account, the *robo2* morpholino induces even after 7 days a strong reduction in mRNA expression, which means that it is unlikely that the morpholino was degraded too quickly to influence mRNA expression in the regenerating RGCs. The possibility of the concentration of the morpholino having been too weak is unlikely because we used high concentrations (up to 32µg per fish) of the morpholinos (no sign of toxicity could be observed since the axons grew as fast and accurately as in control animals). But maybe the induced reduction by the morpholino was not strong enough to cause observable pathfinding effects (even with 16µg morpholino, *robo2* mRNA was still detectable; see section 3.3.5, Figure 47). Other researchers (Veldman, Bemben et al. 2007) had to target 6 different genes with 8 morpholinos to find 2 genes (KLF-6 and KLF-7) whose downregulation would cause discernable phenotypes. Another explanation might be, that in comparison to the *astray* mutant in which functional *robo2* is not expressed in the whole fish, our application influenced gene expression only in the RGCs. But this argument could be counteracted with the known fact, that *robo2* is eye autonomous, meaning after transplanting the eye of an *astray* mutant in a wild type body, optic fibers still commit pathfinding errors (Fricke, Lee et al. 2001). Another reason for no detectable errors could be, that we checked for phenotypes 4 weeks post lesion, the same period as used in the *astray* experiments with regenerated optic projections. Maybe, the activity of the morpholino diminishes after day 7, and at 4 weeks post lesion the fibers, which had no morpholino influence for some period of time, had corrected all their misrouting themselves.

4.4 Summary

In contrast to mammals, zebrafish are able to regenerate their central nervous system (CNS). In this thesis we focused on zebrafish and its optic projection, being part of the CNS, to shed new light on details of regeneration hitherto unknown. Two approaches addressing different aspects of CNS regeneration were chosen as research topics. Both topics deal with genes important during regeneration, the first using an *in vitro* approach the second is based on *in vivo* experiments and observations. The first topic deals with the identification of novel genes which are associated with optic axon regeneration. The second topic is the analysis of pathfinding in regenerating optic axons of adult zebrafish. Identification of novel genes was performed with zebrafish Affymetrix® microarray chips. From the regulated genes we picked the CRMP (collapsin response mediator protein) family for further analysis. CRMPs are cytosolic phosphoproteins, playing important roles in microtubuli assembly and signal transduction. Employing the technique of *in situ* hybridization we tested 6 CRMP family members (CRMP-1 to -5b) for their expression in the developing eye, in the unlesioned adult eye and in the adult eye 11 days after an optic nerve lesion. CRMP-2, -4 and -5a show expression in the retinal ganglion cell (RGC) layer both during development and after lesion and thus show a recapitulation of developmental expression in regeneration. In contrast, CRMP-3 is only expressed in the RGC layer after a lesion, whereas CRMP-5b exhibits expression only during development. Summarizing, CRMP-2, -3, -4 and –5a are upregulated in zebrafish after a lesion and thus seem to be good candidates for further research in the regeneration of the CNS in mammals.

Regenerating optic axons in zebrafish have to make many pathfinding decisions in order to reestablish a correct projection and topography. To gain more insight into pathfinding during regeneration of optic axons, a known developmentally active pathfinding gene, *robo2*, was chosen for observations. The *astray* mutant, carrying a null-mutation of the *robo2* gene, opened up the possibility to test whether *robo2* is needed for correct pathfinding decisions during adult regeneration of the optic projection. The adult optic projection of the *astray* mutant before and after regeneration was morphologically described in detail for the first time. Rostro-caudal pathfinding errors and ectopic midline crossings occur significantly less frequently in *astray* mutants with a regenerated optic projection than in unlesioned adult *astray* mutants. On the other hand irregular growth into the tectum and termination errors in the pretectum and tectum are repeated during regeneration of the optic projection in *astray*

mutants. Summarizing, our results show that pathfinding of regenerating optic axons in part depends on *robo2* function. Additionally, our results seem to suggest, that ectopic tracts were not re-innervated during regeneration of the optic projection. This seems to indicate, that degenerating tracts do not strongly influence the path of regenerating optic axons in the *astray* mutant. Looking at the mammalian CNS, the insufficiency of presenting only growth-promoting glial cells to non-regenerating mammalian CNS axons in order to gain directed growth becomes clear. Thus, navigational cues in CNS regeneration might turn out to be of utmost importance for mammals as demonstrated here for zebrafish.

Zusammenfassung

Im Vergleich zu Säugetieren können Zebrafische ihr zentrales Nervensystem (ZNS) regenerieren. In dieser Arbeit konzentrieren wir uns auf den Zebrafisch und seine optische Projektion, Bestandteil des ZNS, um bisher unbekannte Einzelheiten der Regeneration zu untersuchen. Die ZNS-Regeneration wurde in dieser Arbeit von zwei unterschiedlichen Blickwinkeln, *in vitro* und *in vivo*, beleuchtet, die sich mit für die Regeneration wichtigen Genen beschäftigt. Der erste beschäftigt sich mit der Identifizierung von bisher unbekannten Regenerations-assoziierten Genen, der zweite mit dem Wegfindungsphänomen regenerierender optischer Axone im adulten Zebrafisch. Neue Gene wurden mit Hilfe von spezifischen Zebrafisch Affymetrix® microarray chips identifiziert. Die CRMP (collapsin response mediator protein) Familie wurde aus der Gruppe der regulierten Genen ausgewählt, die zur Gruppe der cytosolischen Phosphoproteine gehören und eine wichtige Rolle beim Zusammenbau von Microtubuli und in der Signaltransduktion spielen. Mit Hilfe der *in situ* Hybridisierung untersuchten wir 6 Mitglieder der CRMP Familie (CRMP-1 bis -5b) auf ihre Expression im sich entwickelnden Auge, im ausgewachsenen nicht-lädierten und dem lädierten Auge (11 Tage nach Läsion). CRMP-2, -4 und -5a werden in der Retina Ganglien Zellschicht (RGZ) sowohl während der Entwicklung als auch nach Läsion des adulten optischen Nervs exprimiert und weisen eine Rekapitulation der in der Entwicklung exprimierten Gene in der Regenerationsphase auf. Andererseits wird CRMP-3 nur nach einer Läsion in der RGZ-Schicht exprimiert, während CRMP-5b ausschliesslich im sich entwickelnden Auge exprimiert wird. Zusammenfassend lässt sich feststellen, dass CRMP-2, -3, -4 und 5a nach einer Läsion im Zebrafisch hochreguliert sind und sich daher als Kandidaten für weitere Forschungen im Feld der ZNS Regeneration bei Säugetieren anbieten.

Regenerierende optische Axone im Zebrafisch müssen zahlreiche Wegfindungsentscheidungen treffen, um eine korrekte Projektion und Topographie wieder zu erstellen. Um einen tieferen Einblick in die Wegfindungsmechanismen während der Regeneration optischer Axone zu gewinnen, wurde ein bekanntes, in der Entwicklung aktives Wegfindungs-Gen, *robo2*, für unsere Untersuchungen gewählt. Die *astray*-Mutante, welche eine Null-Mutation für das *robo2* Gen trägt, ermöglichte die Beantwortung der Frage, ob *robo2* während der adulten optischen Regeneration an korrekten Wegfindungsentscheidungen beteiligt ist. In diesem Zusammenhang wurde die optische Projektion der *astray*-Mutante vor und nach der Regeneration zum ersten Mal morphologisch detailliert beschrieben. Rostro-kaudale Wegfindungsfehler und ektopisches Kreuzen der Mittellinie traten mit signifikant verringerter

Häufigkeit in *astray*-Mutanten mit regenerierter optischer Projektion auf. Andereseits wiederholen sich während der Regeneration der optischen Projektion der *astray*-Mutanten Fehler des Einwachsens in das Tectum und Terminationsfehler im Prätectum und Tectum. Zusammenfassend zeigen unsere Resultate, daß *robo2* teilweise verantwortlich für die korrekte Wegfindung regenerierender optischer Axone ist. Zusätzlich lassen die Ergebnisse vermuten, daß ektopische Trakte nicht reinnerviert wurden. Dies kann als Hinweis darauf gewertet werden, daß degenerierende Trakte keinen starken Einfluß auf die Wegfindung regenerierender optischer Axone in der *astray*-Mutante haben. Betrachtet man in diesem Zusammenhang das ZNS der Säuger, wird offensichtlich, dass wachstumsfördernde Gliazellen, die man mit nicht regenerierenden ZNS Axonen der Säuger zusammenbringt nicht ausreichend sind, um zielgerichtetes Wachstum zu induzieren. So könnten auch für die ZNS-Regeneration in Säugern Navigationshilfen, wie in dieser Arbeit für den Zebrafish gezeigt, äußerst wichtig sein.

5 Supplementary Material

5.1 Genes Chosen from Affy-List for *in situ* Probes

Gene Name	Gene Identifier – Affy ID; to be found on Ensembl	Size (bp)	Temperature and cycles used in PCR
AANAT2	**Dr.8142.1.S1_at**	1000	58 °C; 30 cycles
Alcam	**Dr.20912.1.S2_at**	1000	58 °C; 30 cycles
Fabp3	**Dr.6814.1.S1_at**	Didn't work	
Jun	**Dr.7608.1.A1_at**	1000	60 °C; 40 cycles
Ndrg11	**Dr.8090.1.A1_at**	1000	60 °C; 30 cycles
Nf1	**Dr.15268.1.A1_at**	360	58.8 °C; 40 cycles
Plexin B3	**Dr.22796.1.A1_at**	280	60 °C; 40 cycles
Rx3	**Dr.540.1.S1_at**	1000	
Sox11a	**Dr.4763.3.S1_at**	1000	60 °C; 40 cycles
Tboxbg1	**Dr.10723.1.S1_at**	480	
Thra	**Dr.454.1.S1_at**	1000	
Vsx1	**Dr.558.1.S1_at**	1000	58 °C; 30 cycles
Wnt7b	**Dr.22588.1.A1_at**	320	54 °C; 40 cycles

Jörns Midis / in situs

Her4	**Dr.5372.7.A1_at**
Tf12	**Dr.10346.1.S1_at**
Lim domain	**Dr.18163.2.S1_at**

Sp5	**Dr.23472.1.S1_at**
BMPR 1a	**Dr.8154.1.S1_at**

5.2 Primers for Cloning *in situ* Probes

	Forward Primer	Reverse Primer
AANAT2	cga gca gac aaa tcc acc aac	ttt ggc cag taa agc atg cag
Alcam	tag cag ccg ctt tgt ttg ct	ggc ttg cat cca gaa agc tc
Deltex4	tac tcc gtt ttc gtg tgg ac	tag ttg tat cat gtg gcg ca
Fabp3	gct gcg ctt cag ctc aaa c	gat gag gac gga ttc agg ctc
Jun	gtc cca aga acg tga cgg at	gca gtc gcg tcc ctg ttt ta
Ndrg11	acc gtc cta cca tcc tga cct	cgg aaa ctg agt gac ccg at
Nf1	aac ggt gat gtt tga tat ca	aga gtc ctg gag gtg tga acg
Plexin B3	ttg cgc ccg gct cga gtt	aat gat cca ttt cac tca tg
Rx3	tcc ccg aaa aag gac tcg a	atg cca aat gcg att caa tg
Sox11a	aag aca gcc acc gga cac at	aac caa gtc cga aaa gtt cgc
Tboxbg1	aat agc tac ata tat taa a	ttg caa gta agc aca cca caa
Thra	gtt tgg aag ggt atc gca gc	aca act cgt gtg atg gca gg
Vsx1	cga ggt gaa tta aag aaa ctg cc	ctg aat cgt ccg ctc cat tag
Wnt7b	gtg ttg gac cac tca gct ca	tgt aaa caa cat gtc atc tt

5.3 Primers for Identifing Appropriate and Aberrant Splice Site Sequences in *robo2* Morpholino Treated Animals

*robo2*ex1 forward	5'AAACGTGTTCTGGGGTTGAG 3'
*robo2*ex2 reverse	5'CAGATCGGAGGGGTGTTCTA3'

5.4 Morpholino Sequences

CRMP-2 Intron Exon 2.Morph:	5'CACTCTGGAAACACAGATAAACACA 3'
CRMP-4B:	5' GGTCCAGGCGTCTGCCCTCAGCCAT 3'
robo2:	5' TAAAAAGTAGCGCAACTCACCATCC 3'
Non-active control:	5' GCTCCGCCACATCACAACACGCGC 3'

5.5 List of Faber Chip Results

Common Name	**Fold Change**	**Gene Name**
Class 1 Beta Tubulin	17,17344382	AI626492
GAP-43	16,16748735	L27645
ß-thymosin	6,538554627	AF006831
Acyl-Coenzyme A	6,265417087	AI942982
Annexin	5,650401815	BI707699
plasticin	5,579113439	AF024598
ubiqutin hydrolase	5,557099314	BM185181
Interferon induced precursor IFI 6	5,333258434	BM036339
neurolin	5,009660556	BI704249
unknown	4,89777755	AI943132
unknown	4,771823181	AW019716
Neurofilament protein	4,743929031	BM102193
Acetyl-CoA carboxylase	4,116621007	BG727211

MARCKS	4,019228549	AI965249
adenylate cyclase peptide	3,712033115	AF329730
zfNLRR	3,706893745	BI879864
gefiltin	3,568268769	U89710
alpha tubulin	3,561683638	BM185116
Pre-prosomatostatin 2	3,560340624	BI533259
Cytochrome b561	3,54305011	AI545321
Sox 11B	3,513100238	U85091
phosphoinositol 3 protein	3,441315509	AW077850
unknown	3,376504273	AI522608
stathmin	3,322193921	BI430135
unknown	3,277791528	AW232839
CD9 antigen	3,238476445	AW174625
tubulin alpha 1 chain	3,235426574	AI877819
DNAH5	3,229188672	AI496943
thy1	3,150749025	BM181792
unknown	3,085498004	BI875670
PACAP	2,971312846	BI844108
unknown	2,94148213	AI641655
unknown	2,849504986	BF937964
S-cyclophilin	2,743514869	AW567464
SCAMP1	2,742124133	AW170934
ZHX1	2,732121796	AI793802
RAB-6	2,722694548	BM034772
unknown	2,721015659	BM004967
unknown	2,720654507	BI473122
ATF-3	2,708608027	AW422298
GHMP Kinase	2,705610571	BG884493
synapsin	2,704758872	BI534277
unknown	2,697252113	BI476319
GP 70	2,696701478	AW826462
unknown	2,695429656	AW826305
Tubulin beta2 chain	2,675347874	AW077024
unknown	2,636355759	AW232713

unknown	2,63399586	AJ400363
unknown	2,630496388	AB046866
unknown	2,628929373	BI880136
calcium channel beta 1B subunit	2,624738486	BM156105
unknown	2,590003387	AW171071
DRP-2	2,584717016	AI957812
vimentin	2,547659189	AF069994
unknown	2,543263499	AI667071
beta-tubulin	2,542719181	BM186665
unknown	2,539607327	BI865888
unknown	2,537041236	BM072431
unknown	2,521617602	BE693143
unknown	2,515876447	AA494787
VAP-1	2,512949672	BI534211
RPE65	2,505323775	BI670861
unknown	0,399114821	BI889657
unknown	0,397919087	BG307172
unknown	0,397641486	BI891596
unknown	0,397353963	X81128
CRM1	0,397157928	BI672394
unknown	0,396684766	BI671809
unknown	0,396038119	AF359436
unknown	0,394310423	BI705908
unknown	0,393008622	BG884411
unknown	0,392088035	U08870
unknown	0,391828603	AF260240
unknown	0,391173353	AI658011
unknown	0,390386774	BI890954
unknown	0,390294821	AW826769
unknown	0,389674156	BE017424
unknown	0,389547213	BI979989
unknown	0,388606123	BG305944
unknown	0,386256776	AW826882
unknown	0,385259046	BI846940

unknown	0,384797266	AI721417
unknown	0,384405062	AF201451
FOXG1	0,384128243	BF937564
unknown	0,380934005	AI353412
unknown	0,380749138	BI892200
11 beta-hydroxysteroid dehydrogenase	0,377727936	BG882996
unknown	0,377099677	BI890453
unknown	0,375410317	BI887958
unknown	0,374880678	AW154514
unknown	0,37380088	AI958097
unknown	0,37162977	BM153935
unknown	0,369558033	BI840692
unknown	0,368226607	BE693178
unknown	0,366375806	AW510092
unknown	0,364946978	AI667513
unknown	0,364892494	AF315947
unknown	0,362562164	BG985730
unknown	0,362168001	BI881918
RalGEF	0,361321002	BG306097
unknown	0,360801463	BG985698
ATP-binding cassette	0,360276481	AI959644
unknown	0,359797986	AW019131
unknown	0,359407519	AJ236884
unknown	0,359122449	BE016992
unknown	0,358634812	BE017358
unknown	0,357795047	AI959735
unknown	0,356584902	BI890375
NDRG1	0,356020936	BG306016
unknown	0,355442728	AI957711
unknown	0,35313512	AW077420
unknown	0,351241482	BI981903
unknown	0,350109195	BM083940
unknown	0,34774596	AF195851
unknown	0,347558965	BI892017

unknown	0,347170878	AF071255
unknown	0,345993553	AW232871
unknown	0,345587893	AW232559
unknown	0,345060933	BM185901
unknown	0,344587831	BM025875
unknown	0,342482654	BI891706
unknown	0,341783574	BI881145
unknown	0,340361996	BI673753
unknown	0,340215614	BI889086
unknown	0,340029545	BI882203
integrin alpha 3 oder 6	0,339235796	AW076731
unknown	0,338733195	BE605503
unknown	0,338378292	BI563231
MHC II protein	0,337290411	BI844145
unknown	0,337044542	AI331515
unknown	0,33584443	BI878700
unknown	0,334951636	BE605402
stathmin	0,334387581	BI891936
desmoplakin	0,331287545	AI793384
TGF beta	0,330689173	BI890131
unknown	0,328468075	AI958627
paraplegin	0,327119551	AI793442
unknown	0,326770589	BI981442
unknown	0,325636708	BM154445
unknown	0,325030949	BI474827
unknown	0,324297485	AI959432
unknown	0,323717675	AW420367
calpain1	0,323376493	BI888432
NF1	0,320881641	BI878384
unknown	0,320573211	BG306017
unknown	0,317105589	AW019622
unknown	0,316082202	BG304212
unknown	0,315092883	AW455046
unknown	0,313996626	BG884388

unknown	0,311523096	BM156878
unknown	0,310037213	BE016291
unknown	0,308045889	BE017917
homogenin	0,306376023	AW117001
unknown	0,306000992	BI842933
RDS2	0,305958754	AF210643
unknown	0,304551738	BG985503
claudin a	0,304327872	AF359423
ribosomal protein L11	0,303445149	AW077286
unknown	0,301472064	BI878459
rev-erb beta	0,295893772	AF342941
unknown	0,295344327	BM026051
gelsolin mRNA	0,292967552	AF175294
Epd	0,292753074	M89643
ucp2	0,289330771	AJ243250
robo	0,287606467	BM154725
GPE1	0,28756283	AW019436
Gelsolin precursor	0,285171697	BG303563
unknown	0,284914471	BM095399
unknown	0,28144219	AI330535
unknown	0,279708749	AW233044
Ran binding protein 11	0,277450261	BG308899
catechol-O-methyltransferase	0,277347947	BI888550
unknown	0,276567966	AI106503
TRF1	0,275840551	BM071213
Profilin	0,274492204	AW454561
unknown	0,274045406	AW078044
unknown	0,269843623	BI881121
unknown	0,268914008	AW203093
unknown	0,268661704	AI601748
unknown	0,266972567	AW466858
unknown	0,266446514	BE557057
unknown	0,266326211	BI889835
unknown	0,264192593	AI384268

caspy2	0,264030601	AF327410
ECHS1	0,26352426	BE605535
unknown	0,262519563	BI840469
fibulin	0,261703507	BI842809
unknown	0,258791831	BE202131
kearatin 8	0,258390948	BI704281
acyl-Coenzyme A oxidase 3	0,254529419	AW420988
XAG-2	0,254385876	AW233227
unknown	0,254383201	BI886789
centaurin	0,251702935	AI558301
unknown	0,249407407	BI318816
CXC-R3	0,246416002	BE200843
unknown	0,244420092	BI843080
claudin e	0,242986675	AF359425
unknown	0,241276997	BG883806
Ribosomal protein S10	0,240534339	BI842936
unknown	0,239113508	AI958983
unknown	0,237199403	BG799281
unknown	0,235241431	AW280290
unknown	0,234768506	BI706981
mitogen-activated protein kinase	0,230398126	BM102580
unknown	0,230282558	U27121
unknown	0,228699655	AW420822
Keratin complex 1	0,225459577	BE200731
Appollo	0,222344912	AW058811
calmodulin	0,221320198	BI671162
myeloperoxidase	0,220733045	AF349034
unknown	0,218991844	AW115519
unknown	0,218314495	BI982878
XSA-1	0,217735718	BI890609
EBP-2	0,216908038	BE017827
Alpha crystallin A	0,213194427	AI626489
tenascin-W	0,21042534	AJ001423
serine protease inhibitor	0,209678257	BI980261

Annexin 1a.	0,205095073	BI889370
E-cadherin	0,203436441	AF364811
unknown	0,202677346	BE605502
SK3	0,201779119	BM101698
unknown	0,199911447	BE017652
unknown	0,197274846	AI723241
Catenin delta-1	0,191159166	BI878775
unknown	0,189529504	AW174653
aquaporin 3	0,185313022	BI882594
taurine transporter	0,18500432	AW116367
unknown	0,184180135	AW184660
Dynein light intermediate chain 1	0,183194809	BI844162
krüppel-like factor 2a	0,182567859	AF392992
threonyl-tRNA synthetase	0,181324814	BI886492
Catenin delta-1	0,179825121	AW128428
unknown	0,1782677	AI959704
unknown	0,177594668	AW455027
ictacalcin	0,177360539	AW595487
unknown	0,173156813	BM102459
unknown	0,165719032	AW174620
unknown	0,164311962	BI672347
unknown	0,160347966	BI846374
claudin b	0,160266705	AF359426
unknown	0,158667448	AW344023
unknown	0,157958226	AJ011788
unknown	0,155990783	BM101640
claudin i	0,149979874	AF359428
epithelial membrane protein 2	0,141596668	BE605325
unknown	0,140460571	BI890287
aquaporin 3	0,139196372	AW422269
Keratin	0,134372883	AI397347
Ck2a1	0,128999295	BI866713
cytokeratin	0,125952971	AF134850
EGP	0,110828716	BI888943

Annexin 1a	0,106219965	AW077961
Keratin	0,09954538	BE200701
unknown	0,075638379	AI384943
unknown	0,074747871	AF197880
unknown	0,059010209	AW280179
calsequestrin	0,056818419	BI533854
regulator of G-protein signaling	0,006967796	AW115899

5.6 List of Affymetrix Chip Results

5.6.1 Time After Lesion: 6 Hours

Sorted by categories and fold change – *in situ* probes have been generated from the genes in bold letters

Common name (Affy definitions 17Sept '05)	**Fold Change**	**Gene Name**
Transcription Factors		
thyroid hormone receptor alpha	**3,299**	**Dr.454.1.S1_at**
similar to SWI/SNF-related, matrix-associated actin-dependent regulator of chromatin, subfamily a, containing DEAD/H box 1	3,071	Dr.3950.1.A1_at
hairy-related 4 gene	**2,376**	**Dr.5372.7.A1_at**
Signaling		
Wnt-7b	**4,435**	**Dr.22588.1.A1_at**
neuropeptide FF-amide peptide precursor like	2,036	Dr.18308.1.A1_at
N-myc downstream regulated gene 1, like	**0,412**	**Dr.8090.1.A1_at**
Clock / Photoreceptor		

guanylate cyclase activator 1A	3,182	Dr.12592.1.S1_at
DNA photolyase	2,922	Dr.23983.1.A1_at
opsin 1 (cone pigments), long-wave-sensitive, 1	0,316	AFFX-Dr-NM_131175-1_s_at

Cytoskeleton

Transcribed locus, moderately similar to XP_421389.1 similar to kinesin light chain 1J; KLC1J [Gallus gallus]	2,19	Dr.15378.2.A1_at
Centrin, EF-hand protein, 2	2,092	Dr.16367.1.A1_at

Stress/Repair/ Metabolism

Cryptochrome DASH	4,431	Dr.18310.2.A1_at
Solute carrier family 13 (sodium/sulphate symporters), member 1	4,383	Dr.12354.1.A1_at
Transcribed locus, weakly similar to XP_422077.1 similar to 25-hydroxyvitamin D-1 alpha hydroxylase, mitochondrial precursor	4,068	Dr.11380.1.A1_at
pyrimidine 5'-nucleotidase	3,502	Dr.4794.2.S1_at
heme binding protein 2	2,811	Dr.18410.1.S1_at
ACN9, mitocondrial	2,749	Dr.19854.1.S1_at
SOLUTE CARRIER FAMILY 23, MEMBER 2 (SODIUM-DEPENDENT VITAMIN C TRANSPORTER 2)	2,728	Dr.7636.1.A1_at
similar to paraplegin	2,711	Dr.18511.1.A1_at
thymidine kinase 2, mitochondrial	2,669	Dr.18401.1.S1_a_at
ATP-binding cassette, sub-family C (CFTR/MRP), member 4	2,629	Dr.14489.1.A1_at
thymidine kinase 2, mitochondrial	2,624	Dr.18401.1.S1_at
thymidine kinase 2, mitochondrial	2,61	Dr.18401.1.S1_x_at
similar to Acyl-Coenzyme A dehydrogenase, very long chain	2,593	Dr.3523.1.A1_at
similar to Adrenodoxin, mitochondrial precursor (Adrenal ferredoxin) (Hepatoredoxin) (Ferredoxin 1)	2,474	Dr.13680.1.S1_at
Ribonucleotide reductase M2 b	2,472	Dr.23801.1.A1_at
similar to stanniocalcin 2	2,455	Dr.23461.1.A1_at
Stanniocalcin 2	2,395	Dr.26379.1.A1_at
Apo-F	2,384	Dr.7857.1.A1_at

Eukaryotic translation initiation factor 4A, isoform 1A	2,352	Dr.26328.1.A1_at
Transcribed locus, weakly similar to NP_061092.3 presenilin associated, rhomboid-like [Homo sapiens]	2,275	Dr.20668.1.A1_at
succinate dehydrogenase complex, subunit A, flavoprotein (Fp)	2,246	Dr.11239.1.S1_at
electron-transfer-flavoprotein, alpha polypeptide	2,215	Dr.5170.1.S1_at
thymidine kinase 2, mitochondrial	2,196	Dr.18401.2.A1_at
wu:fc14h11	2,183	Dr.171.1.A1_at
similar to ubiquitin-conjugating enzyme E2D 4 (putative)	2,17	Dr.20096.1.S1_at
translocase of inner mitochondrial membrane 23 homolog (yeast)	2,169	Dr.7713.1.S1_at
similar to GrpE protein homolog 1, mitochondrial precursor (Mt-GrpE#1) (HMGE)	2,147	Dr.5829.1.A1_at
Surfeit 1	2,063	Dr.14568.1.S1_at
selenoprotein W, 1	2,042	Dr.10201.1.S1_at
glutamic pyruvate transaminase (alanine aminotransferase) 2	2,042	Dr.12011.1.A1_at
Heat shock 60kD protein 1 (chaperonin)	2,034	Dr.7108.1.S1_at
similar to cytochrome c-1	2,018	Dr.1044.1.S1_at

Unidentified

hypothetical protein LOC406605	10,56	Dr.23441.1.S1_at
heme binding molecule	9,361	Dr.7799.1.A1_at
Transcribed locus, weakly similar to XP_510395.1 similar to Very-long-chain acyl-CoA synthetase [Pan troglodytes]	5,69	Dr.12740.1.A1_at
similar to MGC81751 protein	4,887	Dr.2906.1.S1_at
similar to CG6282-PA, isoform A	4,849	Dr.18661.1.A1_at
Zgc:91996	3,282	Dr.26014.1.A1_at
histidine triad	3,257	Dr.26332.1.A1_s_at
Zgc:92102	3,217	Dr.3959.1.A1_at
Zgc:66117	3,082	Dr.4794.1.A1_at
Zgc:77038	2,976	Dr.9617.1.A1_at
Wu:fj82d09	2,928	Dr.22988.1.A1_at

WD repeat and FYVE domain containing 2	2,92	Dr.18512.1.A1_at
Wu:fj81c05	2,908	Dr.1870.1.A1_at
Transcribed locus	2,897	Dr.9901.1.S1_at
Zgc:103456	2,841	Dr.20778.1.S1_at
Transcribed locus, strongly similar to XP_415647.1 similar to RIKEN cDNA 2010004I09 [Gallus gallus]	2,804	Dr.14827.1.A1_at
Wu:fb12d05	2,745	Dr.4069.1.A1_at
Wu:fj05h12	2,735	Dr.6401.1.S1_at
zgc:64123	2,638	Dr.5040.1.S1_at
Wu:fb13g09	2,633	Dr.23583.1.A1_at
similar to Nitrogen fixation gene, yeast homolog 1	2,582	Dr.26514.1.A1_at
Zgc:86620	2,474	Dr.434.1.S1_at
zgc:77513	2,465	Dr.24259.1.A1_at
Wu:fj30e04	2,384	Dr.8010.1.S1_at
Zgc:103765	2,367	Dr.10113.1.S1_at
Wu:fc96f12	2,36	Dr.7939.1.A1_at
Zgc:86909	2,35	Dr.3730.1.A1_at
Zgc:101660	2,338	Dr.9292.1.A1_at
dZ265N4.4 (novel protein)	2,332	Dr.16925.1.S1_at
Wu:fj94h02	2,302	Dr.9616.1.A1_at
Sb:cb464	2,302	Dr.21921.1.A1_at
Transcribed locus	2,296	Dr.23415.1.A1_at
Wu:fc84a10	2,277	Dr.3972.1.S1_at
Transcribed locus, strongly similar to NP_060528.3 cartilage acidic protein 1 [Homo sapiens]	2,254	Dr.6210.1.S1_at
Zgc:73384	2,227	Dr.3515.1.A1_at
Wu:fa94b01	2,196	Dr.23558.1.A1_at
similar to evolutionarily conserved signaling intermediate in Toll pathway	2,192	Dr.2345.1.A1_at
Zgc:92822	2,173	Dr.13967.1.A1_at

carnitine deficiency-associated gene expressed in ventricle 3	2,173	Dr.390.1.S1_at
Zgc:76970	2,172	Dr.24916.2.S1_at
Wu:fj30e04	2,145	Dr.6728.1.A1_at
Wu:fd55e03	2,138	Dr.22231.1.A1_at
Wu:fj87f08	2,106	Dr.10240.1.S1_at
Transcribed locus	2,1	Dr.25879.1.A1_at
Wu:fj48b05	2,069	Dr.6765.1.A1_at
Transcribed locus, weakly similar to XP_417161.1 similar to NPAT [Gallus gallus]	2,029	Dr.12034.1.A1_at
CDNA clone IMAGE:6911175, partial cds	2,014	Dr.5372.7.A1_x_at
Zgc:91854	2,008	Dr.5399.1.S1_at
Transcribed locus	2,006	Dr.12694.1.A1_at
Transcribed locus	0,5	Dr.5060.1.A1_at
fd48h02.y1 Zebrafish WashU MPIMG EST Danio rerio cDNA clone IMAGE:3733011 5', mRNA sequence	0,466	Dr.23916.1.S1_at

5.6.2 Time After Lesion: 12 Hours

All info ensemble/NCBI and Affy 17.Sep05	**Fold Change**	**Gene Name**
Transcription Factors		
TRANSCRIPTION FACTOR 12 (TRANSCRIPTION FACTOR HTF-4) (E-BOX-BINDING PROTEIN)	**5,631**	**Dr.10346.1.S1_at**
TRANSCRIPTION FACTOR 12 (TRANSCRIPTION FACTOR HTF-4) (SALIVARY-SPECIFIC CAMP RESPONSE ELEMENT)	**5,581**	**Dr.25174.1.A1_at**
close to NUCLEAR FACTOR 1 TYPE NUCLEAR FACTOR NF1 NFI NF CCAAT BOX BINDING TRANSCRIPTION FACTOR	5,344	Dr.15268.1.A1_at
TRANSCRIPTION FACTOR 12 (TRANSCRIPTION FACTOR HTF-4) (E-BOX-BINDING PROTEIN) (SALIVARY-SPECIFIC CAMP Rec.)	**4,809**	**Dr.12842.1.S1_at**
Far upstream element binding protein 1 (FUSE binding protein 1) (FBP)	3,944	Dr.683.1.A1_at
regulator of G-protein signaling 12 isoform repressor of transcription	3,755	Dr.21449.1.S1_at
close to SKI - like protein	3,203	Dr.17141.1.A1_at
similar to high-mobility group box 2	3,184	Dr.9746.12.S1_at

similar to NLI interacting factor (1E869)	3,14	Dr.5629.1.A1_at
LIM-only protein 3 (Neuronal specific transcription factor DAT1) (Rhombotin-3)	**2,882**	**Dr.18163.2.S1_at**
Sp5 transcription factor (related to WNT signaling)	**2,732**	**Dr.23472.1.S1_at**
similar to visual system homeobox 1 protein (Vsx1)	**2,675**	**Dr.558.1.S1_at**
similar to Polycomb protein Suz12 (Suppressor of zeste 12 protein homolog)	2,076	Dr.3815.1.A1_at
nuclear respiratory factor 1	2,01	Dr.8179.1.S1_at

Signaling

similar to human sec oncogene or TPA: human lymphocyte specific protein tyrosine kinase (lck) (related to RAS signaling)	9,555	Dr.9616.1.A1_at
tumor necrosis factor receptor superfamily, member 21	4,808	Dr.964.1.A1_at
Axin-1 up-regulated gene 1 protein (TAIP-3)	4,196	Dr.2490.1.A1_at
rad and gem related GTP binding protein 1 (REM1) (related to RAS signaling)	4,141	Dr.15089.1.S1_at
phospholipase C-like 3	4,05	Dr.18810.1.A1_at
Transcribed locus, moderately similar to NP_671700.1 A-kinase anchor protein 9 isoform 1	3,991	Dr.9964.1.S1_at
Transcribed locus, moderately similar to NP_671700.1 A-kinase anchor protein 9 isoform 1	3,761	Dr.9964.2.S1_at
neuropeptide FF-amide peptide precursor like	3,054	Dr.18308.1.A1_at
faciogenital dysplasia	2,698	Dr.8178.1.S1_at
dual specificity phosphatase 2 (DUSP2)	2,594	Dr.22685.1.A1_at
male germ cell-associated kinase	2,502	Dr.24934.1.S1_at
crestin (related to BMP signaling)	2,434	Dr.8124.1.S1_at
ensemble: close to TBC1 DOMAIN FAMILY MEMBER 4 AKT SUBSTRATE OF 160 KDA AS160	2,36	Dr.17288.1.A1_at
mitogen-activated protein kinase-activated protein kinase 2	2,15	Dr.25777.1.S1_at
ensemble: close to EPHRIN B1 PRECURSOR EPH RELATED RECEPTOR TYROSINE KINASE LIGAND 2 LERK 2 ELK LIGAND	2,102	Dr.18005.1.A1_at

Axon guidance

Transcribed locus, weakly similar to XP_424356.1 PREDICTED: similar to Hyaluronidase 1 [Gallus gallus]	5,708	Dr.14360.1.A1_at

close to CMP-N-acetylneuraminate-poly-alpha-2,8-sialyl transferase	3,784	Dr.11360.1.A1_at
protocadherin 2 alpha c /// protocadherin 2 alpha b2 /// protocadherin 2 alpha b 1 /// protocadherin 2 alpha b 3…	2,834	Dr.19866.1.S1_at
similar to Syndecan-4 precursor (Ryudocan core protein)	2,099	Dr.26405.1.S1_at
ensemble: close to plexin B3	2,074	Dr.22796.1.A1_at
tissue inhibitor of metalloproteinase 2	2,01	Dr.240.1.A1_at

Clock / Photoreceptor

arylalkylamine N-acetyltransferase (AANAT)	13,58	Dr.8142.1.S1_at
tryptophan hydroxylase 1 (tryptophan 5-monooxygenase)	9,075	Dr.15967.1.A1_at
guanylate cyclase activator 1A	5,063	Dr.12592.1.S1_at
cryptochrome 3	3,614	Dr.10441.1.S1_at
opsin 1 (cone pigments), medium-wave-sensitive, 1	3,523	Dr.8102.1.S1_at
opsin 1 (cone pigments), long-wave-sensitive, 1	3,076	AFFX-Dr-NM_131175-1_s_at
similar to cryptochrome 2a	2,588	Dr.2518.1.A1_at
similar to harmonin a1	2,28	Dr.22228.1.S1_at

Cytoskeleton

similar to Nesprin 2 (Nuclear envelope spectrin repeat protein 2) (Syne-2) (Synaptic nuclear envelope protein 2) (Nucleus and actin connecting element protein)	4,25	Dr.4661.1.A1_at
similar to Septin-4 (Peanut-like protein 2) (Brain protein H5)	3,736	Dr.8575.1.A1_at
similar to septin 9	3,26	Dr.11967.1.A1_at
Gefiltin	**0,487**	**Dr.264.1.S1_at**
tubulin beta	0,343	Dr.24758.1.A1_at

Differentiation

similar to Follistatin	9,216	Dr.198.1.S2_at
myocyte enhancer factor 2c	8,636	Dr.267.1.S1_at

bone morphogenetic protein receptor, type 1a	**8,088**	**Dr.8154.1.S1_at**
similar to type I serin/threonine kinase receptor	5,098	Dr.25506.3.S1_at
thyroid hormone receptor alpha	4,076	Dr.454.1.S1_at
N-myc downstream regulated gene 1, like	**3,893**	**Dr.8090.1.A1_at**
retinal homeobox gene 3	**2,599**	**Dr.540.1.S1_at**
similar to Neural proliferation differentiation and control protein-1 precursor (NPDC-1 protein)	2,55	Dr.23064.2.S1_at
jagged 2	2,521	Dr.8287.1.S1_a_at
inhibitor of DNA binding 2, dominant negative helix-loop-helix protein	2,511	Dr.5428.1.S1_at
N-myc downstream regulated family member 3b	2,184	Dr.20738.1.S1_at
connexin 35	2,029	DrAffx.1.63.S1_at

Stress/repair/metabolism

similar to Chloride intracellular channel	6,925	Dr.22661.1.A1_at
close to APOLIPOPROTEIN F PRECURSOR APO F; in GDNF FAMILY RECEPTOR ALPHA PRECURSOR GFR ALPHA RECEPTOR ALPHA ALPHA TGF BETA RELATED NEUROTROPHIC FACTOR RECEPTOR	5,13	Dr.7857.1.A1_at
F-box only protein 25	3,634	Dr.25520.1.A1_at
growth arrest and DNA-damage-inducible, alpha like	3,468	Dr.23587.1.A1_at
adiponectin receptor 1a	2,685	Dr.11449.1.A1_at
similar to choline kinase alpha isoform a, b	2,377	Dr.13284.2.S1_at
similar to chromodomain helicase DNA binding protein 7	2,255	Dr.18319.2.A1_at
ensemble: close to: CARNITINE O PALMITOYLTRANSFERASE MITOCHONDRIAL EC_2.3.1.21 CPT; ncbi the same	2,246	Dr.4467.1.S1_at
similar to U6 snRNA-associated Sm-like protein LSm8	2,194	Dr.17055.1.S1_at
nucleophosmin 1	2,177	Dr.19937.1.S1_at
cyclin-dependent kinase 8	2,115	Dr.18577.1.S2_at
IMP (inosine monophosphate) dehydrogenase 2	2,103	Dr.2636.1.S1_at
similar to stanniocalcin 2	2,006	Dr.23461.1.A1_at
electron-transfer-flavoprotein, alpha polypeptide	0,477	Dr.5170.1.S1_at
Pyrophosphatase (inorganic)	0,368	Dr.26347.1.A1_at

Unidentified

close to HEAT-like (PBS lyase) repeat containing 1	20,34	Dr.9901.1.S1_at
Transcribed locus	14,92	Dr.18123.1.A1_at
Transcribed locus	14,86	Dr.11384.1.A1_at
Transcribed locus	13,7	Dr.23415.1.A1_at
wu:fc05b06	9,936	Dr.3182.1.A1_at
Transcribed locus	7,234	Dr.17780.1.S1_at
looks like affy-piece belongs to bmpr1-similar to that in human - nothing known in Fubu	6,829	Dr.25506.1.A1_at
close to IMP dehydrogenase/GMP reductase; similar to: RIMKLP ribosomal modification protein	6,402	Dr.20131.8.S1_at
Transcribed locus	5,035	Dr.16949.1.A1_at
BTB/POZ domain containing protein 6 (Lens BTB domain protein)	4,958	Dr.25528.1.A1_at
wu:fj41a03	4,816	Dr.6568.1.A1_at
Wu:fb49f03	4,655	Dr.19408.1.A1_at
Transcribed locus	4,529	Dr.9880.1.A1_at
zgc:85956	4,339	Dr.25174.2.A1_at
wu:fb38e11	4,185	Dr.4135.1.A1_at
CDNA clone IMAGE:7151033	3,569	Dr.9531.1.A1_at
wu:fd02a07	3,546	Dr.21996.1.A1_at
Transcribed locus	3,491	Dr.12770.1.S1_at
Im:7138430	3,364	Dr.18495.1.A1_at
similar to type I serin/threonine kinase receptor	3,36	Dr.25506.2.A1_at
---	3,278	Dr.12902.1.A1_at
between CIRCADIAN LOCOMOTER OUTPUT CYCLES KAPUT; and TRANSMEMBRANE PFT27 TPA REGULATED LOCUS	3,277	Dr.16319.1.A1_at
wu:fc80b03	3,27	Dr.5351.1.A1_at
Transcribed locus	3,211	Dr.15953.1.A1_at
close to cyclin fold protein 1 (danio)	3,117	Dr.5060.1.A1_at

wu:fc11d07	3,062	Dr.3115.1.A1_at
Transcribed locus	3,043	Dr.11957.1.A1_at
Transcribed locus	3,029	Dr.25257.1.A1_at
Transcribed locus	2,97	Dr.11243.1.A1_at
zgc:110149	2,945	Dr.15657.1.S1_at
wu:fc29g09	2,916	Dr.21573.1.A1_at
hypothetical protein	2,913	Dr.5476.1.A1_at
sb:cb578	2,862	Dr.10103.1.A1_at
Transcribed locus	2,8	Dr.16724.1.A1_at
transmembrane protein 16A	2,786	Dr.17740.2.A1_at
wu:fi04a03	2,773	Dr.15149.1.A1_at
Transcribed locus	2,768	Dr.14129.1.A1_at
Transcribed locus	2,762	Dr.14340.2.S1_a_at
zgc:56271	2,715	Dr.13039.1.S1_at
similar to High mobility group protein 4 (HMG-4) (High mobility group protein 2a) (HMG-2a)	2,691	Dr.6932.3.S1_at
wu:fc64h01	2,684	Dr.2270.1.A1_at
Transcribed locus	2,629	Dr.16339.1.A1_at
wu:fc52a02	2,616	Dr.1782.1.A1_at
im:7140576	2,61	Dr.11999.1.A1_at
zgc:77038	2,604	Dr.9617.1.A1_at
zgc:110149	2,588	Dr.18163.1.S1_at
similar to CXXC finger 5	2,561	Dr.18724.1.A1_at
wu:fj99c09	2,514	Dr.6617.1.A1_at
zgc:66367	2,491	Dr.3569.1.S1_at
wu:fj66h02	2,482	Dr.12028.1.A1_at
Transcribed locus	2,44	Dr.15298.1.S1_at
wu:fj59b03	2,436	Dr.9146.1.S1_at

chromosome 6 open reading frame 115 (H. sapiens)	2,404	Dr.5677.1.S1_at
close to Homo sapiens bicaudal D homolog 2 (*Drosophila*) (BICD2)	2,391	Dr.12381.1.A1_at
zgc:56544	2,383	Dr.9633.1.A1_at
---	2,377	Dr.13953.1.A1_at
wu:fb49f03	2,357	Dr.23735.1.A1_at
similar to High mobility group protein 4 (HMG-4) (High mobility group protein 2a) (HMG-2a)	2,323	Dr.25683.9.S1_at
wu:fj13h01	2,323	Dr.7365.1.A1_at
---	2,301	Dr.23203.1.A1_at
wu:fj84d10	2,284	Dr.17070.1.A1_at
BTBD6 protein /// similar to novel BTB (POZ) domain containing protein	2,282	Dr.20785.1.S1_a_at
---	2,278	Dr.23040.1.A1_at
CDNA clone IMAGE:7012610	2,268	Dr.16385.1.A1_at
ncbi: origin recognition complex	2,26	Dr.17944.1.S1_at
Transcribed locus	2,253	Dr.11231.1.A1_at
Transcribed locus	2,252	Dr.17613.1.A1_at
zgc:110417	2,245	Dr.15855.1.A1_at
wu:fb78f01	2,24	Dr.21131.1.A1_at
ensembl: close to 60S ACIDIC RIBOSOMAL P1	2,236	Dr.12688.1.A1_at
wu:fb53a11	2,235	Dr.18027.1.A1_at
Transcribed locus	2,233	Dr.12304.1.S1_at
ensemble: close to unknown transcription factor	2,211	Dr.23916.1.S1_at
zgc:110767	2,189	Dr.18287.2.A1_at
zgc:73292	2,185	Dr.18088.1.S1_at
---	2,178	Dr.6493.1.A1_at
zgc:63471	2,167	Dr.23975.1.A1_at
Transcribed locus	2,165	Dr.23046.1.A1_at
Transcribed locus	2,145	Dr.16584.1.S1_at

Transcribed locus	2,138	Dr.2845.1.A1_at
CDNA clone IMAGE:7146797	2,134	Dr.15510.1.S1_at
wu:fb98d04	2,132	Dr.4336.1.A1_at
collagen type II, alpha-1 /// similar to collagen alpha 1(II) chain precursor - bovine (tentative sequence) (fragments)	2,132	Dr.3761.1.S1_at
LanC antibiotic synthetase component C-like 1 (bacterial)	2,13	Dr.1004.1.S1_at
zgc:101854	2,127	Dr.9743.1.S1_at
wu:fa02e12	2,127	Dr.125.1.A1_at
similar to high mobility group protein	2,114	Dr.24802.2.A1_at
wu:fd45a11	2,091	Dr.8915.1.A1_at
zgc:64022	2,08	Dr.26458.1.S1_at
Transcribed locus, weakly similar to XP_426590.1 PREDICTED: similar to aortic preferentially expressed gene 1 [Gallus gallus]	2,079	Dr.15230.1.A1_at
Transcribed locus	2,073	Dr.24873.1.A1_at
Transcribed locus	2,071	Dr.12764.1.A1_at
zgc:66401	2,071	Dr.4117.1.A1_at
Zgc:100960	2,063	Dr.15757.2.A1_at
similar to MGC81063 protein	2,062	Dr.6114.1.A1_at
zgc:92682	2,05	Dr.11215.1.A1_at
wu:fa94b01	2,049	Dr.23558.1.A1_at
Transcribed locus	2,047	Dr.19445.1.S1_at
Transcribed locus	2,04	Dr.14614.1.A1_at
wu:fc08a10	2,039	Dr.3118.1.A1_a_at
Transcribed locus	2,038	Dr.13569.1.A1_at
Transcribed locus	2,037	Dr.14865.1.A1_at
similar to Fam13a1 protein	2,035	Dr.7236.1.A1_at
zgc:77366	2,034	Dr.5122.1.S1_at
Transcribed locus	2,02	Dr.14317.1.A1_at
---	2,018	Dr.12804.1.S1_at

ensemble: close to ATP BINDING CASSETTE SUB FAMILY G MEMBER	2,013	Dr.22792.1.A1_at
wu:fc63h04	2,01	Dr.2751.1.A1_at
wu:fj59h01	2,01	Dr.6789.1.A1_at
ensemble: close to METAL REGULATORY TRANSCRIPTION FACTOR 1	0,494	Dr.15136.1.A1_at
ensemble: between rlbp1l and abhd2	0,49	Dr.23638.1.A1_at
---	0,483	Dr.14322.1.A1_at
Transcribed locus	0,479	Dr.17224.1.S1_at
wu:fj81c05	0,472	Dr.1870.1.A1_at
zgc:86909	0,455	Dr.3730.1.A1_at
zgc:92822	0,443	Dr.13967.1.A1_at
---	0,354	Dr.16375.1.A1_at
Transcribed locus, weakly similar to NP_038529.1 crystallin, alpha A	0,185	Dr.17476.1.A1_at

5.6.3 Time After Lesion: 11 Days

Description	**Fold Change**	**Gene Name**
Transcription factors		
SRY-box containing gene 11b	8,115	**Dr.5112.1.S3_at**
activating transcription factor 3	7,805	**Dr.14282.1.S1_at**
SRY-box containing gene 11b	4,68	Dr.5112.1.S2_at
v-jun sarcoma virus 17 oncogene homolog (avian)	2,554	Dr.7608.1.A1_at
similar to T-box brain gene 1	2,225	Dr.10723.1.S1_at
similar to High mobility group protein 4 (HMG-4) (High mobility group protein 2a) (HMG-2a)	2,114	Dr.25683.9.S1_at
core promoter element binding protein /// hypothetical protein LOC554994	2,063	Dr.20339.1.S1_at
SRY-box containing gene 11a	2,03	Dr.4763.3.S1_at
SRY-box containing gene 11a	2,026	Dr.4763.1.S1_at
SRY-box containing gene 11a	2,018	Dr.4763.1.S2_at

Signaling

adenylate cyclase activating polypeptide 1b	4,126	Dr.10739.2.S1_a_at
PREDICTED: similar to annexin A13 isoform 1	3,779	Dr.16504.1.A1_at
junction plakoglobin	3,274	Dr.25119.1.S1_s_at
beta-catenin-interacting protein	2,763	Dr.1102.1.S1_at
similar to A-kinase anchor protein 6	2,348	Dr.12901.1.A1_at
similar to phosphodiesterase 9A isoform b	2,123	Dr.20838.1.A1_at

Guidance

sulfatase 2	5,196	**Dr.12717.1.S1_at**
close to fibronectin 1	4,57	Dr.12367.1.A1_at
lectin, galactoside-binding, soluble, 1 (galectin 1)-like 2	3,113	Dr.13015.1.S1_at
dihydropyrimidinase-like 5a (CRMP-5)	2,929	**Dr.21550.1.S1_at**
Activated leukocyte cell adhesion molecule (ALCAM)	2,886	Dr.20912.1.S2_at
dihydropyrimidinase-like 3 (CRMP-4)	2,435	**Dr.16753.2.A1_at**
CD99 antigen-like 2	2,066	Dr.25120.3.S1_at
fibronectin 1	2,038	Dr.19965.1.S1_at

Clock/(Photoreceptor)

arylalkylamine N-acetyltransferase	2,083	Dr.8142.1.S1_at

Cytoskeleton

thymosin, beta	25,39	**Dr.19380.1.S1_at**
Thy-1 cell surface antigen	17,99	**Dr.20019.1.S1_at**
growth associated protein 43	14,72	**Dr.92.1.A1_at**
Tubulin, beta 5	14,43	**Dr.4416.3.A1_at**
tubulin, beta 5	12,8	**Dr.4416.1.A1_at**

plasticin	7,956	**Dr.263.2.S1_x_at**
plasticin	7,626	**Dr.263.1.S1_a_at**
plasticin	7,385	**Dr.263.2.S1_at**
Tubulin, alpha 8 like 3	5,135	**Dr.20214.1.A1_at**
gefiltin	4,873	**Dr.264.1.S1_at**
Neuron-specific class III beta-tubulin	4,349	Dr.7928.1.A1_at
close to stathmin-like 2	4,273	Dr.1841.1.A1_at
Stathmin-like 4	4,125	Dr.6183.1.A1_at
Myristoylated alanine-rich protein kinase C substrate	3,923	Dr.3153.1.A1_at
similar to tubulin, alpha 2 isoform 2	3,231	Dr.11310.3.S1_at
similar to tubulin, alpha 2 isoform 2	2,943	Dr.11310.3.S1_x_at
Actin related protein 2/3 complex, subunit 5A	2,9	Dr.5621.1.A1_at
myristoylated alanine rich protein kinase C substrate	2,306	Dr.24758.2.S1_at
Tubulin, alpha 2	2,277	Dr.26381.1.A1_at
actin related protein 2/3 complex, subunit 5B	2,201	Dr.10390.1.S1_at
similar to gamma filamin	2,058	Dr.3713.1.A1_at

Differentiation

fatty acid binding protein 3, muscle and heart	2,738	Dr.6814.1.S1_at
muscle-specific beta 1 integrin binding protein 2	2,51	Dr.781.1.S1_at

Regulation of translation

similar to g-RICH sequence factor 1	6,587	Dr.6804.1.A1_at
ELAV (embryonic lethal, abnormal vision, *Drosophila*)-like 4 (Hu antigen D)	2,321	Dr.424.1.S1_at

(stress/repair) / metabolism

ubiquitin carboxyl-terminal esterase L1 (ubiquitin thiolesterase)	6,112	Dr.8724.1.S1_at
solute carrier family 25 (mitochondrial carrier	2,811	Dr.13990.1.A1_at

Peptidylprolyl isomerase A (cyclophilin A)	2,507	Dr.9654.1.A1_at
Caspase 3, apoptosis-related cysteine protease	2,359	Dr.4796.1.A1_at
non-metastatic cells 2, protein (NM23B) expressed in	2,323	Dr.1320.1.S1_at
Peptidylprolyl isomerase A (cyclophilin A)	2,301	Dr.12423.1.S1_at
beta-2-microglobulin	2,25	Dr.184.1.S1_at
Reticulon 1	2,199	Dr.4188.2.S1_at
eukaryotic translation elongation factor 2, like	2,147	Dr.908.1.S1_at
Proteasome (prosome, macropain) subunit, alpha type,5	2,132	Dr.20156.1.S1_at
acyl-CoA synthetase long-chain family member 4	2,125	Dr.16391.1.A1_at
selenoprotein W, 1	2,084	Dr.10201.1.S1_at
Zgc:92164	2,061	Dr.20131.8.S1_at

Unidentified

Transcribed locus	6,29	**Dr.14570.1.S1_at**
Transcribed locus	4,46	Dr.9901.1.S1_at
Transcribed locus	4,028	Dr.12824.1.A1_at
Transcribed locus	3,76	Dr.18055.1.S1_at
Transcribed locus, weakly similar to XP_426590.1 similar to aortic preferentially expressed gene 1 [Gallus gallus]	3,695	Dr.15230.1.A1_at
Transcribed locus	3,595	Dr.12222.1.A1_at
Zgc:100829	3,552	Dr.9484.1.A1_at
Transcribed locus	3,36	Dr.24284.1.A1_at
Putative ISG12-1 protein	3,344	Dr.14950.1.A1_at
hypothetical protein LOC561769	3,126	Dr.26497.1.A1_at
Wu:fc66h11	3,105	Dr.3294.1.A1_at
Transcribed locus	3,098	Dr.23415.1.A1_at
Transcribed locus	3,096	Dr.12321.1.A1_at
Transcribed locus, weakly similar to XP_535715.1 PREDICTED: hypothetical protein XP_535715 [Canis familiaris]	3,067	Dr.15964.1.A1_at

Wu:fj55d04	2,97	Dr.7862.1.A1_at
Transcribed locus	2,967	Dr.16132.1.A1_at
Wu:fj20a04	2,882	Dr.6156.1.A1_at
Transcribed locus	2,874	Dr.13489.1.S1_at
Zgc:66052	2,861	Dr.3966.1.A1_at
Zgc:92925	2,845	Dr.19516.1.S1_at
Wu:fc95e01	2,803	Dr.1851.1.A1_at
similar to hematological and neurological expressed 1	2,782	Dr.1162.1.S1_at
ft01f08.y1 Zebrafish neuronal Danio rerio cDNA clone IMAGE:5080454 5', mRNA sequence.	2,709	Dr.13879.1.A1_at
Hypothetical protein LOC407664	2,704	Dr.15448.1.A1_at
Transcribed locus	2,619	Dr.906.1.S1_at
Zgc:101522	2,587	Dr.14036.1.A1_at
Wu:fa92g05	2,505	Dr.956.1.S1_at
Zgc:65908	2,456	Dr.14120.1.A1_at
Zgc:103707	2,446	Dr.1894.1.S1_at
Wu:fa27c07	2,4	Dr.20010.3.S2_at
Wu:fj42f06	2,396	Dr.7825.1.A1_at
Transcribed locus	2,376	Dr.26043.1.A1_at
chromosome 6 open reading frame 115 (H. sapiens)	2,355	Dr.5677.1.S1_at
Transcribed locus	2,355	Dr.15562.1.A1_at
Wu:fb53c10	2,339	Dr.4444.1.S1_at
Transcribed locus	2,337	Dr.15379.1.A1_at
Wu:fc05b06	2,301	Dr.3182.1.A1_at
similar to complement C4-1	2,278	Dr.6623.1.A1_at
Transcribed locus	2,258	Dr.12304.1.S1_at
Wu:fk54g08	2,225	Dr.23253.1.A1_at
Transcribed locus	2,219	Dr.11247.1.A1_at

Transcribed locus	2,183	Dr.21811.1.S1_at
Zgc:101095	2,176	Dr.12174.1.A1_at
Transcribed locus	2,173	Dr.17780.1.S1_at
Transcribed locus	2,15	Dr.5976.1.A1_at
Transcribed locus	2,11	Dr.14448.1.A1_at
Wu:fc95d03	2,056	Dr.16247.1.A1_at
Wu:fl05f10	2,028	Dr.24492.1.A1_at
Wu:fb98b06	2,028	Dr.955.1.A1_at
Transcribed locus, weakly similar to NP_038529.1 crystallin, alpha A	0,415	Dr.17476.1.A1_at

5.7 Abbreviations

ANOVA **Analysis of Variance**
cDNA **Copy Deoxyribonucleic Acid**
CNS **Central Nervous System**
CPN **Central Pretectal Nucleus**
CRMP **Collapsin Response Mediator Protein**
DHP **Dihydropyrimidinase**
DiI **1,1'-dioctadecyl-3,3,3'3'-tetramethylindocarbocyanine perchlorate**
DIV **Diencephalic Ventricle**
DNA **Deoxyribonucleic Acid**
dpf **Days Post Fertilization**
GO **Gene Ontology**
hpf **Hours Post Fertilization**
LCM **Laser Capture Microscope**
LONL **Left Optic Nerve Lesion**
MAG **Myelin-Associated Glycoprotein**
mRNA **Messenger Ribonucleic Acid**
MS222 **3-Aminobenzoic Acid Ethylmethylester**
NMLF **Nucleus Medial Longitudinal Fascicle**

ODC	**Ocular Dominance Column**
ON	**Oculomotor Nucleus**
PCR	**Polymerase Chain Reaction**
PPd	**Periventricular Pretectal Nucleus**
RGC	**Retinal Ganglion Cell**
RNA	**Ribonucleic Acid**
SAC	**Stratum Album Centrale**
SEM	**Standard Error of the Mean**
SFGS	**Stratum Fibrosum et Griseum Superficiale**
SGC	**Stratum Griseum Centrale**
TL	**Torus Longitudinalis**
VL	**Ventrolateral Thalamic Nucleus**
WT	**Wild Type**

6 Literature

Ankerhold, R., C. A. Leppert, et al. (1998). "E587 antigen is upregulated by goldfish oligodendrocytes after optic nerve lesion and supports retinal axon regeneration." Glia **23**(3): 257-70.

Arimura, N., A. Hattori, et al. (2009). "CRMP-2 directly binds to cytoplasmic dynein and interferes with its activity." J Neurochem **111**(2): 380-90.

Arimura, N., C. Menager, et al. (2004). "Role of CRMP-2 in neuronal polarity." J Neurobiol **58**(1): 34-47.

Arimura, N., C. Menager, et al. (2005). "Phosphorylation by Rho kinase regulates CRMP-2 activity in growth cones." Mol Cell Biol **25**(22): 9973-84.

Arora, V., D. C. Knapp, et al. (2000). "c-Myc antisense limits rat liver regeneration and indicates role for c-Myc in regulating cytochrome P-450 3A activity." J Pharmacol Exp Ther **292**(3): 921-8.

Asch, W. S., D. Leake, et al. (1998). "Cloning of zebrafish neurofilament cDNAs for plasticin and gefiltin: increased mRNA expression in ganglion cells after optic nerve injury." J Neurochem **71**(1): 20-32.

Ayaz, D., M. Leyssen, et al. (2008). "Axonal injury and regeneration in the adult brain of Drosophila." J Neurosci **28**(23): 6010-21.

Ayroles, J. F. and G. Gibson (2006). "Analysis of variance of microarray data." Methods Enzymol **411**: 214-33.

Barnett, S. C. and J. S. Riddell (2007). "Olfactory ensheathing cell transplantation as a strategy for spinal cord repair--what can it achieve?" Nat Clin Pract Neurol **3**(3): 152-61.

Beattie, C. E., M. Granato, et al. (2002). "Cellular, genetic and molecular mechanisms of axonal guidance in the zebrafish." Results Probl Cell Differ **40**: 252-69.

Becker, C. G. and T. Becker (2002). "Repellent guidance of regenerating optic axons by chondroitin sulfate glycosaminoglycans in zebrafish." J Neurosci **22**(3): 842-53.

Becker, C. G. and T. Becker (2007). "Growth and pathfinding of regenerating axons in the optic projection of adult fish." J Neurosci Res **85**(12): 2793-9.

Becker, C. G., B. C. Lieberoth, et al. (2004). "L1.1 is involved in spinal cord regeneration in adult zebrafish." J Neurosci **24**(36): 7837-42.

Becker, C. G., R. L. Meyer, et al. (2000). "Gradients of ephrin-A2 and ephrin-A5b mRNA during retinotopic regeneration of the optic projection in adult zebrafish." J Comp Neurol **427**(3): 469-83.

Becker, C. G., J. Schweitzer, et al. (2004). "Tenascin-R as a repellent guidance molecule for newly growing and regenerating optic axons in adult zebrafish." Mol. Cell Neurosci. **26**: 376-389.

Becker, C. G., J. Schweitzer, et al. (2004). "Tenascin-R as a repellent guidance molecule for newly growing and regenerating optic axons in adult zebrafish." Mol Cell Neurosci **26**(3): 376-89.

Becker, C. G. a. B., T. (2007). Model Organisms in Spinal Cord Regeneration, Wiley-VCH.

Becker, T., M. F. Wullimann, et al. (1997). "Axonal regrowth after spinal cord transection in adult zebrafish." J Comp Neurol **377**(4): 577-95.

Bernhardt, R. R., E. Tongiorgi, et al. (1996). "Increased expression of specific recognition molecules by retinal ganglion cells and by optic pathway glia accompanies the

successful regeneration of retinal axons in adult zebrafish." J Comp Neurol **376**(2): 253-64.

Bohmann, D., T. J. Bos, et al. (1987). "Human proto-oncogene c-jun encodes a DNA binding protein with structural and functional properties of transcription factor AP-1." Science **238**(4832): 1386-92.

Bormann, P., L. W. Roth, et al. (1999). "zfNLRR, a novel leucine-rich repeat protein is preferentially expressed during regeneration in zebrafish." Mol Cell Neurosci **13**(3): 167-79.

Bormann, P., V. M. Zumsteg, et al. (1998). "Target contact regulates GAP-43 and alpha-tubulin mRNA levels in regenerating retinal ganglion cells." J Neurosci Res **52**(4): 405-19.

Brittain, J. M., A. D. Piekarz, et al. (2009). "An atypical role for collapsin response mediator protein 2 (CRMP-2) in neurotransmitter release via interaction with presynaptic voltage-gated calcium channels." J Biol Chem **284**(45): 31375-90.

Brose, K., K. S. Bland, et al. (1999). "Slit proteins bind Robo receptors and have an evolutionarily conserved role in repulsive axon guidance." Cell **96**(6): 795-806.

Burrill, J. D. and S. S. Easter, Jr. (1995). "The first retinal axons and their microenvironment in zebrafish: cryptic pioneers and the pretract." J Neurosci **15**(4): 2935-47.

Cameron, D. A., K. L. Gentile, et al. (2005). "Gene expression profiles of intact and regenerating zebrafish retina." Mol Vis **11**: 775-91.

Campbell, D. S., S. A. Stringham, et al. (2007). "Slit1a inhibits retinal ganglion cell arborization and synaptogenesis via Robo2-dependent and -independent pathways." Neuron **55**(2): 231-45.

Charrier, E., S. Reibel, et al. (2003). "Collapsin response mediator proteins (CRMPs): involvement in nervous system development and adult neurodegenerative disorders." Mol Neurobiol **28**(1): 51-64.

Charron, F., E. Stein, et al. (2003). "The morphogen sonic hedgehog is an axonal chemoattractant that collaborates with netrin-1 in midline axon guidance." Cell **113**(1): 11-23.

Chaudhry, N. and M. T. Filbin (2007). "Myelin-associated inhibitory signaling and strategies to overcome inhibition." J Cereb Blood Flow Metab **27**(6): 1096-107.

Cole, A. R., A. Knebel, et al. (2004). "GSK-3 phosphorylation of the Alzheimer epitope within collapsin response mediator proteins regulates axon elongation in primary neurons." J Biol Chem **279**(48): 50176-80.

Cole, A. R., W. Noble, et al. (2007). "Collapsin response mediator protein-2 hyperphosphorylation is an early event in Alzheimer's disease progression." J Neurochem **103**(3): 1132-44.

Czech, T., J. W. Yang, et al. (2004). "Reduction of hippocampal collapsin response mediated protein-2 in patients with mesial temporal lobe epilepsy." Neurochem Res **29**(12): 2189-96.

de Martino, S., Y. L. Yan, et al. (2000). "Expression of sox11 gene duplicates in zebrafish suggests the reciprocal loss of ancestral gene expression patterns in development." Dev Dyn **217**(3): 279-92.

Deininger, S. O., L. Rajendran, et al. (2003). "Identification of teleost Thy-1 and association with the microdomain/lipid raft reggie proteins in regenerating CNS axons." Mol Cell Neurosci **22**(4): 544-54.

Devine, C. A. and B. Key (2008). "Robo-Slit interactions regulate longitudinal axon pathfinding in the embryonic vertebrate brain." Dev Biol **313**(1): 371-83.

Diaz, M. L., M. Becerra, et al. (2002). "Distribution of thyrotropin-releasing hormone (TRH) immunoreactivity in the brain of the zebrafish (Danio rerio)." J Comp Neurol **450**(1): 45-60.

Dickson, B. J. and G. F. Gilestro (2006). "Regulation of commissural axon pathfinding by slit and its Robo receptors." Annu Rev Cell Dev Biol **22**: 651-75.

Diekmann, H., M. Klinger, et al. (2005). "Analysis of the reticulon gene family demonstrates the absence of the neurite growth inhibitor Nogo-A in fish." Mol Biol Evol **22**(8): 1635-48.

Diekmann, H. and C. A. Stuermer (2009). "Zebrafish neurolin-a and -b, orthologs of ALCAM, are involved in retinal ganglion cell differentiation and retinal axon pathfinding." J Comp Neurol **513**(1): 38-50.

Draper, B. W., P. A. Morcos, et al. (2001). "Inhibition of zebrafish fgf8 pre-mRNA splicing with morpholino oligos: a quantifiable method for gene knockdown." Genesis **30**(3): 154-6.

Ekker, S. C. and J. D. Larson (2001). "Morphant technology in model developmental systems." Genesis **30**(3): 89-93.

Ernst, A. F., G. Gallo, et al. (2000). "Stabilization of growing retinal axons by the combined signaling of nitric oxide and brain-derived neurotrophic factor." J Neurosci **20**(4): 1458-69.

Erskine, L., S. E. Williams, et al. (2000). "Retinal ganglion cell axon guidance in the mouse optic chiasm: expression and function of robos and slits." J Neurosci **20**(13): 4975-82.

Erter, C. E., T. P. Wilm, et al. (2001). "Wnt8 is required in lateral mesendodermal precursors for neural posteriorization in vivo." Development **128**(18): 3571-83.

Feldner, J., M. M. Reimer, et al. (2007). "PlexinA3 restricts spinal exit points and branching of trunk motor nerves in embryonic zebrafish." J Neurosci **27**(18): 4978-83.

Fricke, C., J. S. Lee, et al. (2001). "astray, a zebrafish roundabout homolog required for retinal axon guidance." Science **292**(5516): 507-10.

Fujisawa, H., R. Ohtani-Kaneko, et al. (2008). "Involvement of post-translational modification of neuronal plasticity-related proteins in hyperalgesia revealed by a proteomic analysis." Proteomics **8**(8): 1706-19.

Fukata, Y., T. J. Itoh, et al. (2002). "CRMP-2 binds to tubulin heterodimers to promote microtubule assembly." Nat Cell Biol **4**(8): 583-91.

Gu, Y. and Y. Ihara (2000). "Evidence that collapsin response mediator protein-2 is involved in the dynamics of microtubules." J Biol Chem **275**(24): 17917-20.

Hall, C., M. Brown, et al. (2001). "Collapsin response mediator protein switches RhoA and Rac1 morphology in N1E-115 neuroblastoma cells and is regulated by Rho kinase." J Biol Chem **276**(46): 43482-6.

Harel, N. Y. and S. M. Strittmatter (2006). "Can regenerating axons recapitulate developmental guidance during recovery from spinal cord injury?" Nat Rev Neurosci **7**(8): 603-16.

Harman, A. M., J. Rodger, et al. (2003). "PSA-NCAM is up-regulated during optic nerve regeneration in lizard but not in goldfish." Exp Neurol **182**(1): 180-5.

Heasman, J. (2002). "Morpholino oligos: making sense of antisense?" Dev Biol **243**(2): 209-14.

Herdegen, T., S. Brecht, et al. (1993). "Long-lasting expression of JUN and KROX transcription factors and nitric oxide synthase in intrinsic neurons of the rat brain following axotomy." J Neurosci **13**(10): 4130-45.

Hjorth, J. and B. Key (2002). "Development of axon pathways in the zebrafish central nervous system." Int J Dev Biol **46**(4): 609-19.

Honnorat, J., T. Byk, et al. (1999). "Ulip/CRMP proteins are recognized by autoantibodies in paraneoplastic neurological syndromes." Eur J Neurosci **11**(12): 4226-32.

Hou, S. T., S. X. Jiang, et al. (2006). "Calpain-cleaved collapsin response mediator protein-3 induces neuronal death after glutamate toxicity and cerebral ischemia." J Neurosci **26**(8): 2241-9.

Hou, S. T., S. X. Jiang, et al. (2008). "Permissive and repulsive cues and signaling pathways of axonal outgrowth and regeneration." Int Rev Cell Mol Biol **267**: 125-81.

Hutson, L. D. and C. B. Chien (2002). "Pathfinding and error correction by retinal axons: the role of astray/robo2." Neuron **33**(2): 205-17.

Inatome, R., T. Tsujimura, et al. (2000). "Identification of CRAM, a novel unc-33 gene family protein that associates with CRMP3 and protein-tyrosine kinase(s) in the developing rat brain." J Biol Chem **275**(35): 27291-302.

Irizarry, R. A., B. Hobbs, et al. (2003). "Exploration, normalization, and summaries of high density oligonucleotide array probe level data." Biostatistics **4**(2): 249-64.

Isenmann, S., S. Engel, et al. (1999). "Bax antisense oligonucleotides reduce axotomy-induced retinal ganglion cell death in vivo by reduction of Bax protein expression." Cell Death Differ **6**(7): 673-82.

Itoh, A., T. Miyabayashi, et al. (1998). "Cloning and expressions of three mammalian homologues of Drosophila slit suggest possible roles for Slit in the formation and maintenance of the nervous system." Brain Res Mol Brain Res **62**(2): 175-86.

Jankowski, M. P., P. K. Cornuet, et al. (2006). "SRY-box containing gene 11 (Sox11) transcription factor is required for neuron survival and neurite growth." Neuroscience **143**(2): 501-14.

Jankowski, M. P., S. L. McIlwrath, et al. (2009). "Sox11 transcription factor modulates peripheral nerve regeneration in adult mice." Brain Res **1256**: 43-54.

Kandel, E. (2000). Principles of Neuronal Science, McGraw Hill.

Kanninen, K., G. Goldsteins, et al. (2004). "Glycosylation changes in Alzheimer's disease as revealed by a proteomic approach." Neurosci Lett **367**(2): 235-40.

Karlstrom, R. O., T. Trowe, et al. (1996). "Zebrafish mutations affecting retinotectal axon pathfinding." Development **123**: 427-38.

Kaslin, J. and P. Panula (2001). "Comparative anatomy of the histaminergic and other aminergic systems in zebrafish (Danio rerio)." J Comp Neurol **440**(4): 342-77.

Kawano, Y., T. Yoshimura, et al. (2005). "CRMP-2 is involved in kinesin-1-dependent transport of the Sra-1/WAVE1 complex and axon formation." Mol Cell Biol **25**(22): 9920-35.

Kee, N. J., E. Preston, et al. (2001). "Enhanced neurogenesis after transient global ischemia in the dentate gyrus of the rat." Exp Brain Res **136**(3): 313-20.

Kidd, T., K. Brose, et al. (1998). "Roundabout controls axon crossing of the CNS midline and defines a novel subfamily of evolutionarily conserved guidance receptors." Cell **92**(2): 205-15.

Kidd, T., C. Russell, et al. (1998). "Dosage-sensitive and complementary functions of roundabout and commissureless control axon crossing of the CNS midline." Neuron **20**(1): 25-33.

Kowara, R., M. Menard, et al. (2007). "Co-localization and interaction of DPYSL3 and GAP43 in primary cortical neurons." Biochem Biophys Res Commun **363**(1): 190-3.

Kullander, K., S. J. Butt, et al. (2003). "Role of EphA4 and EphrinB3 in local neuronal circuits that control walking." Science **299**(5614): 1889-92.

Lee, J. S. and C. B. Chien (2004). "When sugars guide axons: insights from heparan sulphate proteoglycan mutants." Nat Rev Genet **5**(12): 923-35.

Lee, J. S., R. Ray, et al. (2001). "Cloning and expression of three zebrafish roundabout homologs suggest roles in axon guidance and cell migration." Dev Dyn **221**(2): 216-30.

Lee, S., J. H. Kim, et al. (2002). "Collapsin response mediator protein-2 inhibits neuronal phospholipase D(2) activity by direct interaction." J Biol Chem **277**(8): 6542-9.

Lewis, K. E. and J. S. Eisen (2003). "From cells to circuits: development of the zebrafish spinal cord." Prog Neurobiol **69**(6): 419-49.

Linda, H., F. Piehl, et al. (1992). "Expression of GAP-43 mRNA in the adult mammalian spinal cord under normal conditions and after different types of lesions, with special reference to motoneurons." Exp Brain Res **91**(2): 284-95.

Liu, B. P. and S. M. Strittmatter (2001). "Semaphorin-mediated axonal guidance via Rho-related G proteins." Curr Opin Cell Biol **13**(5): 619-26.

Liu, W., X. W. Zhou, et al. (2009). "Calpain-truncated CRMP-3 and -4 contribute to potassium deprivation-induced apoptosis of cerebellar granule neurons." Proteomics **9**(14): 3712-28.

Marcus, R. C., C. L. Delaney, et al. (1999). "Neurogenesis in the visual system of embryonic and adult zebrafish (Danio rerio). off." Vis Neurosci **16**(3): 417-24.

Mario F. Wullimann, B. R., Heinrich Reichert (1996). Neuroanatomy of the zebrafish brain: a topological atlas, Birkhäuser.

McDowell, A. L., L. J. Dixon, et al. (2004). "Visual processing of the zebrafish optic tectum before and after optic nerve damage." Vis Neurosci **21**(2): 97-106.

McGill, M. A. and C. J. McGlade (2003). "Mammalian numb proteins promote Notch1 receptor ubiquitination and degradation of the Notch1 intracellular domain." J Biol Chem **278**(25): 23196-203.

McLaughlin, D., M. Vidaki, et al. (2008). "Localization of CRMP5 mRNA by in situ hybridization during development of the mouse forebrain." Neurosci Lett **432**(2): 117-20.

Meyer, D. K., M. I. Phillips, et al. (1982). "Studies on the presence of angiotensin II in rat brain." J Neurochem **38**(3): 816-20.

Meyronet, D., P. Massoma, et al. (2008). "Extensive expression of collapsin response mediator protein 5 (CRMP5) is a specific marker of high-grade lung neuroendocrine carcinoma." Am J Surg Pathol **32**(11): 1699-708.

Mimura, F., S. Yamagishi, et al. (2006). "Myelin-associated glycoprotein inhibits microtubule assembly by a Rho-kinase-dependent mechanism." J Biol Chem **281**(23): 15970-9.

Mitsui, N., R. Inatome, et al. (2002). "Involvement of Fes/Fps tyrosine kinase in semaphorin3A signaling." Embo J **21**(13): 3274-85.

Nasevicius, A. and S. C. Ekker (2000). "Effective targeted gene 'knockdown' in zebrafish." Nat Genet **26**(2): 216-20.

Neuhauss, S. C., O. Biehlmaier, et al. (1999). "Genetic disorders of vision revealed by a behavioral screen of 400 essential loci in zebrafish." J Neurosci **19**(19): 8603-15.

Nguyen Ba-Charvet, K. T., K. Brose, et al. (1999). "Slit2-Mediated chemorepulsion and collapse of developing forebrain axons." Neuron **22**(3): 463-73.

Nguyen, Q. T., J. R. Sanes, et al. (2002). "Pre-existing pathways promote precise projection patterns." Nat Neurosci **5**(9): 861-7.

Nishimura, T., Y. Fukata, et al. (2003). "CRMP-2 regulates polarized Numb-mediated endocytosis for axon growth." Nat Cell Biol **5**(9): 819-26.

Oudega, M. and X. M. Xu (2006). "Schwann cell transplantation for repair of the adult spinal cord." J Neurotrauma **23**(3-4): 453-67.

Park, K. K., K. Liu, et al. (2008). "Promoting axon regeneration in the adult CNS by modulation of the PTEN/mTOR pathway." Science **322**(5903): 963-6.

Park, K. W., C. M. Morrison, et al. (2003). "Robo4 is a vascular-specific receptor that inhibits endothelial migration." Dev Biol **261**(1): 251-67.

Parkinson, D. B., A. Bhaskaran, et al. (2008). "c-Jun is a negative regulator of myelination." J Cell Biol **181**(4): 625-37.

Pasterkamp, R. J., R. J. Giger, et al. (1999). "Expression of the gene encoding the chemorepellent semaphorin III is induced in the fibroblast component of neural scar tissue formed following injuries of adult but not neonatal CNS." Mol Cell Neurosci **13**(2): 143-66.

Petrausch, B., M. Jung, et al. (2000). "Lesion-induced regulation of netrin receptors and modification of netrin-1 expression in the retina of fish and grafted rats." Mol Cell Neurosci **16**(4): 350-64.

Plachez, C., W. Andrews, et al. (2008). "Robos are required for the correct targeting of retinal ganglion cell axons in the visual pathway of the brain." Mol Cell Neurosci **37**(4): 719-30.

Plump, A. S., L. Erskine, et al. (2002). "Slit1 and Slit2 cooperate to prevent premature midline crossing of retinal axons in the mouse visual system." Neuron **33**(2): 219-32.

Plunet, W., B. K. Kwon, et al. (2002). "Promoting axonal regeneration in the central nervous system by enhancing the cell body response to axotomy." J Neurosci Res **68**(1): 1-6.

Quach, T. T., G. Massicotte, et al. (2008). "CRMP3 is required for hippocampal CA1 dendritic organization and plasticity." Faseb J **22**(2): 401-9.

Quinn, C. C., E. Chen, et al. (2003). "TUC-4b, a novel TUC family variant, regulates neurite outgrowth and associates with vesicles in the growth cone." J Neurosci **23**(7): 2815-23.

Quinn, C. C., G. E. Gray, et al. (1999). "A family of proteins implicated in axon guidance and outgrowth." J Neurobiol **41**(1): 158-64.

Ricard, D., B. Stankoff, et al. (2000). "Differential expression of collapsin response mediator proteins (CRMP/ULIP) in subsets of oligodendrocytes in the postnatal rodent brain." Mol Cell Neurosci **16**(4): 324-37.

Rosslenbroich, V., L. Dai, et al. (2005). "Collapsin response mediator protein-4 regulates F-actin bundling." Exp Cell Res **310**(2): 434-44.

Roth, L. W., P. Bormann, et al. (1999). "Beta-thymosin, a modulator of the actin cytoskeleton is increased in regenerating retinal ganglion cells." Eur J Neurosci **11**(10): 3488-98.

Schebesta, M. and F. C. Serluca (2009). "olig1 Expression identifies developing oligodendrocytes in zebrafish and requires hedgehog and notch signaling." Dev Dyn **238**(4): 887-98.

Schmidt, E. F. and S. M. Strittmatter (2007). "The CRMP family of proteins and their role in Sema3A signaling." Adv Exp Med Biol **600**: 1-11.

Schmidt, J. T., M. Buzzard, et al. (2000). "MK801 increases retinotectal arbor size in developing zebrafish without affecting kinetics of branch elimination and addition." J Neurobiol **42**(3): 303-14.

Schulte-Merker, S., F. J. van Eeden, et al. (1994). "no tail (ntl) is the zebrafish homologue of the mouse T (Brachyury) gene." Development **120**(4): 1009-15.

Schweitzer, J., C. G. Becker, et al. (2005). "Expression of collapsin response mediator proteins in the nervous system of embryonic zebrafish." Gene Expr Patterns **5**(6): 809-16.

Schweitzer, J., T. Becker, et al. (2003). "Expression of protein zero is increased in lesioned axon pathways in the central nervous system of adult zebrafish." Glia **41**(3): 301-17.

Schweitzer, J., D. Gimnopoulos, et al. (2007). "Contactin1a expression is associated with oligodendrocyte differentiation and axonal regeneration in the central nervous system of zebrafish." Mol Cell Neurosci **35**(2): 194-207.

Seeger, M., G. Tear, et al. (1993). "Mutations affecting growth cone guidance in Drosophila: genes necessary for guidance toward or away from the midline." Neuron **10**(3): 409-26.

Smith, D. S. and J. H. Skene (1997). "A transcription-dependent switch controls competence of adult neurons for distinct modes of axon growth." J Neurosci **17**(2): 646-58.

Solomon, K. S. and A. Fritz (2002). "Concerted action of two dlx paralogs in sensory placode formation." Development **129**(13): 3127-36.

Stenmark, P., D. Ogg, et al. (2007). "The structure of human collapsin response mediator protein 2, a regulator of axonal growth." J Neurochem **101**(4): 906-17.

Stuermer, C. A. (1988). "Trajectories of regenerating retinal axons in the goldfish tectum: II. Exploratory branches and growth cones on axons at early regeneration stages." J Comp Neurol **267**(1): 69-91.

Stuermer, C. A., M. Bastmeyer, et al. (1992). "Trying to understand axonal regeneration in the CNS of fish." J Neurobiol **23**(5): 537-50.

Stuermer, C. A. and S. S. Easter, Jr. (1984). "A comparison of the normal and regenerated retinotectal pathways of goldfish." J Comp Neurol **223**(1): 57-76.

Stuermer, C. A. and S. S. Easter, Jr. (1984). "Rules of order in the retinotectal fascicles of goldfish." J Neurosci **4**(4): 1045-51.

Sumanas, S. and J. D. Larson (2002). "Morpholino phosphorodiamidate oligonucleotides in zebrafish: a recipe for functional genomics?" Brief Funct Genomic Proteomic **1**(3): 239-56.

Summerton, J. (1999). "Morpholino antisense oligomers: the case for an RNase H-independent structural type." Biochim Biophys Acta **1489**(1): 141-58.

Summerton, J. and D. Weller (1997). "Morpholino antisense oligomers: design, preparation, and properties." Antisense Nucleic Acid Drug Dev **7**(3): 187-95.

Suzuki, Y., S. Nakagomi, et al. (2003). "Collapsin response mediator protein-2 accelerates axon regeneration of nerve-injured motor neurons of rat." J Neurochem **86**(4): 1042-50.

Tanaka, E. M. and P. Ferretti (2009). "Considering the evolution of regeneration in the central nervous system." Nat Rev Neurosci **10**(10): 713-23.

Taylor, J. S., Y. Van de Peer, et al. (2001). "Comparative genomics provides evidence for an ancient genome duplication event in fish." Philos Trans R Soc Lond B Biol Sci **356**(1414): 1661-79.

Turner, J. E. and M. Singer (1974). "The ultrastructure of regeneration in the severed newt optic nerve." J Exp Zool **190**(3): 249-68.

Udvadia, A. J. (2008). "3.6 kb genomic sequence from Takifugu capable of promoting axon growth-associated gene expression in developing and regenerating zebrafish neurons." Gene Expr Patterns **8**(6): 382-8.

Van de Peer, Y., J. S. Taylor, et al. (2002). "Wanda: a database of duplicated fish genes." Nucleic Acids Res **30**(1): 109-12.

Veldman, M. B., M. A. Bemben, et al. (2007). "Gene expression analysis of zebrafish retinal ganglion cells during optic nerve regeneration identifies KLF6a and KLF7a as important regulators of axon regeneration." Dev Biol **312**(2): 596-612.

Veyrac, A., N. Giannetti, et al. (2005). "Expression of collapsin response mediator proteins 1, 2 and 5 is differentially regulated in newly generated and mature neurons of the adult olfactory system." Eur J Neurosci **21**(10): 2635-48.

Wang, L. H. and S. M. Strittmatter (1997). "Brain CRMP forms heterotetramers similar to liver dihydropyrimidinase." J Neurochem **69**(6): 2261-9.

Watson, W. E. (1974). "Cellular responses to axotomy and to related procedures." Br Med Bull **30**(2): 112-5.

Westerfield, M. (1989). The Zebrafish Book.

White, F. A. and O. Behar (2000). "The development and subsequent elimination of aberrant peripheral axon projections in Semaphorin3A null mutant mice." Dev Biol **225**(1): 79-86.

Woo, Y., J. Affourtit, et al. (2004). "A comparison of cDNA, oligonucleotide, and Affymetrix GeneChip gene expression microarray platforms." J Biomol Tech **15**(4): 276-84.

Yamashita, N., A. Morita, et al. (2007). "Regulation of spine development by semaphorin3A through cyclin-dependent kinase 5 phosphorylation of collapsin response mediator protein 1." J Neurosci **27**(46): 12546-54.

Yamashita, N., Y. Uchida, et al. (2006). "Collapsin response mediator protein 1 mediates reelin signaling in cortical neuronal migration." J Neurosci **26**(51): 13357-62.

Yang, Z., H. A. Quigley, et al. (2007). "Changes in gene expression in experimental glaucoma and optic nerve transection: the equilibrium between protective and detrimental mechanisms." Invest Ophthalmol Vis Sci **48**(12): 5539-48.

Yiu, G. and Z. He (2006). "Glial inhibition of CNS axon regeneration." Nat Rev Neurosci **7**(8): 617-27.

Yoshimura, T., Y. Kawano, et al. (2005). "GSK-3beta regulates phosphorylation of CRMP-2 and neuronal polarity." Cell **120**(1): 137-49.

Yuan, Q., B. Hu, et al. (2009). "GAP-43 expression correlates with spinal motoneuron regeneration following root avulsion." J Brachial Plex Peripher Nerve Inj **4**: 18.

Yuan, W., L. Zhou, et al. (1999). "The mouse SLIT family: secreted ligands for ROBO expressed in patterns that suggest a role in morphogenesis and axon guidance." Dev Biol **212**(2): 290-306.

Zearfoss, N. R., J. M. Alarcon, et al. (2008). "A molecular circuit composed of CPEB-1 and c-Jun controls growth hormone-mediated synaptic plasticity in the mouse hippocampus." J Neurosci **28**(34): 8502-9.

Zhang, Y., X. H. Feng, et al. (1998). "Smad3 and Smad4 cooperate with c-Jun/c-Fos to mediate TGF-beta-induced transcription." Nature **394**(6696): 909-13.

Zhang, Z., A. K. Ottens, et al. (2007). "Calpain-mediated collapsin response mediator protein-1, -2, and -4 proteolysis after neurotoxic and traumatic brain injury." J Neurotrauma **24**(3): 460-72.

7 Danksagung

Als erstes möchte ich PD Dr. Catherina Becker danken, dass sie mir die Möglichkeit gegeben hat, in ihrer Gruppe meine Doktorarbeit zu schreiben und sich mit viel Zeit und Einsatz um mich gekümmert hat. Ein besonders herzlicher Dank gilt meinem Betreuer PD Dr. Thomas Becker für seine kompetente, immer freundliche und konstruktive Begleitung meiner Doktorarbeit. Jederzeit konnte ich Ideen und Schwierigkeiten während meiner Arbeit ganz offen mit ihm austauschen.

Mein Dank gilt Prof. Lothar Renwrantz vom Zoologischen Institut der Universität Hamburg für die Begutachtung meiner Dissertation.

Ganz besonders möchte ich mich bei Dr. Michell Reimer, meinem Doktorandenkollegen und Mitstreiter im Labor, bedanken. Viele Stunden im Labor und wissenschaftliche Diskussionen bei komplizierten Themen haben mir sehr geholfen.

Ein ganz spezieller Dank geht an Prof. Ron Hart von der Rutgers University, der mir mit Rat und Tat zur Seite stand.

Danke natürlich den vielen Freunden (Dr. Dymtro Puchkov, Dr. Ingo Meier, Dr. Aparna Shetty, Jonathan Davila und Dr. Loyal Goff, um nur einige zu nennen) in den verschiedenen Laboren in Deutschland und im Ausland, die mich immer überaus freundlich empfangen und aufgenommen haben. Eure Hilfe war von unschätzbarem Wert. Ihr habt jedes Labor zu dem gemacht, was es für mich war: Lehrreich, aufregend und unvergesslich.

Vielen Dank auch meinen Verwandten Angela und Chris für das englische Korrekturlesen.

Die konstante Unterstützung meiner Eltern und meiner Schwester, ihre positive Einstellung und tatkräftige Hilfe, haben mir die nötige Energie gegeben, um diese Arbeit fertigzustellen.

Zu guter Letzt möchte ich mich bei Max und Moni dafür bedanken, dass sie während der letzten Phase der Arbeit so intensiv für mich da waren und mir viel Geduld entgegen gebracht haben.